PNL-3828
UC-85

Examination of Stainless Steel-Clad Connecticut Yankee Fuel Assembly S004 After Storage in Borated Water

September 1982

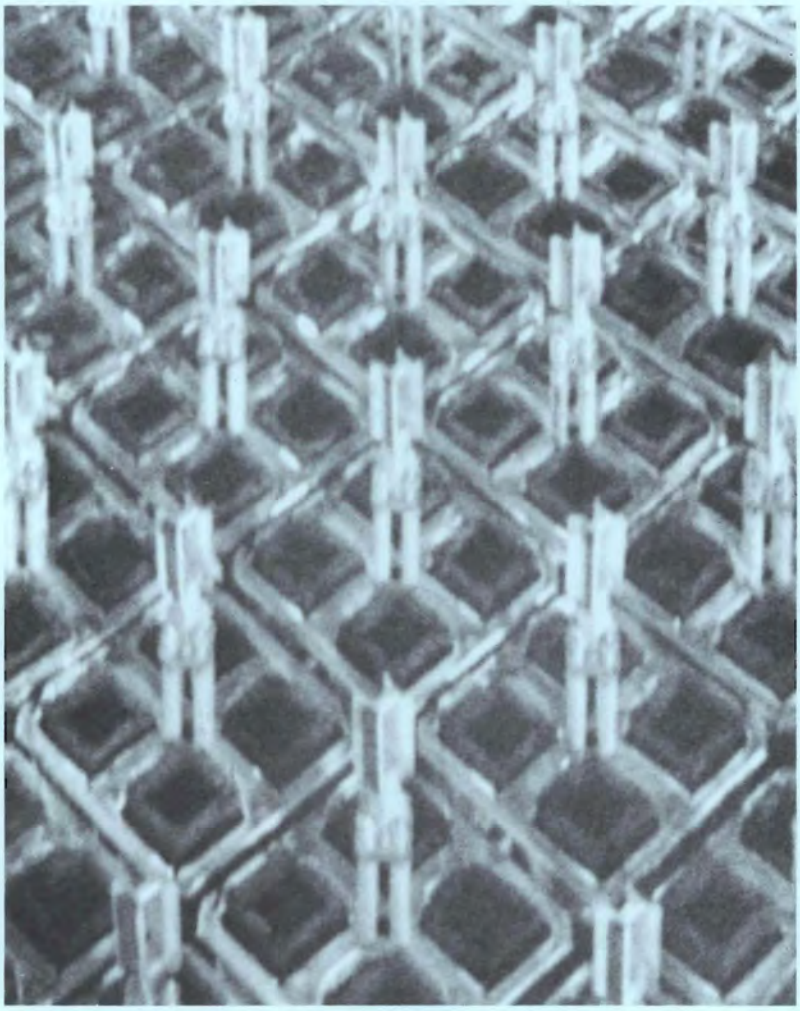

Prepared for the U.S. Department of Energy
under Contract DE-AC06-76RLO 1830

Pacific Northwest Laboratory
Operated for the U.S. Department of Energy
by Battelle Memorial Institute

Battelle

PNL-3828

DISCLAIMER

PACIFIC NORTHWEST LABORATORY
operated by
BATTELLE
for the
UNITED STATES DEPARTMENT OF ENERGY
under Contract DE-AC06-76RLO 1830

Printed in the United States of America
Available from
National Technical Information Service
United States Department of Commerce
5285 Port Royal Road
Springfield, Virginia 22151

NTIS Price Codes
Microfiche A01

Printed Copy

Pages	Price Codes
001-025	A02
026-050	A03
051-075	A04
076-100	A05
101-125	A06
126-150	A07
151-175	A08
176-200	A09
201-225	A010
226-250	A011
251-275	A012
276-300	A013

DOE-Richland, WA

PNL-3828
UC-85

EXAMINATION OF STAINLESS STEEL-CLAD CONNECTICUT YANKEE FUEL ASSEMBLY S004 AFTER STORAGE IN BORATED WATER

D. C. Langstaff(a)
W. J. Bailey
A. B. Johnson, Jr.
M. P. Landow(b)
V. Pasupathi(b)
R. W. Klingensmith(b)

September 1982

Prepared for
the U.S. Department of Energy
under Contract DE-AC06-76RLO 1830

Pacific Northwest Laboratory
Richland, Washington 99352

(a) Under subcontract to PNL from Columbia Engineers Services, Inc., and later from TAD Technical Services Corp.
(b) Battelle Columbus Laboratories.

ACKNOWLEDGMENTS

This document was published under the U.S. Department of Energy's Commercial Spent Fuel Management Program. The contributions from the following individuals are gratefully acknowledged.

M. T. Pitek and R. W. Bishop and Northeast Utilities Service Company arranged the transfer of Connecticut Yankee Qualification Fuel Assembly S004 to this program and supplied background information on the fuel.

L.F.A. Raven and J. Naylor of British Nuclear Fuels Limited provided background information on Connecticut Yankee Qualification Fuel Assembly S004.

D. M. Rainey of Babcock & Wilcox Company provided information on calculated fuel rod power and burnup.

T. W. Rees of Superior Tube Company supplied information on fabrication and mechanical properties of the unirradiated cladding.

We especially appreciate the guidance and participation of W. H. Baker of the Savannah River Plant in planning and implementing the program.

SUMMARY

Stainless steels are susceptible to stress corrosion cracking in a variety of environments. Investigations have shown, for example, that a few stainless steel pipes at domestic PWR spent fuel pools have developed intergranular stress corrosion cracks at weld heat-affected zones (Giacobbe 1981). Intergranular stress corrosion cracking was the apparent cause of the failure of stainless steel components in a domestic PWR fuel assembly (NSP 1982). Intergranular corrosion also occurred on some domestic and foreign stainless steel-clad gas reactor fuel as a result of sensitization during reactor exposure. These considerations suggest that stainless steel-clad water reactor fuel could be more susceptible to stress-related corrosion than Zircaloy-clad fuel, even though sensitization is not a significant factor during water residence times.

The general lack of data has pointed out the need for a program to study the corrosion of stainless steel-clad fuel during storage in water. Because the United States has the largest current and potential inventory of stainless steel-clad fuel,[(a)] it was concluded that examination of stainless steel-clad fuel stored in borated water should be incorporated into the U.S. spent fuel examination programs.

SELECTION OF FUEL FOR EXAMINATION

A Connecticut Yankee (Haddam Neck) qualification fuel assembly was chosen for examination by Pacific Northwest Laboratory (PNL) under a program sponsored by the U.S. Department of Energy (DOE). Connecticut Yankee is a pressurized water reactor (PWR) that has operated since startup (1967) with stainless steel-clad fuel. Spent fuel stored at the reactor pool had characteristics that were attractive to this investigation:

- fuel assemblies characterized before and during irradiation
- relatively high burnups (>30,000 M,Wd/MTU or >2600 Gj/kgU)
- substantial storage times (5 to 8 yr) in borated water.

(a) Of the commercial light-water reactor fuel assemblies stored in the United States as of mid-1979, approximately 7% (nearly 1500 fuel assemblies) contained stainless steel-clad fuel rods.

Assembly S004 was selected for examination because it had no known reactor-induced defects, had a relatively high burnup (32,000 MWd/MTU), had been stored for 5 yr, and was a well-characterized qualification assembly. At about the same time, hot-cell examinations of two other Connecticut Yankee fuel assemblies, H07 and G11, were planned under a separate program jointly sponsored by the Northwest Utilities Service Company (NUSCO) and the Electric Power Research Institute (EPRI) to investigate a fuel failure mechanism that occurred during reactor residence. The principal aim of the investigation was to determine the cause of cladding failure in H07. However, NUSCO and EPRI agreed to provide the DOE program with any evidence regarding the presence or absence of pool-induced effects on the two assemblies. PNL, NUSCO, and EPRI also agreed on the interchange of a few rods between the three assemblies when they are reconstituted prior to shipment from the hot cell for subsequent extended storage.

The selection of these Connecticut Yankee fuel assemblies for the two programs provided a data base on pool storage effects on three related assemblies that contain fuel rods with stainless steel (304L and 304 types) cladding, burnups up to 37,500 MWd/MTU, and a range of pool storage times. The examinations of all three assemblies were conducted at the hot-cell facility at the Battelle Columbus Laboratories.

CLADDING DEGRADATION MECHANISMS ADDRESSED AND INSPECTION METHODS USED

The S004 fuel examination was designed to address all mechanisms regarded as possible contributors to cladding degradation (see table below).

Mechanism	Method of Inspection
Uniform Corrosion	Visual Inspection, Metallography
Crud-Localized Corrosion	Visual Inspection, Metallography
Stress Corrosion	Visual Inspection, Metallography, Eddy Current
Pitting	Visual Inspection, Metallography, Eddy Current
Corrosion at Cladding Defects[a]	Visual Inspection, Metallography
Fission Product Attack	Visual Inspection, Metallography
Corrosion of Weld-Sensitized Areas	Visual Inspection, Metallography
Fretting Corrosion	Visual Inspection, Metallography (at grid spacer-cladding contact points)

(a) Applicable only to assembly H07.

At the same time, characteristics of the fuel rods were determined so comparisons could be made with similar data obtained during prior examinations at the reactor pool (see table below), and to establish baseline information in case future examinations of the assembly were considered desirable after additional storage periods.

Parameter	Measurement
Cladding Mechanical Properties	Tensile Test, Ring Crush Test
Cladding Ovality	Fuel Rod Profilometry
Fuel Swelling	Fuel Rod Profilometry
Fuel Swelling Degradation	Visual Inspection, Metallography
Grid Spacer Spring Forces	Measure Fuel Rod Withdrawal Forces
Cladding Incipient Defects	Profilometry/Eddy Current
Fuel Rod Weight	Weighing
Fuel Rod Length and Diameter	Dimensions/Determinations

RESULTS OF NONDESTRUCTIVE AND DESTRUCTIVE EXAMINATIONS

The following conclusions are drawn from nondestructive and destructive examinations of assembly S004:

- Fuel rod weight measurements indicated that no significant weight changes had occurred.
- Eddy current measurements showed no strong indications of incipient cladding defects.
- The visual appearance of the fuel rods suggested no significant deterioration.
- The results of the metallurgical examination showed that cladding and fuel were typical of irradiated PWR fuel rods. At most locations, oxide layers and crud layers were to thin to be discrenible.
- No significant cladding deterioration was observed in the metallographic examination of the end cap-to-cladding welds and the cladding seam welds.

- The results of the mechanical properties testing indicated that the cladding had retained some ductility and did not behave in a brittle manner.
- Visual inspection suggested that the fuel assembly componets (end fittings and rod spacers) had not undergone noticeable degradation.

In general, the cladding surface was free of crud and oxide layers, although some localized areas did show surface layers from 1/2 to 6 microns thick. Isolated areas with oxide layers occurred on both the outside and inside surfaces of the cladding. Measurements made from photomicrographs indicated that no detectable change in cladding thickness occurred. This result supported the visual observation of no significant general corrosion. Visual, metallographic, and eddy current examinations failed to reveal any evidence of pitting corrosion or cracking in either the seam-welded cladding or in the end cap-to-cladding weld areas.

Based on the results, it was concluded that no obvious degradation of the 304L stainless steel-clad spent fuel from assembly S004 occurred during 5 yr of storage in borated water. Furthermore, no obvious degradation due to the pool environment occurred on 304 stainless steel-clad rods in assemblies H07 and G11, which were stored for shorter periods but contained operationally induced cladding defects. The seam welds in the cladding on fuel rods from assembly S004, H07, and G11 were similar in that they showed a wrought microstructure with grains noticeably smaller than those in the cladding base metal. The end cap welds showed a dendritically cored structure, typical of rapidly quenched austenitic weld metal. Some intergranular melting may have occurred in the heat-affected zone (HAZ) in the cladding adjacent to the end cap welds in rods from assemblies S004 an H07. However, the weld areas did not show evidence of corrosion-induced degradation.

CONTENTS

FIGURES

TABLES

INTRODUCTION

Storage of spent nuclear fuel in water has been and will continue to be an important factor in nuclear fuel management. Currently, water storage of spent nuclear fuel is the only licensed option in the United States. The last commercial reprocessing of spent fuel occurred in 1971. Since then, the commercial spent fuel inventory stored in U.S. water pools has risen to about 28,000 fuel assemblies (Carter 1980). Another option, dry storage, is also being investigated as an interim fuel management measure (Anderson and Meyer 1980; Johnson, Gilbert, and Guenther 1982). However, even with that option, spent fuel will continue to be discharged to water storage for a cooling period before being transferred to dry storage.

Spent fuel examinations conducted in Canada, the Federal Republic of Germany, and the United Kingdom have investigated the possible effects of water storage. Only one stainless steel-clad fuel rod has been examined in those programs. Although there has been no evidence of degradation in stainless steel-clad water reactor fuel stored for over a decade in water, there have been a few cases of stress corrosion cracking of stainless steel: 1) intergranular stress-corrosion cracks developed in the weld heat-affected zones of stainless steel pipes at domestic PWR spent fuel pools (Giacobbe 1981); 2) intergranular stress corrosion cracking was the apparent cause of failure of stainless steel components in one domestic PWR fuel assembly (NSP 1982); and 3) some stainless steel-clad gas reactor fuel underwent intergranular corrosion as a result of sensitization during the reactor exposure.

Because the U.S. has the largest current and potential inventory of stainless steel-clad water reactor fuel, the Department of Energy (DOE) has included the examination of such fuel in the Spent Fuel and Fuel Pool Component Integrity Program, which DOE has implemented to establish the corrosion and metallurgical condition of spent light-water reactor (LWR) fuel assemblies after extended storage in water. The program was designed to provide insight into fuel behavior of value in licensing and operating spent fuel storage pools. As part of that program, Pacific Northwest Laboratory (PNL) has examined the

Connecticut Yankee qualifiation fuel assmbly S004 with the objective of establishing its condition after 5 yr of storage in borated water. The S004 assembly contains stainless steel-clad fuel rods, 20 of which were well characterized prior to irradiation. The incentives for investigation such a fuel assembly were: 1) of the nuclear fuel stored in the United States as of mid-1979, approximately 7%, nearly 1500 fuel assemblies, contained stainless steel-clad fuel (Johnson 1980); and 2) stainless steel is known to show susceptibility to stress-corrosion cracking in some environments and in certain metallurgical conditions. Some standard commercial fuel assemblies stored at the Connecticut Yankes spent fuel pool had higher burnups (i.e., irradiation exposures to 36,800 MWd/MTU or 3180 GJ/kgU) or longer times (to 10 yr versus 5 yr for S004) in pool storage. However, fuel rods in those assemblies were not characterized as well as some in S004. As of 1979, the highest burnups for fuel assemblies with stainless steel-clad fuel rods discharged from domestic and foreign commercial reactors were 37,500 MWd/MTU (3,240 GJ/kgU) (batch average) and 32,000 MWd/MTU (3,765 GJ/kgU), respectively (Johnson 1980). Some domestic fuel with batch average burnups to the former level were discharged during this 1972-1976 period.

Another objective of the PNL examination was to characterize the fuel to the extent that any significant changes in the assembly condition caused by subsequent extended pool storage would be discernible if future assembly examinations are conducted. Figure 1 provides an overall perspective of the general plan that was developed prior to the examinations. All examinations were made at the Battelle Columbus Laboratories (BCL) Nuclear Materials Technology Facility.

In a complementary program (Pasupathi and Klingensmith 1981), the Northeast Utilities Service Company (NUSCO) and the Electric Power Research Institute (EPRI) examined Connecticut Yankee fuel assemblies to determine the cause of reactor-induced fuel rod failures that had occurred in 36 of 48 Batch-8 fuel assemblies. One Batch-8 fuel assembly (H07) and one Batch-7 fuel assembly (G11) have been examined (Figure 1). Assembly H07 had several fuel rods that failed during operation in the reactor. Fuel rods in Assembly G11 did not fail during operation in the reactor. Fuel pellets for H07 and S004 were fabricated by the same fuel supplier, British Nuclear Fuels Limited

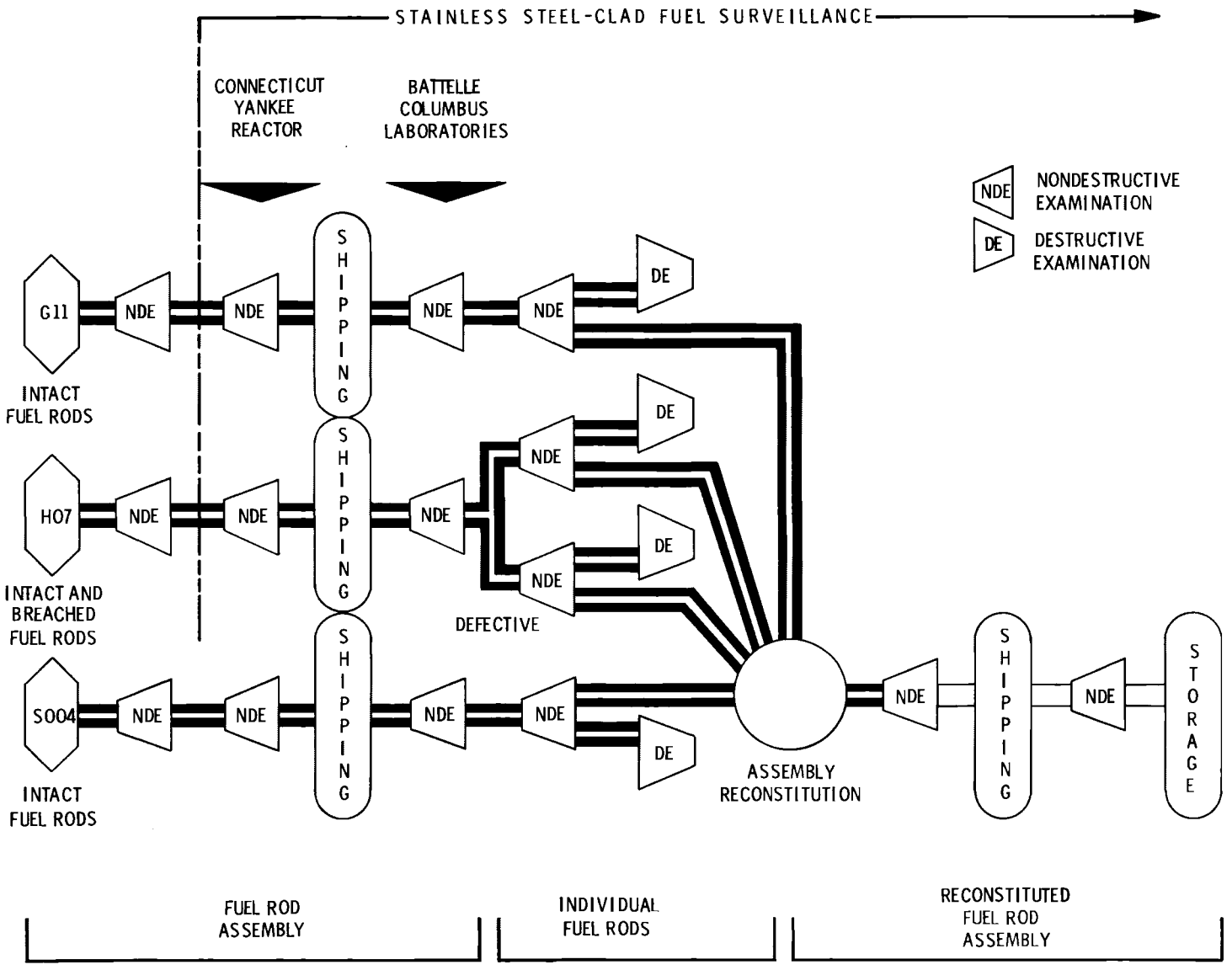

FIGURE 1. General Outline of Connecticut Yankee Qualification Fuel Assembly S004 History: Storage, Transport, and Examination

(BNFL). The examinations of assemblies G11 and H07 were conducted concurrently but independently of the examination of assembly S004 at BCL. However, the concurrent examinations provided an opportunity to select a few G11 and H07 fuel rods for insertion into assembly S004 when it is reconstituted prior to shipment from the hot cell for subsequent extended storage.

As noted in the report from the NUSCO/EPRI program (Pasupathi and Klingensmith 1981), there have been several other documented cases of failures of stainless steel-clad fuel. The Connecticut Yankee fuel rod failures were similar to those in the Vulcain core of the BR-3 reactor (Storen and Locke 1970), and were probably similar to the failures observed in SENA (Multer 1975).

The postirradiation examination of S004 was initiated at BCL in July 1980. This report contains PNL's results from both nondestructive and destructive examinations of assembly S004 and relevant results from assemblies H07 and G11. Also included in a brief history of the fuel assembly fabrication, storage, and transport.

CONCLUSIONS

The studies of the corrosion and metallurgical condition of pool-stored S004, H07, and G11 fuel rods from the Connecticut Yankee (Haddam Neck) Reactor resulted in the following conclusions:

- No obvious degradation of the 304L stainless steel-clad fuel rods from assembly S004 occurred after 5 yr of storage in borated water. With respect to crud and corrosion, the fuel rods from assembly S004 were very similar to 304 stainless steel-clad fuel rods from assemblies H07 and G11, which had been stored for much shorter periods (1.3 and 2.6 yr, respectively).
- Fuel rods from assemblies S004, H07, and G11 were relatively free of crud and oxide films.
- In contrast to the cases with H07 and G11 rods, no pellet chips were lodged in the fuel-cladding gaps of S004 rods. Pellet chips in S004 rods were also much smaller than those found in H07 and G11 rods.
- No cladding breaches, with concomitant loss of fission products and/or fuel, or ingress of coolant occurred in the precharacterized fuel rods examined during postirradiation examination based on:
  - reactor operating data (NRC Docket Reports)
  - sipping test results
  - rod weight measurements
  - eddy current measurements.
- Cladding and weld metallography is very similar for the S004, H07, and G11 fuel rods that were examined.
- Cladding cracks, pitting, or significant general corrosion were not evident from the metallographic examination of the cladding from S004 fuel rods on either the OD or ID of the cladding.
- Cracks, pitting, or significant general corrosion were not evident in cladding or end cap weld areas on fuel rods from assemblies S004, H07, and G11.

- A qualitative indication of good ductility was evident in the ring crush test of S004 fuel rod AHR irradiated cladding.
- Irradiation strengthening, with a concomitant reduction of ductility, was observed in cladding from fuel rod AHR, assuming the unirradiated strength and ductility were similar to those of the 304SS archive cladding used on fuel rods in the H07 assembly.
- The mechanical properties of the irradiated cladding are deformation rate dependent.
- There are at least two operating temperature regimes (i.e., some fuel rods operated with higher centerline fuel temperatures than others) represented in the fuel rods from the S004 fuel assembly, based on fission gas release (order of magnitude difference noted) and fuel microstructural information from the fuel rods that were destructively examined.

FUEL HISTORY AND CHARACTERISTICS

The qualification fuel assembly S004 was irradiated in the Connecticut Yankee (Haddam Neck) reactor, a Westinghouse-designed pressurized water reactor (PWR), operated by the Connecticut Yankee Atomic Power Company and partially owned by the Northeast Utilities Services Company (NUSCO). Commercial operation began in June 1967, with power levels of 575 MWe (1825 MWt). Assembly S004 was supplied to the reactor by Gulf General Atomic (GGA). The assembly was irradiated in the reactor core during cycles 3, 4, and 5 and was stored in the Connecticut Yankee spent fuel pool for 5 yr after it was discharged from the reactor. In May 1980, it was shipped to the Battelle Columbus Laboratories Nuclear Materials Technology Facility at West Jefferson, Ohio, for hot-cell examination.

FUEL FABRICATION

Gulf General Atomic contracted with British Nuclear Fuels Limited (BNFL) to design and fabricate the fuel assembly. The fuel rods contained UO_2 pellets enriched to 4.0% ^{235}U by weight in 10.76-mm (0.4235-in.) OD, seam-welded and drawn Type 304L stainless steel cladding,[(a)] with a 0.42-mm (0.0165-in.) wall thickness. The fuel rod length was 3.2171 m (126.66 in.). The fill gas composition was typically 96 to 98% helium and 2 to 4% air with about 25 to 30 ppm ^{85}Kr, based on results from destructive tests on sample rods; the fill gas pressure was 1 atm. The control rod guide tubes and the instrument tube were fabricated from 12.2-mm (0.480-in.) OD, Type 304L stainless steel tubing witha 0.34-mm (0.0135-in.) wall thickness. The grid spacers and springs were fabricated from Inconel 718. The upper and lower nozzles were made from Type 321 stainless steel. The upper nozzle was not designed to be readily removable. Additional design details are listed in Table 1.

(a) BNFL had specified Type 304 stainless steel for the fuel cladding. However, the results of PNL's analysis of the certified archive sample of the fuel cladding supplied by BNFL showed a carbon content of 0.030%. The maximum carbon content is 0.08% and 0.03% for Types 304 and 304L stainless steel, respectively. For this reason, the fuel cladding is labeled Type 304L in this report.

TABLE 1. Fabrication Data for Connecticut Yankee (Haddam Neck) Qualification Fuel Assembly S004

Fuel Vendor	Gulf General Atomic
Fuel Designer and Fabricator	British Nuclear Fuels Limited
Type (Rod Array)	15 x 15
Control Rod Guide Tubes:	
Number	20
Upper OD	12.2 mm (0.480 in.)
Wall Thickness	0.34 mm (0.0135 in.)
Material	304L Stainless Steel
Instrument Tubes:	
Number	1
OD	12.2 mm (0.480 in.)
Wall Thickness	0.34 mm (0.0135 in.)
Material	304L Stainless Steel
Spacer Grids:	
Number	7
Material	Inconel 718
Spring Material	Inconel 718
Fuel Rods (not prepressurized):	
Number	204
Length	3.2171 mm (126.66 in.)
OD	10.76 mm (0.4235 in.)
Wall Thickness	0.42 mm (0.0165 in.)
Material	304L Stainless Steel(a)
Fuel Pellet Stack Length	3.0798-3.0925 m (121.25-121.75 in.)
Diametral Gap(b)	0.18 mm (0.007 in.)
Orifice Plate Material	321 Stainless Steel
Plenum Springs:	
Working Length	102 mm (4.06 in.)
Material	302 Stainless Steel
Fuel Pellet:	
Geometry	Solid Right Circular Cylinder with Dished Ends
Diameter	9.73-9.75 mm (0.383-0.384 in.)
Material	UO_2
Enrichment	4.00 wt% ^{235}U
Mean Density	10.215 g/cm^3 (93.20% TD)(c)
Mean Weight/Rod	2.264 kg (4.987 lb)
Length	11.4 mm (0.450 in.)

(a) See Footnote (a) under "FUEL FABRICATION."
(b) Diametral gap is cladding inside diameter minus pellet diameter.
(c) Theoretical density (TD) for stoichiometric UO_2 is 10.96 g/cm^3.

The assembly, a 15 x 15 rod array shown schematically in Figure 2, contains 1 instrument tube, 20 control rod guide tubes, and 204 fuel rods. Figure 3 is a schematic drawing of a typical fuel rod in this assembly.

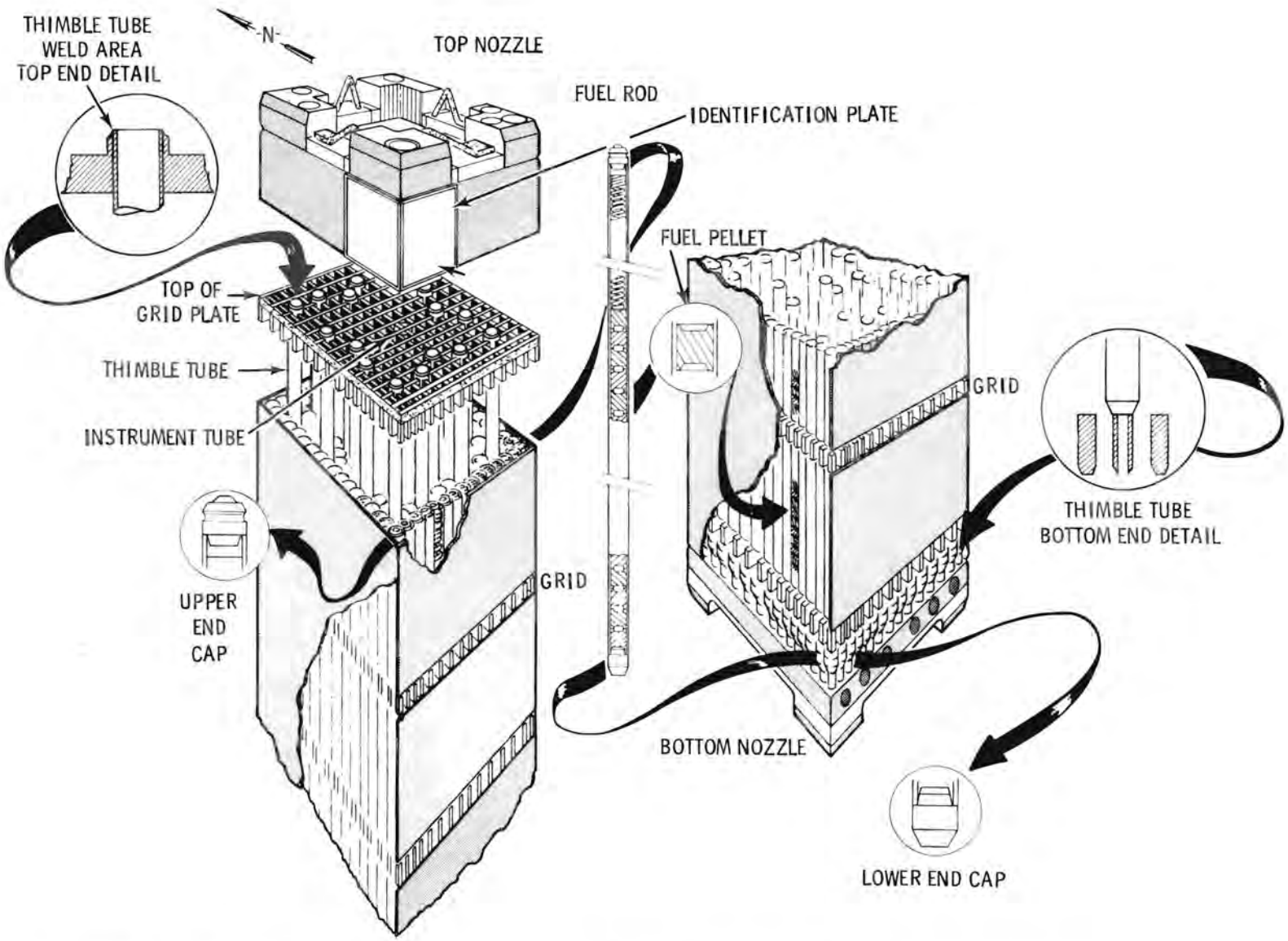

FIGURE 2. Schematic Diagram Showing Structural Features of S004, Including Details of the Thimble Tube Weld Areas

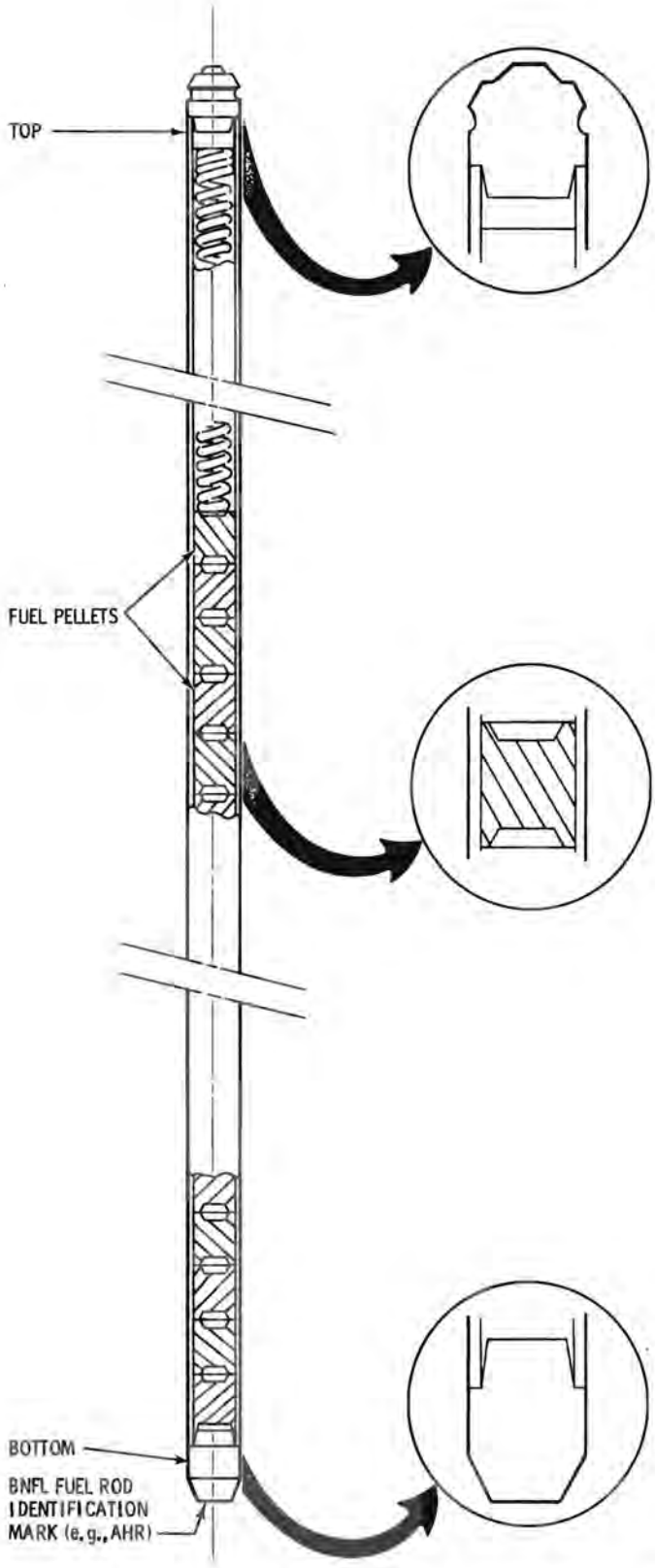

FIGURE 3. Schematic Diagram of Typical Fuel Rod from Fuel Assembly S004

CONPOR (Controlled Porosity) fuel (Heal, Littlechild, and Page 1980; Littlechild and Butler 1976; Raven 1976) was used for the pellets. Pellet information is listed in Table 1. Table 2 lists the fabrication history of the welded and drawn tubing used for fuel rod cladding. The fuel rod loading diagram for S004 is provided in Figure 4.

TABLE 2. Fabrication of Seam-Welded, Stainless Steel Cladding for Fuel Rods

MATERIAL:	1.65 mm thick strip	
RECEIVING INSPECTION:	Physical and Chemical Testing	
FABRICATION:	Bend Strip	
	Tungsten-Inert Gas Weld	
	Draw Degrease Solution Anneal	Repeat to 0.41 mm OD
	Plug Draw	
	Degrease	
	Solution Anneal	
	Pickle (HNO_3 + HF)	
	Plug Draw to Final Size (10-15% Cold-Worked)	
	Final Pickle (HNO_3 + HF)	
TUBE INSPECTION:	Straightness	
	Ovality	
	Ultrasonic Testing on ID/OD-100%, Every Tube	
CORROSION TEST:	Boiling $CuSO_4$ Solution	

FUEL IRRADIATION HISTORY

S004 was first irradiated in cycle 3 at Connecticut Yankee. It was removed from the core at the end of cycle 3 for an interim examination. Irradiation continued in cycle 4 and cycle 5. The assembly was discharged from the reactor at the end of cycle 5 and moved to the reactor fuel storage pool.

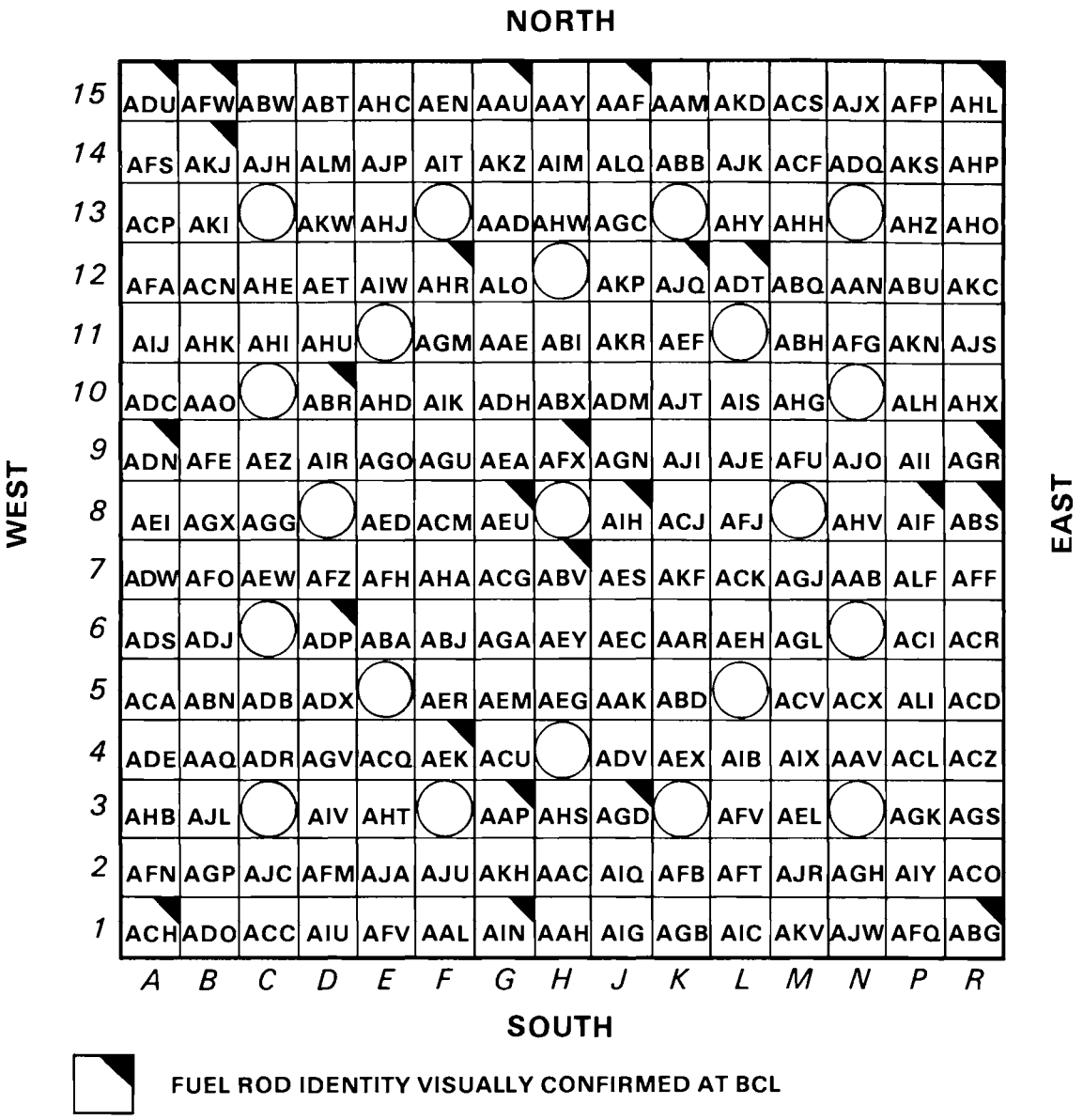

FIGURE 4. Fuel Rod Loading Diagram for S004

Assemblies G11 and H07 (see Introduction) contained fuel from batches 7 and 8, respectively. The irradiation histories of G11, H07, and S004 are summarized in Table 3 and Figure 5. Table 4 describes the S004 irradiation history in greater detail. Figure 6 shows the locations of assemblies S004, G11, and H07 during the various reactor cycles.

Figures 7 and 8 show typical beginning-of-cycle (BOC) and end-of-cycle (EOC) assembly power and end-of-cycle assembly burnup profiles for Connecticut Yankee fuel rods. Figure 9 shows depressions in the flux profiles of assemblies, as measured in Connecticut Yankee.

TABLE 3. Irradiation and Storage Histories for Connecticut Yankee Fuel Assemblies S004, G11, and H07

Assembly Number	Cladding Material	Fuel Burnup Average, MWd/MTU (GJ/kgU)	Pool Storage Time as of May 1980 (yr)	Shutdown Date
S004	304LSS	32,151 (2788)	5.0	May 18, 1975
G11	304SS	36,700 (3171)	2.6	October 15, 1977
H07	304SS	35,800 (3093)	1.3	January 27, 1979

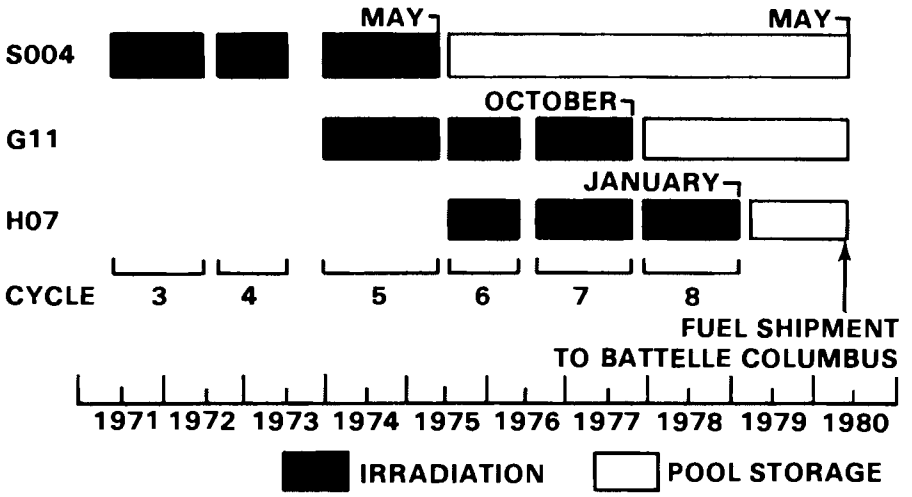

FIGURE 5. Irradiation History of Connecticut Yankee Fuel Assemblies S004, H07, and G11

TABLE 4. Connecticut Yankee (Haddam Neck) Operating Information During Cycles 3, 4, and 5

Cycle Number	Startup Date	Shutdown Date	Irradiation Time Effective Full-Power Days
3	May 21, 1971	June 15, 1972	365
4	July 8, 1972	July 18, 1973	321
5	December 14, 1973	May 18, 1975	460

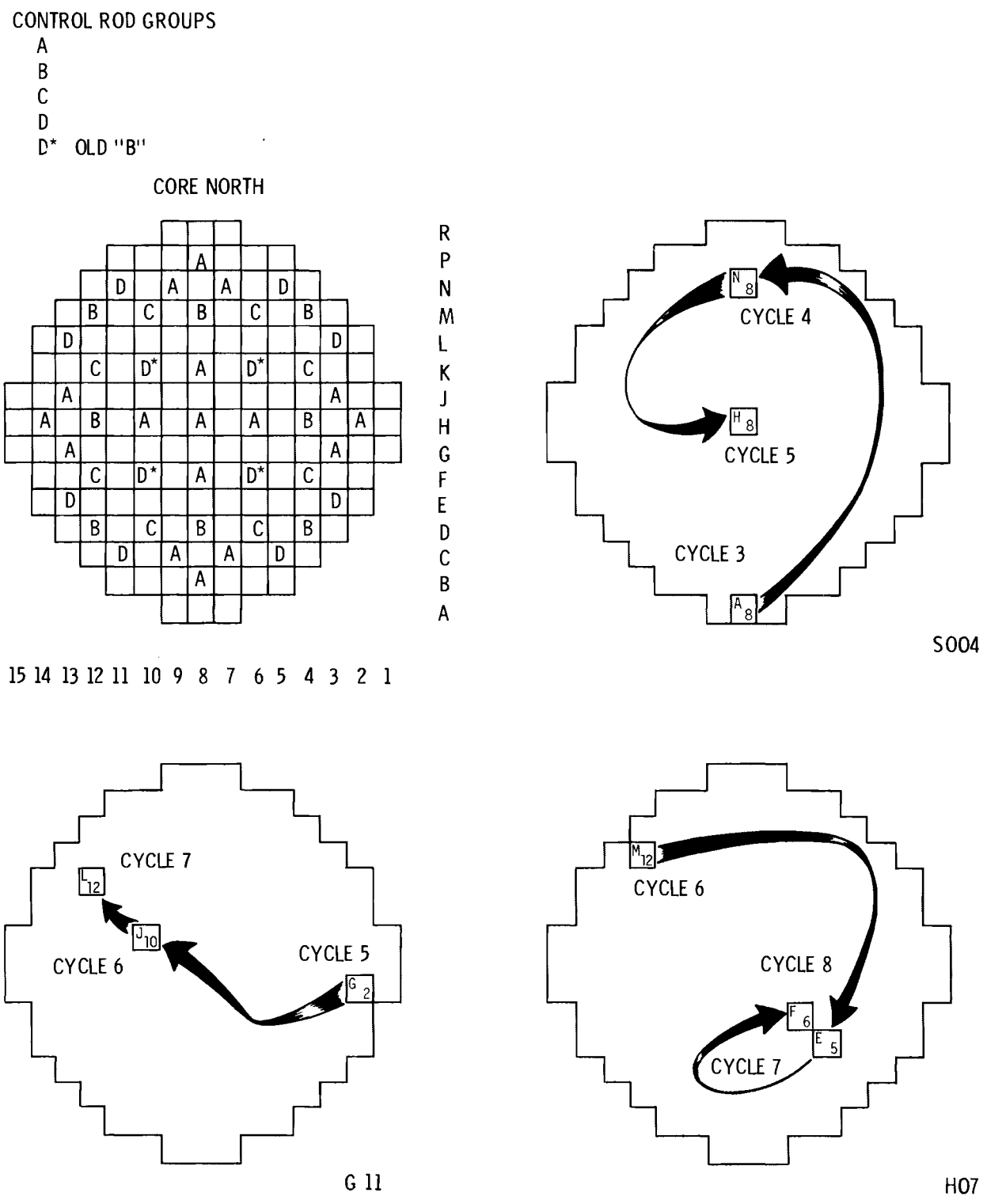

FIGURE 6. Locations of Fuel Assemblies S004, G11, and H07 in the Connecticut Yankee (Haddam Neck) Core During Irradiation

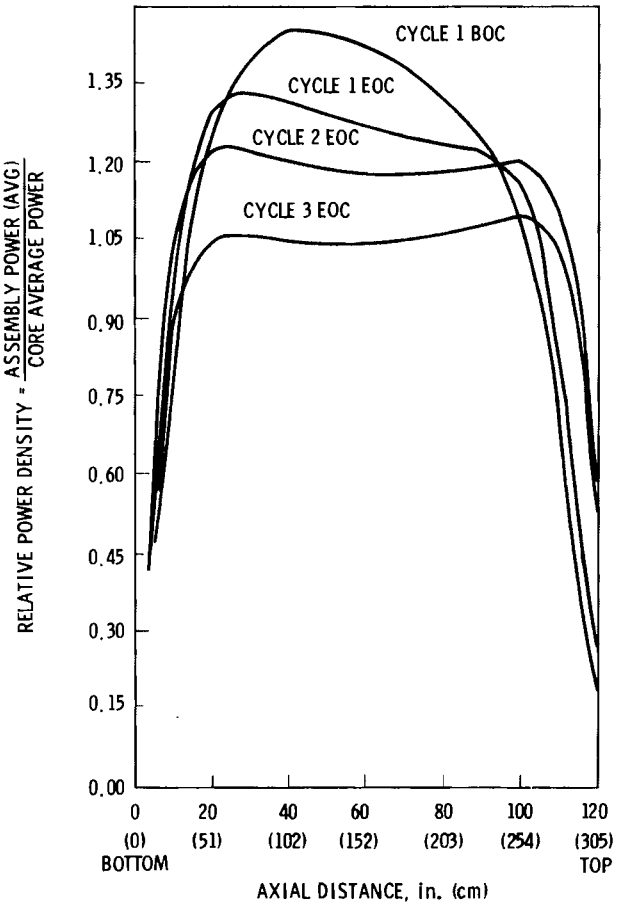

FIGURE 7. Change in the Axial Power Profile With Accumulated Fuel Burnup For a Typical PWR Fuel Assembly (BOC = Beginning of Cycle; EOC = End of Cycle).

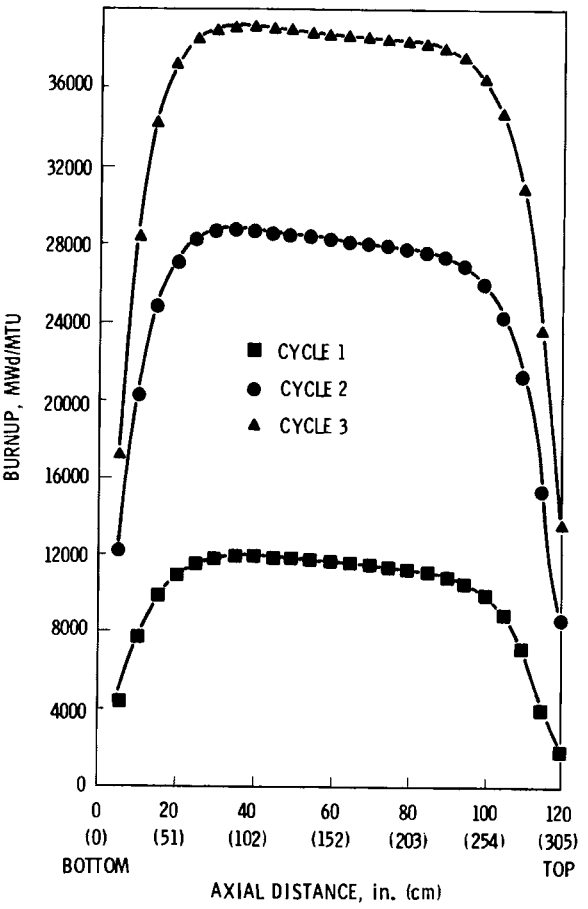

FIGURE 8. Accumulation of Fuel Burnup With Continued Irradiation for a Typical PWR Fuel Assembly

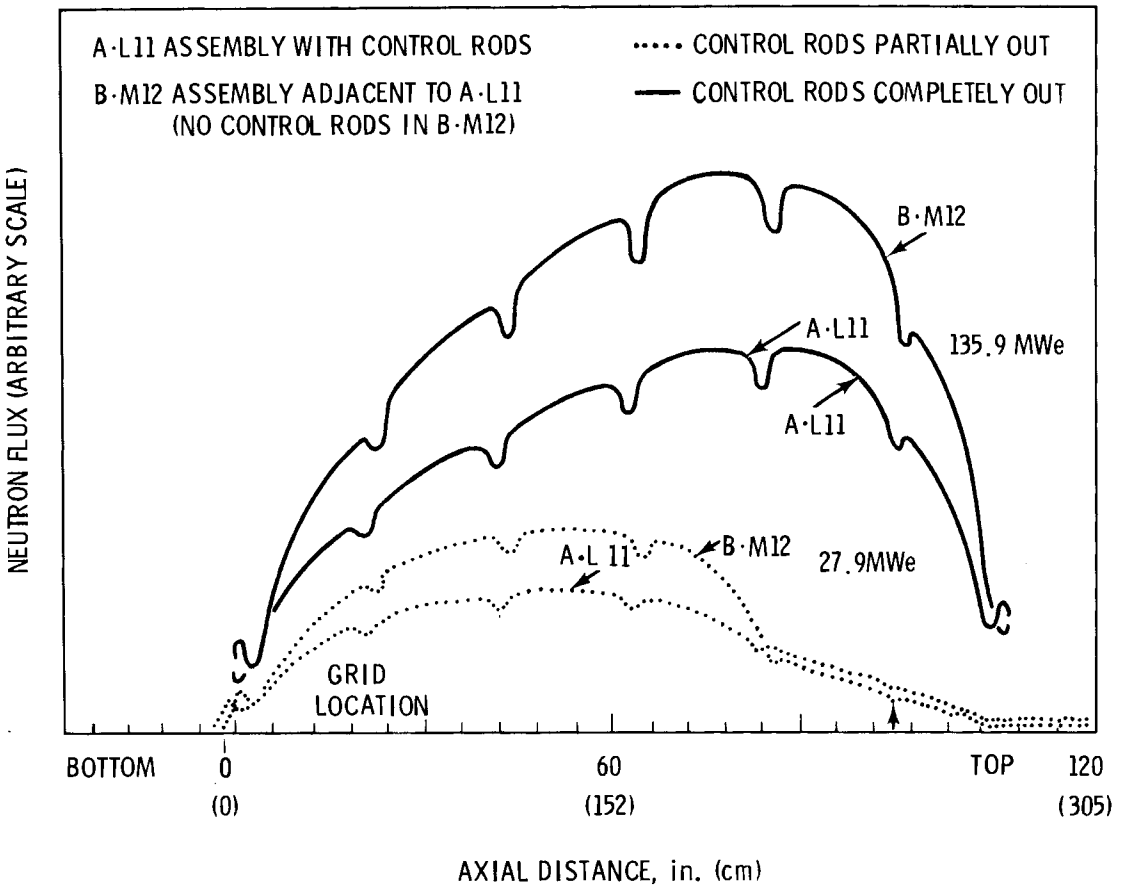

FIGURE 9. Variation in the Axial Neutron Flux Profile Along Two Fuel Assemblies in Connecticut Yankee

FUEL STORAGE, HANDLING, AND TRANSPORT

Assembly S004 was discharged at end-of-life on May 18, 1975, and placed in the reactor fuel storage pool, where it remained for 5 yr. After S004 was selected for examination as part of the Spent Fuel and Fuel Pool Component Integrity Program, it was transported to the examination site at BCL.

The shipment of S004 from Connecticut Yankee to the BCL hot-cell facility was arranged with a qualified carrier by NUSCO as part of the NUSCO/PNL agreement. The periods of pool storage for the individual assemblies are listed in Table 3. Poolside examinations were performed on the three assemblies immediately prior to shipment.

All three assemblies were shipped dry. H07 was shipped first, G11 second, and S004 last. H07 contained several fuel rods known to have failed. The cooling period after reactor discharge was 16 months for H07 compared to 60 months for S004. An increase in the activity of the pool water from 1.1×10^{-4} to 1.1×10^{-2} μCi/ml accompanied the unloading of H07 from the shipping cask in the BCL pool (Klingensmith 1980). The water activity continued at the higher level for 6 weeks. S004 was stored in the BCL pool during this time.

S004 was shipped in an air-filled cask on May 14, 1980, and arrived at the hot-cell facility at BCL on May 15. It was unloaded from the shipping cask in the BCL pool on May 16. Table 5 gives a summary of the nominal environmental conditions encountered by S004 through November 1980.

FUEL EXAMINATION

One criterion for selecting a fuel assembly was that it be well characterized. As shown in Table 6, S004 met the requirements. Because S004 was a qualification fuel assembly, BNFL developed preirradiation data on 20 fuel rods. The fuel stack lengths and stack weights were measured. The cladding diameter was measured at three equally spaced azimuthal locations at 10 axial

TABLE 5. Summary of Nominal Environmental Conditions Encountered by Fuel Assembly S004 Through November 1980

Parameter	Reactor Core (Borated Water)	Reactor Pool (Borated Water)	BCL Storage Pool (Deionized Water)
Temperature, °C	318 Outlet 290 Inlet	41	20-25
pH at 25°C	5.4-10	4.2-4.8	--
Boron, ppm	0.1-3000	2300-2500	--
Conductivity, μmho/cm	2.4-30	0.62-0.72	0.77-1.25
Time, Years	4	5	1/2

TABLE 6. Examination History of S004

Examination	Time	Location	Information
Preirradiation[a]	1971, Prior to shipment	British Nuclear Fuels Ltd., England	Fuel Stack Weight, Fuel Rod Length, Rod Diameter
Interim[b]	1972, End of Cycle 3	Poolside Connecticut Yankee Reactor	Rod Length
Discharge	1975, End of Cycle 5	Poolside, Connecticut Yankee Reactor	Visual
Preshipment[c]	1980, April/May	Poolside, Connecticut Yankee Reactor	Periscope Visual, Rod Diameter
Postirradiation	1980, July	Battelle Columbus Laboratories, Ohio	Hot-cell examination results

(a) See Table 7.
(b) See Table 8.
(c) See Table 9.

locations 30 cm (1 ft) apart, starting 30 cm (1 ft) above the bottom of each rod. Table 7 summarizes results of the BNFL measurements on the rods in the as-fabricated (i.e., preirradiation) condition.

At end of cycle 3, lengths of six fuel rods were measured in the reactor pool (see Table 8) by Gulf General Atomic. The results indicated that changes in length were negligible.

The next examination was conducted by Combustion Engineering[a] and NUSCO personnel on May 6, 1980, before the assembly was shipped to BCL (see Table 9). The assembly was examined visually with an underwater periscope in the Connecticut Yankee pool. Several other fuel assemblies from Connecticut Yankee were also examined at that time, among them G11 and H07. Some color pictures were taken with a 35 mm camera (see Figures 10 and 11 for black-and-white reproductions).

(a) Combustion Engineering, Windsor, Connecticut, was a consultant to NUSCO.

TABLE 7. Characterization of Selected S004 Fuel Rods in the As-Fabricated Condition at BNFL

Fuel Rod[a]	Rod[b] Location	Pellet Batch No.	Fuel Stack Weight (kg)	Kr Count	Rod Length (in.)[c]
ACH	A01	S26	2.264	912	126.665
ADO	B01	S22	2.265	804	126.651
AFQ	P01	S36/S27	2.260	1072	126.669
ABG	R01	S26	2.264	858	126.671
AGV	D04	S34	2.270	789	126.653
AEK	F04	S21	2.280	974	126.663
ADP	D06	S34	2.256	889	126.643
ADW	A07	S34	2.259	870	126.660
AFF	R07	S22	2.266	993	126.651
AEI	A08	S21	2.260	936	126.663
ABS	R08	S36	2.256	962	126.661
ADN	A09	S21/S22	2.271	967	126.664
AGR	R09	S27	2.264	914	126.673
ABR	D10	S34	2.272	928	126.656
AET	D12	S34/S21	2.264	952	126.669
AHR	F12	S34	2.258	959	126.657
ADU	A15	S34	2.258	967	126.659
AFW	B15	S26	2.264	932	126.667
AFP	P15	S26	2.263	897	126.662
AHL	R15	S26	2.262	851	126.679

(a) See Figures 3 and 4.
(b) See Figure 12.
(c) 126.665 in. = 321.729 cm.

TABLE 8. Fuel Rod Length Measurements for Fuel Assembly S004 After One Cycle of Irradiation

Rod	Location[a]	As-Fabricated Fuel Rod Length (in.)	Measured Length (in)	Actual Length[b] (in.)	Fuel Rod Length Increase (in.)
ACH[c]	A01	126.671[d]	126.667	126.678	0.007[e]
AIG	J01	126.673	126.667	126.678	0.005
ABG[c]	R01	126.659	126.653	126.664	0.005
ADU[c]	A15	126.665	126.655	126.666	0.001
AAY	H15	126.663	126.663	126.674	0.011
AHL[c]	R15	126.679	126.671	126.682	0.003

(a) Rod location system described in Figure 12.
(b) Measured length corrected for temperature.
(c) Fuel rods precharacterized by BNFL.
(d) 126.671 in. = 321.744 cm.
(e) 0.007 in. = 0.18 mm.

Crud patterns on S004 were similar to those on G11. S004 had several apparent anomalies (Table 9) including a fuel rod with a location that appeared to be bulged, based on underwater examination; a rod with a small elliptical black spot; and two features on a third rod that posssibly could have been cladding cracks. Also, the four corner rods in S004 were not resting on top of the lower nozzle plate. The observed anomalies are called "apparent" because none of them were observed during the subsequent detailed examination at the BCL hot-cell facility. Poolside observations of components being examined by underwater periscope are occasionally subject to optical distortions. The results of the visual inspection of S004 by periscope are given in Table 9. The convention used to describe the locations of fuel rods in the assembly and of grid spacers and rod spans between spacers is shown in Figure 12.

TABLE 9. Results of Visual Examination of Assembly S004[a] by Underwater Periscope. (This examination was performed by Combustion Engineering and took place prior to the shipment of assembly S004 to the BCL hot-cell facility.)

Fuel Assembly Face Observed	Rod	Location[b]	Span[c]	Observation
East	AHL	R15	5	Fuel rod definitely bulged.[d]
East	AGR	R09	5	Approximately 1/8-in. (3-mm) long elliptical black spot.
East	ALF	P07	6	Two apparent small cladding cracks or cracked deposits.[d]
North	AJX	N15	5	Partially decrudded elliptical surface discolorations.
West	AFA	A12	3	Partially decrudded elliptical surface discolorations.
South	--	--	-	No anomalies on this face.

(a) The four corner rods were not seated on the bottom tie plate in this assembly. At the interim inspection, measurements were made on three of the four rods to determine the force necessary to pull the rods axially.
(b) Rod location and span identified in Figure 12.
(c) Fuel assembly ID not verifiable. Face and rod location indicated assumes maintenance of core orientation in spent fuel storage.
(d) Subsequent hot-cell examinations showed this observation to be incorrect.

80H359-2

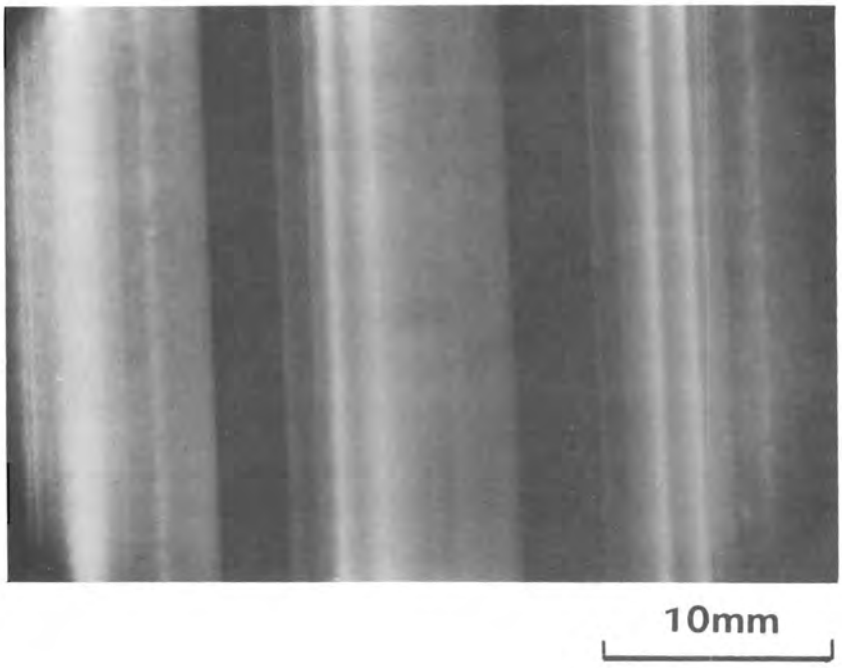

FIGURE 10a. Periscope Photograph Illustrating Typical Appearance of Fuel Rods in Assembly S004 at Connecticut Yankee During Preshipment Poolside Examination

80H359-1

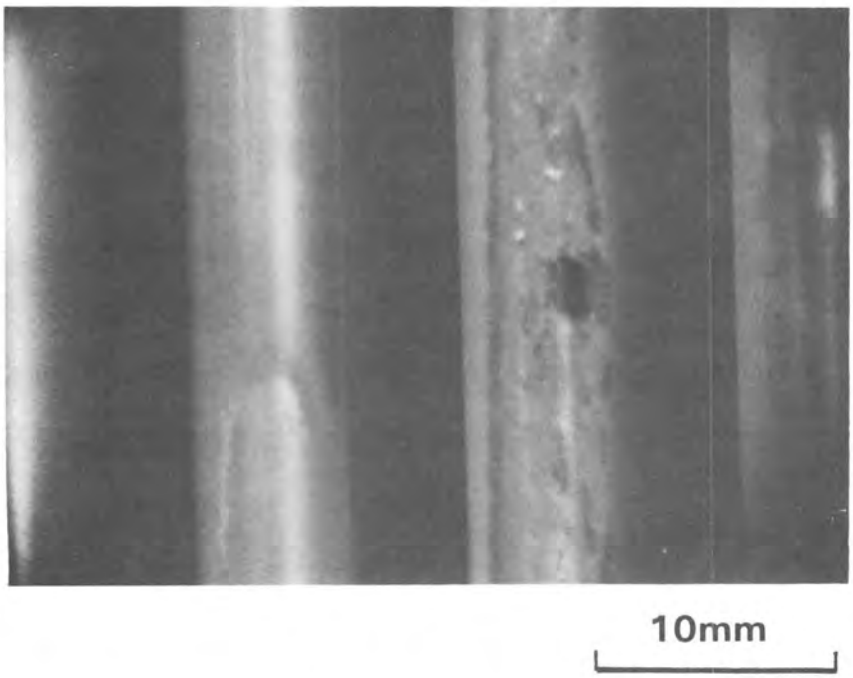

FIGURE 10b. Small Elliptical Black Spot Observed on Fuel Rod in Assembly S004 at Connecticut Yankee During Preshipment Poolside Examination (from Periscope Color Photograph)

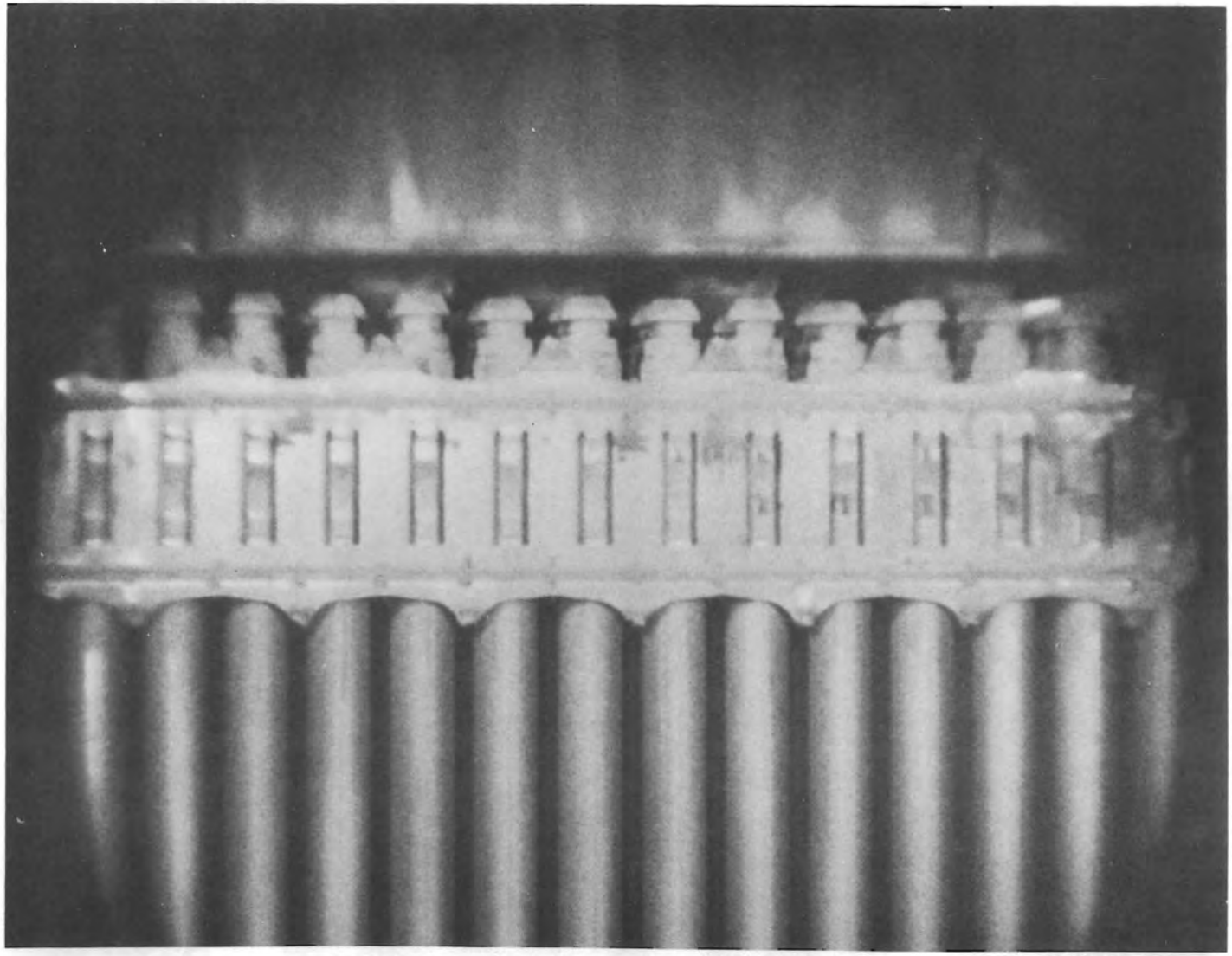

FIGURE 11a. Periscope Photograph Illustrating Typical Appearance of Fuel Rods Including Upper End Caps and Grid Spacer Near Top Nozzle in Assembly G11 at Connecticut Yankee During Preshipment Examination (South Face)

81F342-2 FROM CN R19-2

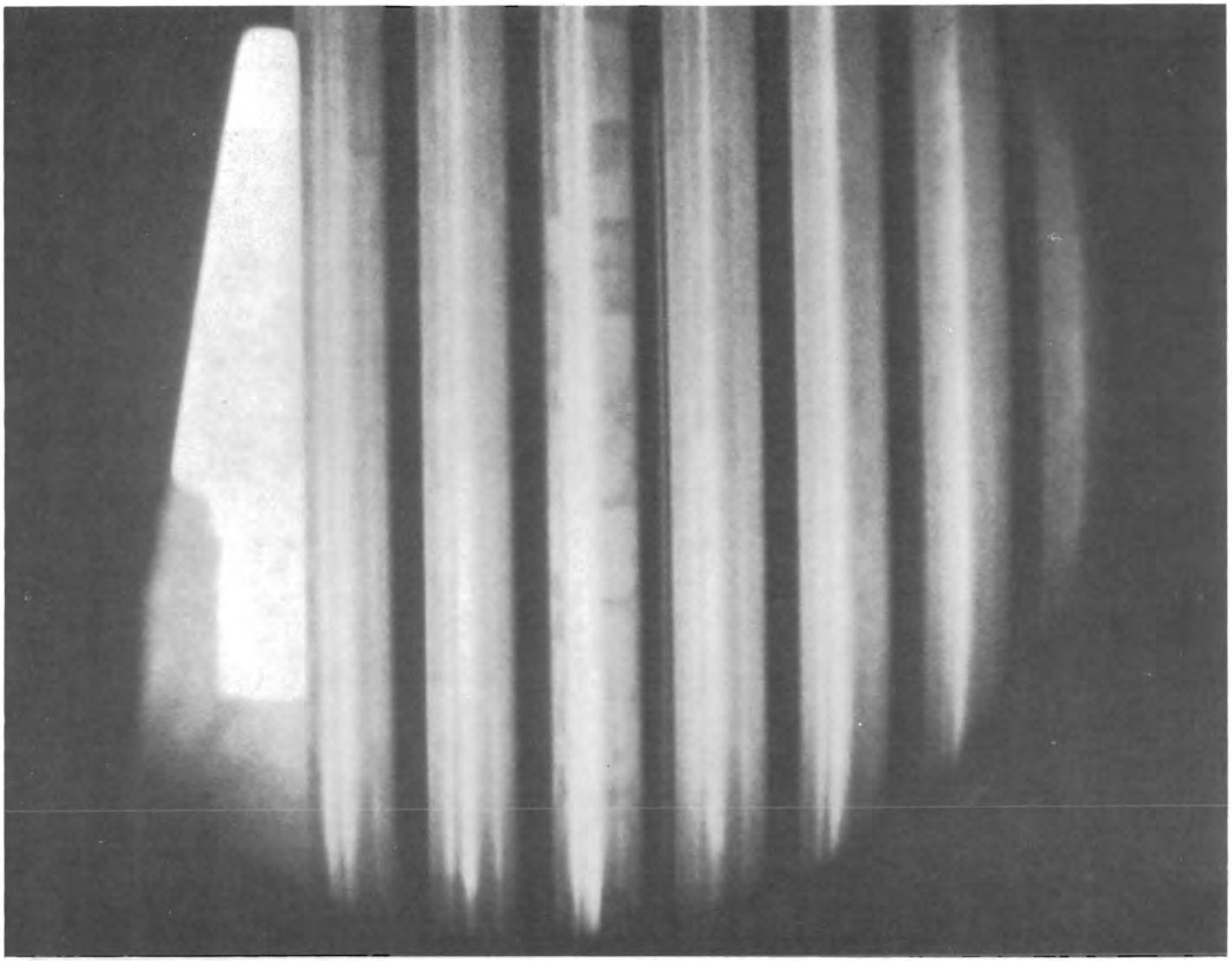

FIGURE 11b. Mottled Appearance of Rod Surface Coinciding with Pellet Interface Locations in Assembly S004 at Connecticut Yankee During Preshipment Examination (Span 5, West Face)

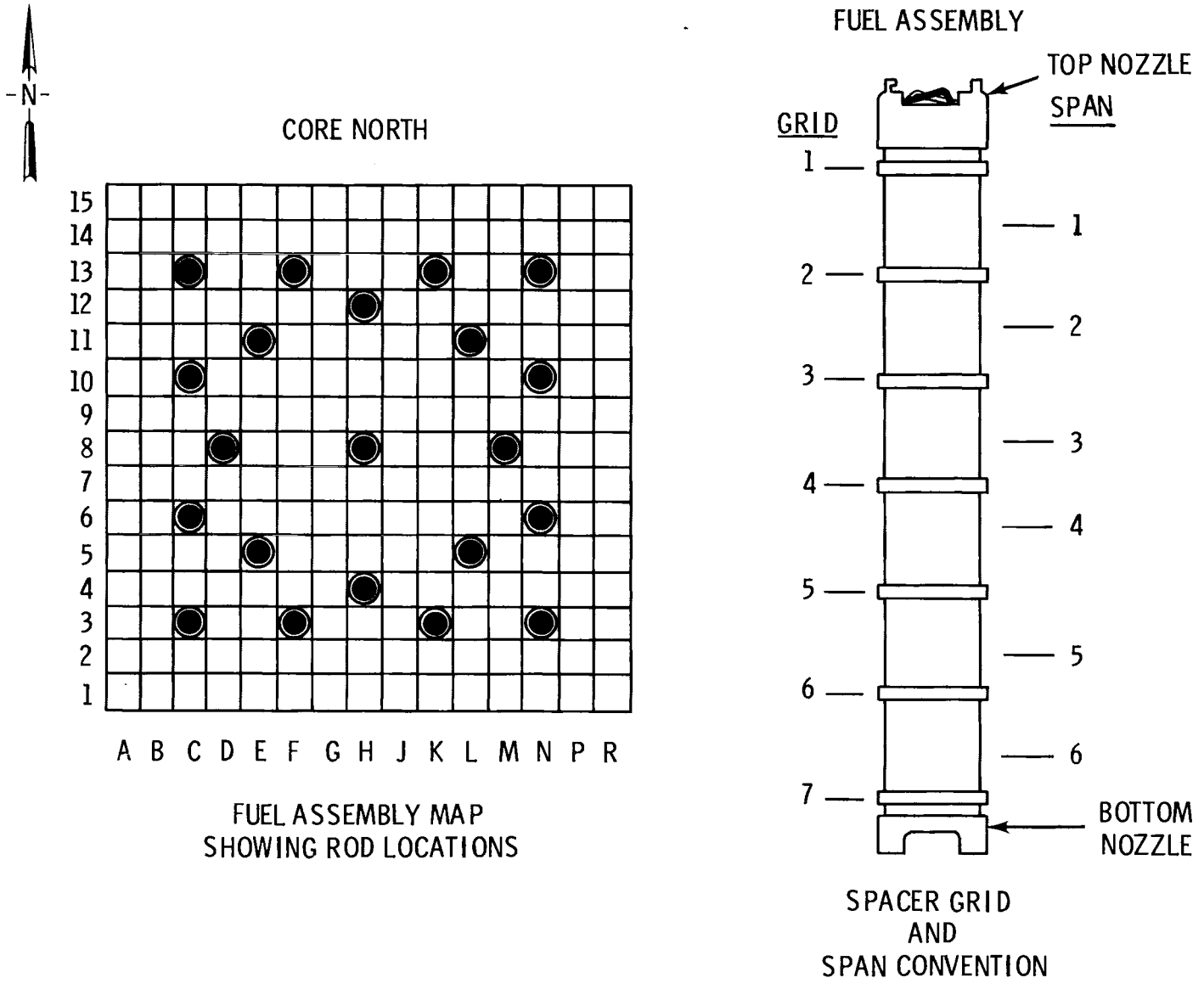

FIGURE 12. Convention Used in This Report To Describe Fuel Rod Locations in the Assembly and Axial Locations of Spacer Grids and Spans

FUEL CHARACTERIZATION RESULTS

Fuel characterization, as used in this report, refers to establishing the present condition of the fuel so that the effects of irradiation and initial pool storage can be determined. Furthermore, by providing a reference condition, significant changes, if they were to occur during subsequent extended pool storage, could be detected. For the S004 examination, both nondestructive and destructive tests were made to determine selected chemical, physical, and mechanical parameters.

Nondestructive examinations were performed on the fuel assembly and also on individual fuel rods. Fuel assembly inspection techniques included sipping (for detecting breached fuel rod cladding within the assembly) and visual examination. Fuel rod inspection techniques included visual examination, profilometry, gamma scanning, eddy current testing, and temperature measurement. The specific examinations performed are shown in Table 10.

TABLE 10. Summary of Nondestructive Examinations Completed on Fuel Rods Removed From Fuel Assembly S004

Rod	Location in Assembly(a)	Profile Spiral	Profile Linear	Videotape Visual	Eddy Current	Gamma Scan (Gross)	Gamma Scan (^{137}Cs)	Rod Weight
AHL	R15	X	–	X	X	X	X	X
AGR	R09	–	–	X	–	–	–	X
ALF	P07	–	–	X	–	–	–	X
ABG	R01	X	–	X	–	X	X	X
AEK	F04	X	–	X	X	–	X	X
AAP	G03	–	–	X	X	–	–	X
AHR	F12	X	X	X	X	–	X	X
AJQ	K12	X	–	X	X	–	X	–

(a) See Figure 12 for location convention.

Destructive examinations were performed on individual fuel rods and included fission gas collection and analysis, void volume determination, rod marking and sectioning, metallographic examination of the fuel and cladding, burnup analysis, autoradiography, fuel density determinations, and cladding mechanical property testing. The specific examinations and specimen locations are listed in Table 11 and are shown in Figure 13.

NONDESTRUCTIVE EXAMINATIONS OF FUEL ASSEMBLY

The SOO4 fuel assembly was examined to determine whether any change in assembly condition had occurred between the poolside visual examination at Connecticut Yankee and the visual examination at BCL.

Sipping Test

When the fuel assembly arrived at BCL on May 15, 1980, the shipping cask underwent a wet sipping test (see Table 12) prior to removal of the fuel assembly. The test results indicated that the fuel rods had not released fission products during shipping. The cask and fuel were transferred to the BCL fuel pool on May 16, and the fuel assembly was removed from the cask.

TABLE 11. Spent Fuel Destructive Examination Plan

	Examination							
Rod	(a)	(b)	(c)	(d)	(e)	(f)	(g)	(h)
AHR	X	X	X	X	X	X	X	X
ABG	X	X						
ADT	X							
AGD	X							

(a) Rod puncture and gas collection, void volume determination, and gas analysis
(b) Fuel and cladding preparation and photomicrography (transverse)
(c) Autoradiography (alpha and beta-gamma)
(d) Fuel burnup analysis
(e) Fuel density measurements
(f) Tensile tests
(g) Ring crush tests (side-pressing)
(h) Cladding-to-end cap weld metallography (longitudinal sections)

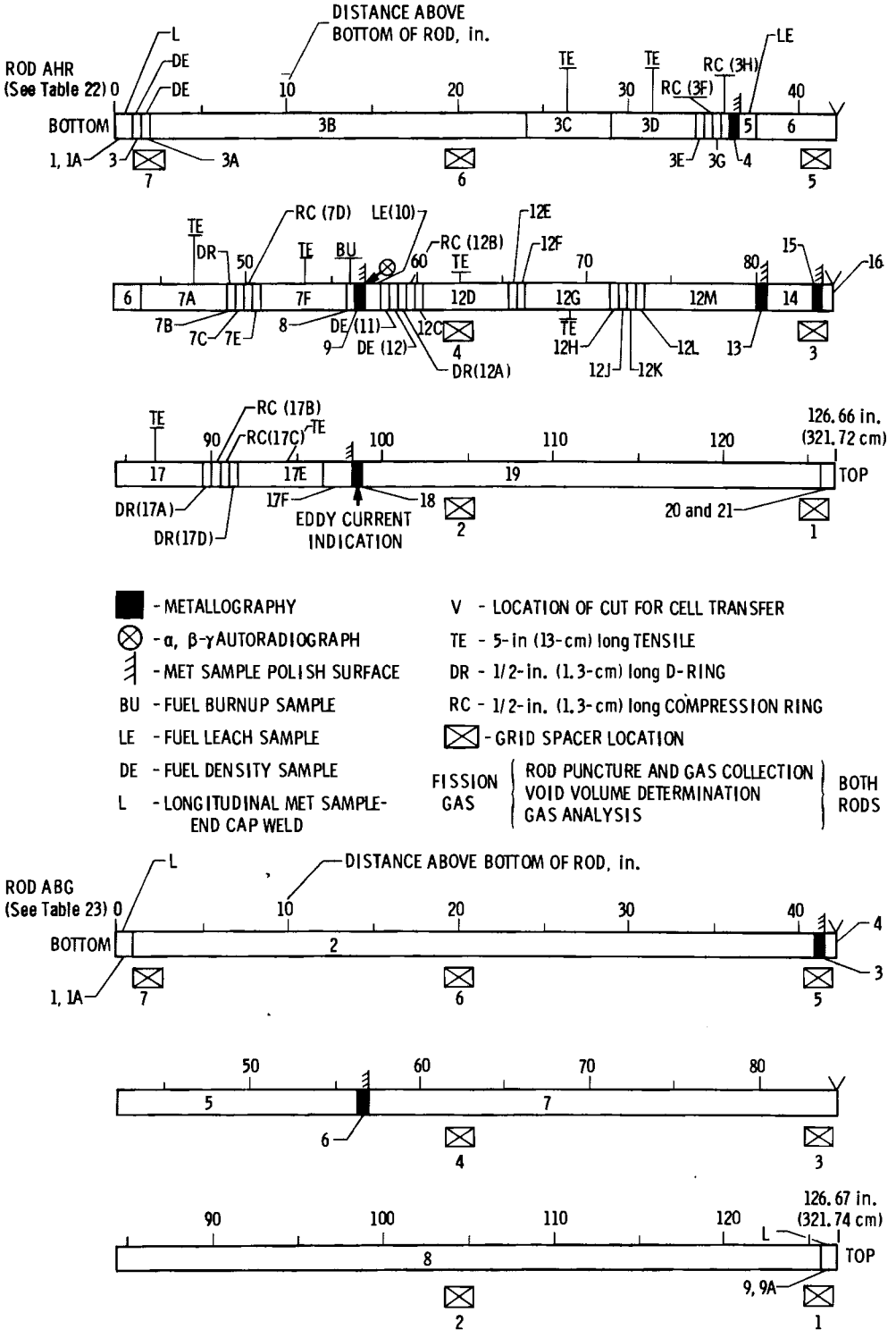

FIGURE 13. Specific Destructive Examinations and Specimen Locations

TABLE 12. Results from Wet Sipping Test of Shipping Cask at BCL Before Assembly S004 Was Removed. (The test involves gamma ray isotopic analysis.)

Sample (Date)	Radioactivity, μCi/ml		
	Cesium-137	Cesium-134	Cobalt-60
First Flush (5/15/80)	5.8×10^{-3}	3.0×10^{-3}	5.4×10^{-1}
1-hr Soak (5/15/80)	1.2×10^{-3}	4.2×10^{-4}	9.1×10^{-2}
Overnight Soak (5/16/80)	7.4×10^{-4}	6.1×10^{-4}	7.9×10^{-2}

The BCL Hot Laboratory sipping procedure for spent fuel shipping casks consists of first flushing the cask with water and then letting water stand in the cask. Samples are collected: a) immediately after flushing, b) after standing 1 hr, and c) after standing 24 hr. The concentration of radioactive material in each sample is then measured.

The cask was back-filled with demineralized water and flushed for 10 to 15 min. A sample was taken to establish a value for background radiation. A value of 5.8×10^{-3} μCi/ml of ^{137}Cs was measured. The water was left in the cask for 1 hr and then a second sample was taken. The ^{137}Cs activity decreased to 1.2×10^{-3} μCi/ml. A third sample was taken after a soak time of approximately 24 hr. The ^{137}Cs activity continued to decrease to 7.4×10^{-4} μCi/ml. A decrease in the ^{137}Cs activity level in the cask with time indicated that none of the fuel rods in the assembly were leaking fission products.

Visual Examination

The fuel assembly was visually examined in the BCL pool with a videotape system. The fuel rods appeared clean. There was no obvious assembly distortion. The system image was of limited clarity and none of the anomalies of the previous periscope examination were observed. Further discussion of the anomalies follows in the section on fuel rod visual examinations.

The top nozzle (Figures 14 and 15) of the fuel assembly was visually examined in air prior to removal from the assembly. Some orange-colored spots were observed near the tops of some of the guide tubes. The top nozzle was removed by drilling out the guide tube-to-nozzle welds on four guide tubes and cutting

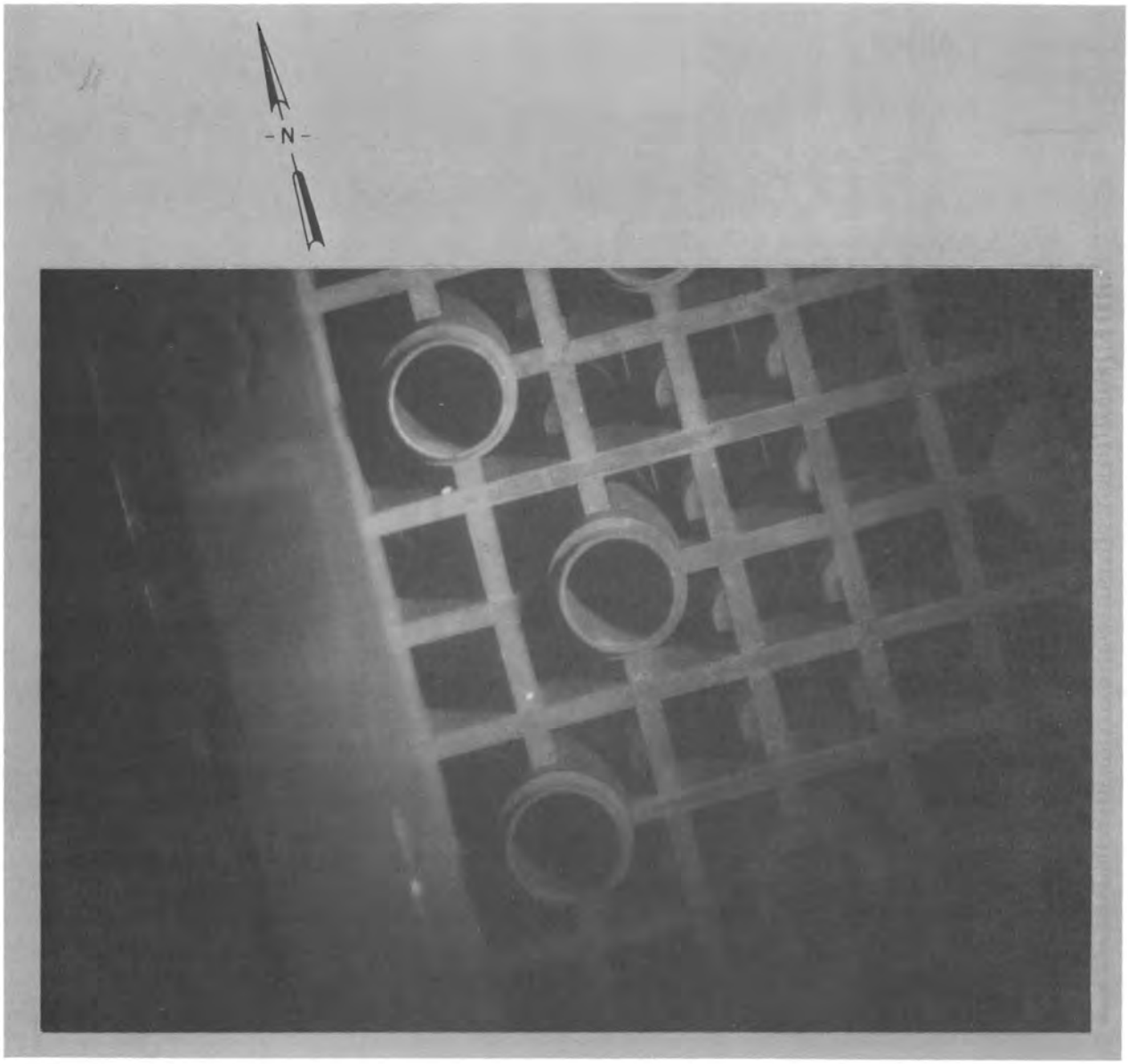

FIGURE 14. Inner Portion of the Top Nozzle Plate of SO04 Showing Nozzle Grid, Upper Thimble Tube Welds, and Fuel Rod Upper End Caps (from periscope color photograph taken during visual examination at the BCL hot-cell facility)

off the other guide tubes just below the nozzle. Eight fuel rods were removed for nondestructive examination; four of the eight were selected for destructive examination (see Tables 10 and 11). The criteria for selection were the presence of anomalies in the previous visual examination and a high calculated fuel burnup. For fuel rods in SO04, high burnup was 2978 GJ/kgU (34,470 MWd/MTU); low burnup was 2139 GJ/kgU (24,750 MWd/MTU).

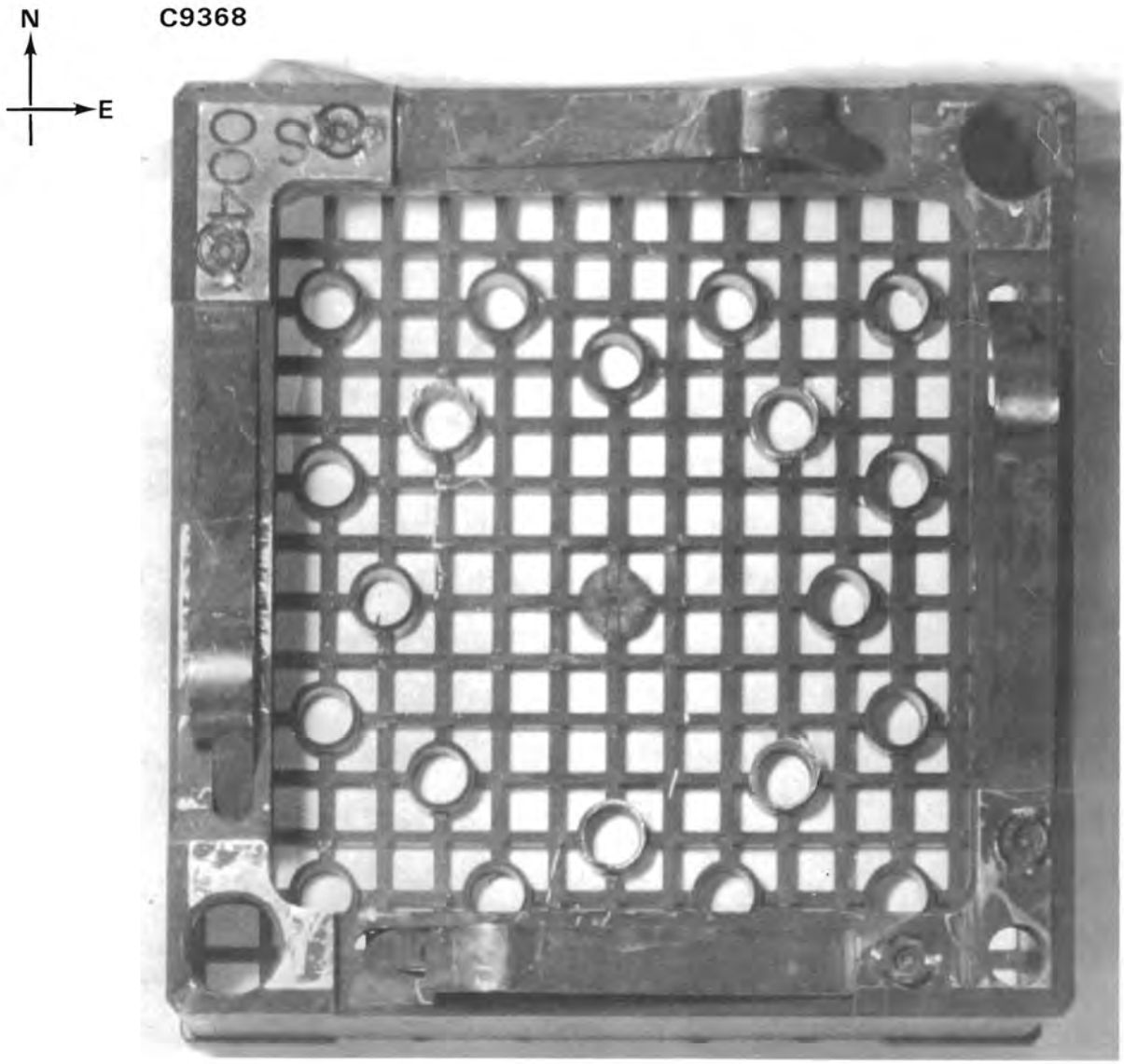

FIGURE 15a. Top View of Top Nozzle

NONDESTRUCTIVE EXAMINATIONS OF FUEL RODS

Fuel rods selected to characterize the S004 assembly were nondestructively examined to establish a baseline for subsequent examinations during extended pool storage.

Visual Examination

Some fuel rods had dull reddish surfaces, which is indicative of an oxide film or a crud layer (see Figure 10). Later metallurgical examinations

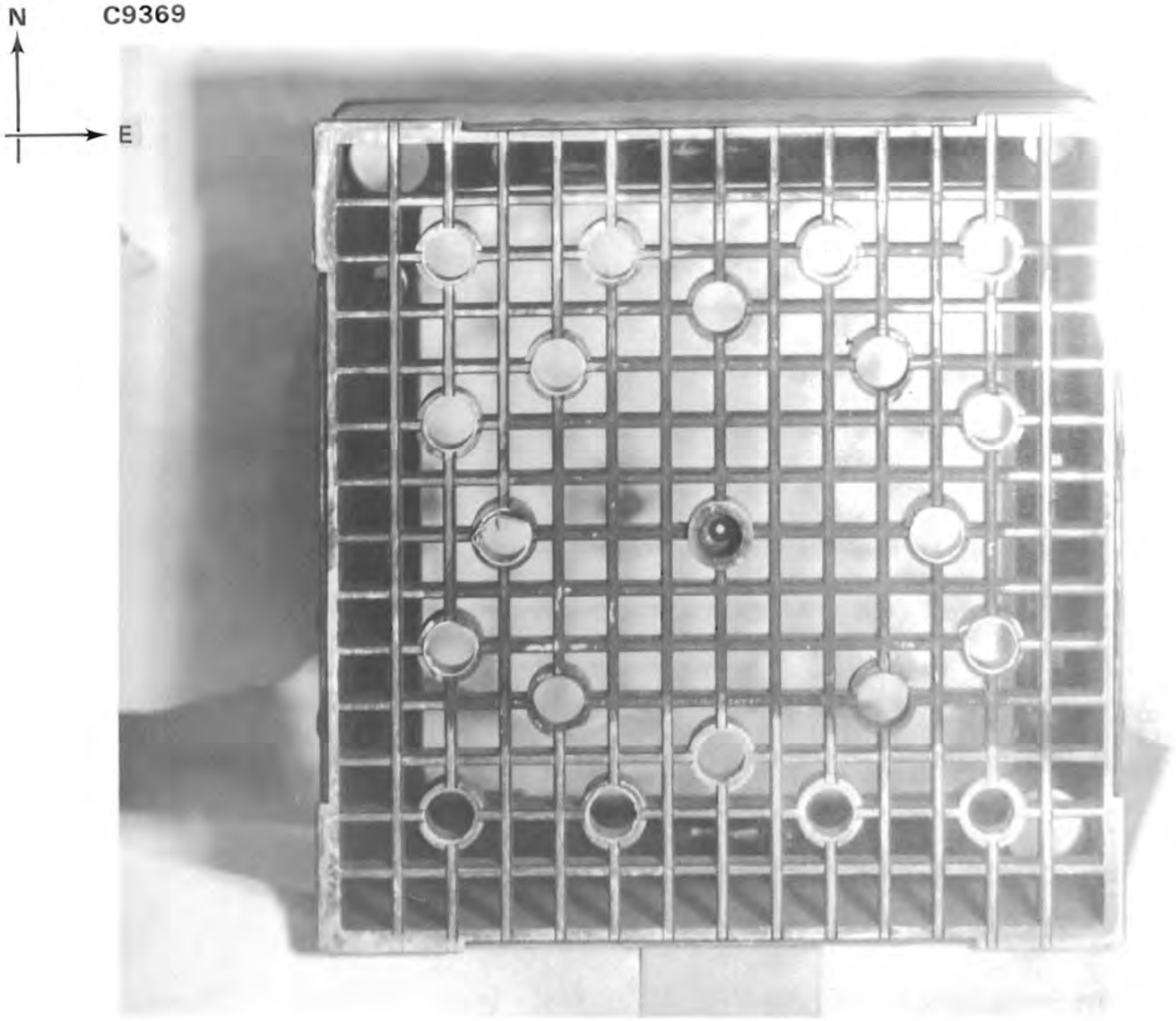

FIGURE 15b. Bottom View of Top Nozzle

indicated that surface deposits were very thin. The fuel rod end cap welds showed no indication of exterior corrosion either in the visual examinations (Figure 16) or in the metallographic examinations (Figure 17). Axial scratches, attributed to abrasion at spacer contacts, were observed when the fuel rods were inserted into or removed from the assembly, and some shallow indentations at cladding-grid spacer spring contact were noted (see Figures 16 and 18). None of the anomalies observed during the underwater periscope examination were discernible. The fuel rods were dry during the visual

HC8499

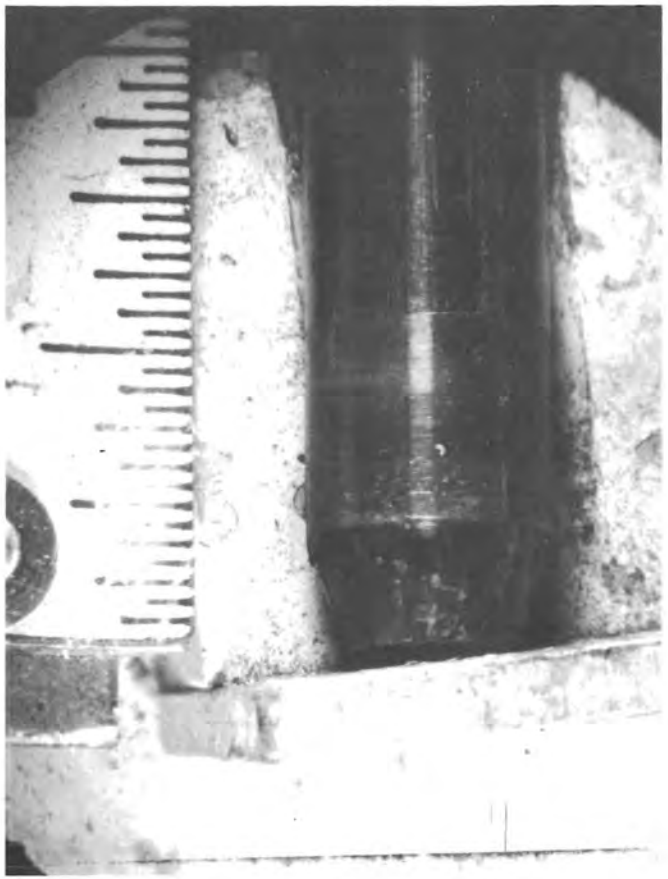

(a) Upper

HC8485

(b) Lower

FIGURE 16. Upper and Lower End Caps and End Cap Weld Areas from S004 Fuel Rods Showing the Machined Area at the Lower End Cap and Handling Marks

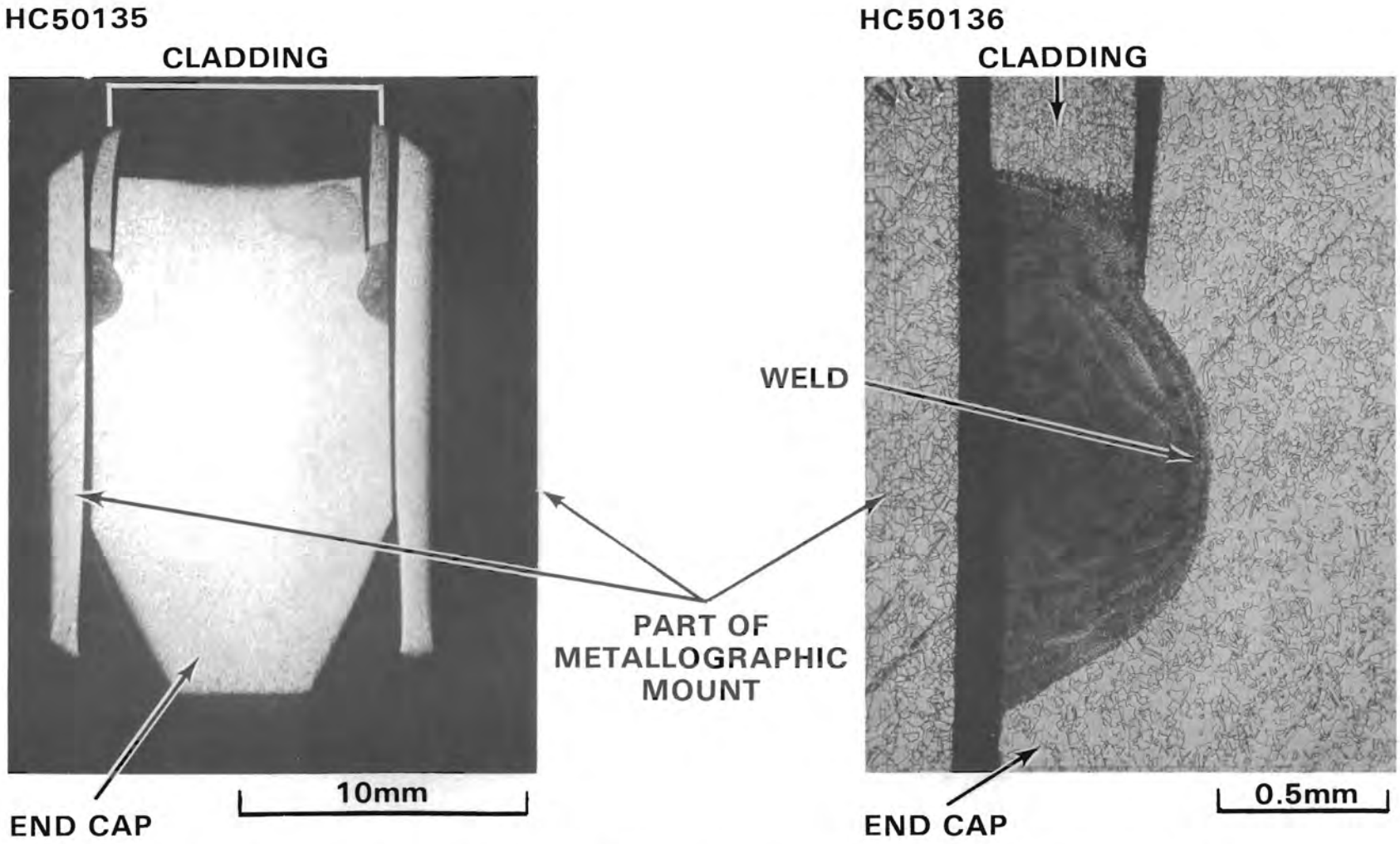

FIGURE 17. Metallography of Longitudinal Section of Lower End Cap Weld from a Stainless Steel-Clad Fuel Rod from S004

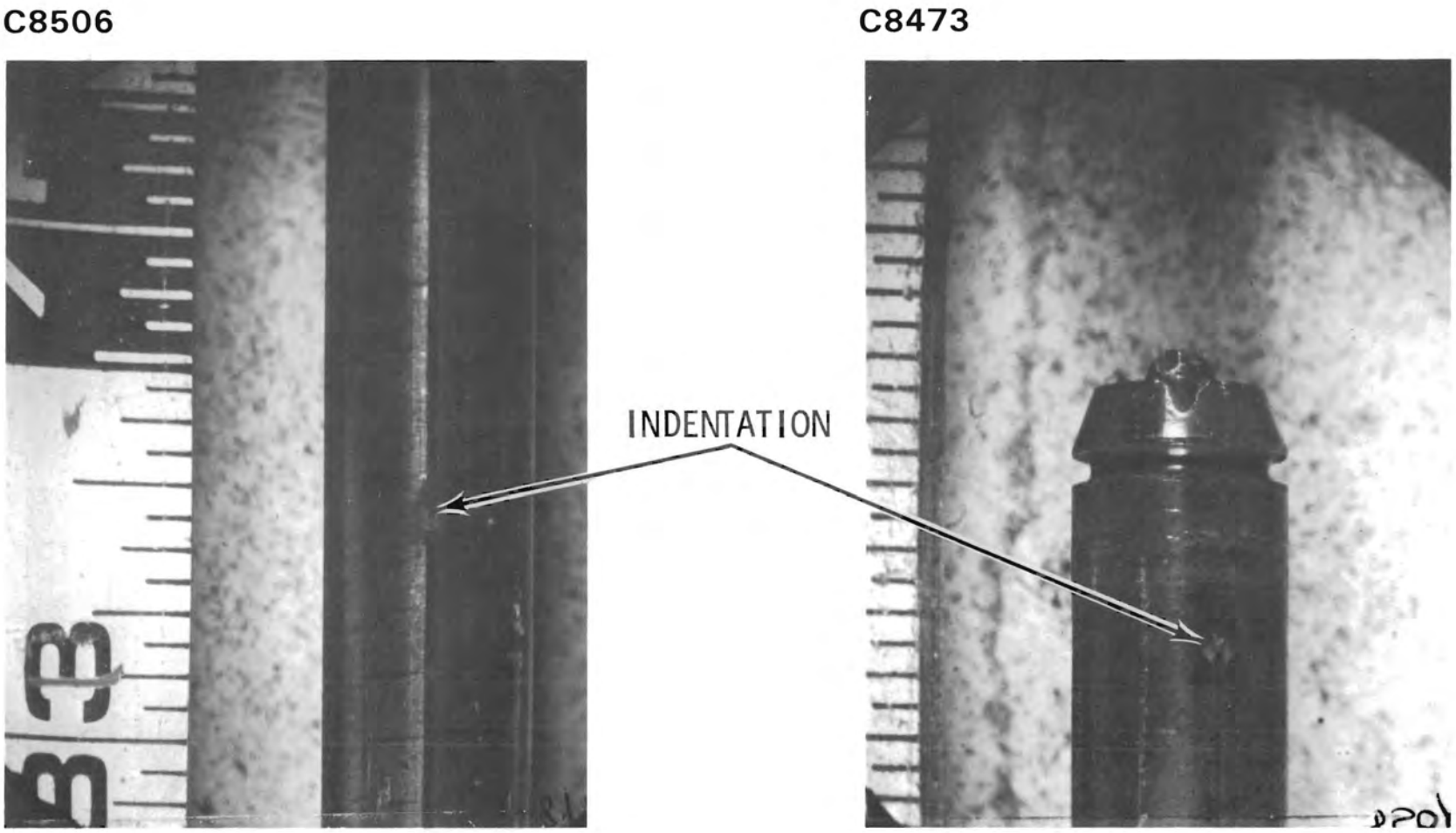

FIGURE 18. Shallow Indentation on Cladding at Grid Spacer Contact Point That was Observed During Visual Examination

examination. Possibly, drying of the cladding surface altered the appearance of stains that were evident under wet conditions. If the black spot was a crud deposit, it may have spalled from the surface when the cladding warmed during transport. If the black spot was a hole that was 1/8 in. (3 mm) in diameter, it would have been seen during visual examination. No defects were observed in either this rod or the other seven visually examined rods.

Videotapes (black and white) showed dull areas, which ranged from gray to black on the otherwise shiny cladding surface. Several rods were shiny at grid spacer locations. Rod AGR was a particularly striking example where the cladding appeared shiny under grid spacers, became duller moving up the rod, and became dark as each grid spacer was approached. This phenomenon was most apparent between the 106.7 cm (42 in.) location and the upper end cap. A similar phenomenon (Figure 19) was observed in an EPRI review of waterside corrosion behavior of PWR, Zircaloy-clad fuel rods (Garzarolli et al. 1980). In this case, the thickness of an oxide layer was changing in the same manner as the apparent, albeit much thinner, layer on the stainless-clad S004 rod. Further discussion of cladding surface layers appears in the section on metallography.

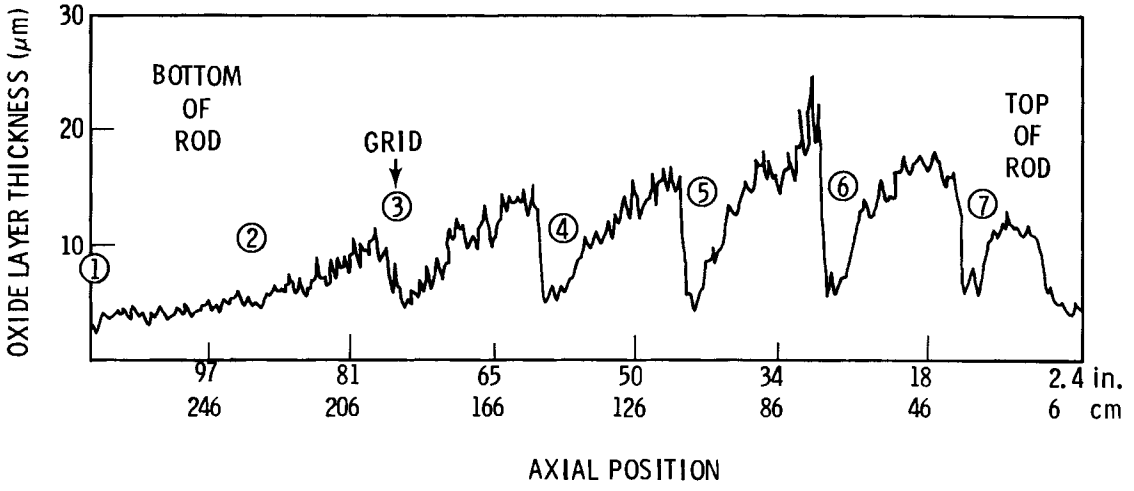

FIGURE 19. Oxide Layer Thickness Trace (from Garzarolli et al. 1980) Similar to the Change in Appearance in the Axial Direction Along S004 Fuel Rod AGR

Rod Weights

Fuel rod weights were measured to establish a basis of comparison for measurements taken during later examinations. Water ingress during operation or storage might have been suggested if measurements had shown a weight increase. No significant increase in rod weight occurred in the precharacterized rods that were measured.

Rod weights were measured at BCL with an 11.35-kg (25-lb) load cell and a Model 1200 strain indicator. Instrument zero and calibration were checked after each rod weighing. Table 13 summarizes the results of the rod weighings.

Five of the eight rods weighed at BCL were precharacterized by BNFL. During the precharacterization, the fuel stack weights were recorded but not the total fabricated rod weight. Consequently, a direct comparison of the weights from the precharacterization with the weights from BCL cannot be made. However, a statistical analysis can be used to indirectly compare the weights. Table 14 summarizes the fuel rod weight statistics for the S004 rods.

TABLE 13. Fuel Rod Weight Data for Assembly S004

Rod Designation	Rod Location	Rod Weight[a] Total (g)	Fuel Stack[b] Weight (g)	Rod Weight Fuel Weight (g)
AHL(c)	R15	2660.0	2262.0	398.0
AGR(c)	R09	2660.0	2264.0	396.0
ALF	P07	2663.0	--	--
ABG(c)	R01	2665.0	2264.0	401.0
AHR(c)	F12	2660.0	2258.0	402.0
AJQ	K12	2665.0	--	--
AEK(c)	F04	2685.0	2280.0	405.0
AAP	G03	2660.0	--	--

(a) Measured at BCL.
(b) Measured at BNFL.
(c) Rods precharacterized at BNFL.

TABLE 14. Fuel Rod Weight Statistics for Assembly S004

	Number of Rods	Average		Standard Deviation, One Sigma	
		Include AEK	Exclude AEK	Include AEK	Exclude AEK
Rod Weight[a]	8	2665.0		8.5	
	7		2662.0		2.4
Rod Weight[b]	5	2666.0		10.8	
	4		2661.0		2.5
Fuel Stack Weight[b]	5	2266.0		8.4	
	4		2662.0		2.8
(BCL-BNFL) Weight[b]	5	400.0		3.5	
	4		399.0		2.8
Stack Weight Fabrication Specification			2264.0		6.0

(a) Rods AHL, AGR, ALF, ABG, AHR, AJQ, AEK, and AAP (see Table 13).
(b) Rods AHL, AGR, ABG, AHR, and AEK (see Table 13).

Possible contributors to rod weight change other than water ingress were considered. For example, corrosion could contribute from 4 to 10 g of weight loss for these rods using calculated values based on corrosion rates of 10 g/dm^2-mo and 26 g/dm^2-mo for 304 stainless steel in a high-temperature irradiation environment typical of a PWR (Johnson 1975). The weight loss/gain occurring in the storage pool would be less because of the lower temperatures involved.

A statistical approach can be used to develop a statement on the occurrence of a significant weight change (i.e., the weight increase expected in the case of a breached fuel rod that had become waterlogged). For instance, Rod AEK is significantly heavier than the average weight of the other rods (i.e., 2685 cf 2662 g, a difference of 23 g, which is equivalent to the weight of 23 cm^3 of water). The measured void volume of rods from S004 is about 22 cm^3. But does a rod weight of 2685 g constitute a weight gain? The standard deviations for the rod and fuel stack weights were comparable, which implied that the variation in weights measured at BCL and BNFL were comparable.

An assumption made at this point is that whatever weight changes occur in sound rods occur uniformly in each rod. To look at those changes, the difference between the rod and fuel stack weights was determined, as well as the average and standard deviation of those values. The one-sigma value was 3.5 g, a number probably consistent with the normal variation in hardware weight for these rods. The rods were relatively clean; oxide, crud, and other debris did not contribute significantly to the measured weights.

The standard deviations were again calculated for rod and fuel stack weights and for the rod and stack weight difference excluding the weights for rod AEK. These values are all comparable at about 3 g, which compares well with the 3.5 g standard deviation originally calculated for the value of the difference between rod and fuel stack weights. The weight data indicate that whatever weight changes did occur were uniform from rod to rod. Based on the other results from this examination, these weight measurements support the contention that there has been no cladding breach followed by water ingress in these rods. The total rod weights now recorded will make evaluation of future rod weight measurements more straightforward.

The weight change of rod AEK is greater ($\sim$2 g) than the standard deviation determined for the other rods. In lieu of additional hardware or as-fabricated rod weight information, the rods weighed do not appear to have significantly changed in weight.

Profilometry Measurements

Spiral profilometry traces were made on the outside surface of each fuel rod to characterize diameter changes that occurred during irradiation. No extraordinary features were observed in the rod profilometry traces. Profilometry can also detect significant localized cladding anomalies such as ovality and ridging. Linear (axial) profilometry traces were made in cases where additional dimensional detail was required.

Before and after profiling the rods, the system was calibrated with the BCL No. 4 Profilometry Standard which contains the following diameters: 0.413140, 0.418120, 0.422180, 0.426110 and 0.431070 $\pm$0.000025 in. The standard was measured in the BCL Standards Laboratory against a standard traceable to the National Bureau of Standards.

The mean diameter in any given rod segment is defined as the average of the maximum and minimum diameter at any axial location along the rod. Rod ovality is defined as the difference between the maximum and minimum rod diameter at a given axial location. A drive pitch of 1/8 in. per revolution was used for the measurements. The accuracy and precision of diametral measurements was ±0.0002 in. (0.0005 cm) at the 95% confidence level. The system is capable of determining the axial rod location to within ±1/16 in. (1.6 mm). The rods were rotated at a lower than normal speed during spiral profilometry because the recorder response was not rapid enough to follow the change in rod diameter at the normal speed (i.e., because of the high cladding ovality).

Spiral profilometry was completed on the lower 40 in. (102 cm) of the corner rods ADU and ACH after full length traces on ABG and AHL failed to show any features that could be correlated with the "bulge" observed in the preshipment visual examination (Figure 20). Strong node-like areas did occur in the fifth span area in the trace from ADU (see Figure 12 for span location). Generally, the traces for these rods were characteristic of the spiral profilometry typical of rods from S004.

Spiral profilometry results from assembly S004 rods indicated that cladding ovality was typically 0.30 to 0.36 mm (12 to 14 mils) in the upper and lower regions of the rods, ranging to a maximum of about 0.46 mm (18 mils).[(a)] Ovality was less in the center region of the rods. Cladding creep-down was up to 0.025 mm (1 mil) on the lower burnup rod and up to 0.038 mm (1-1/2 mil) on the high burnup rod (Figure 21). Most of the creep-down occurred in the upper half of the rods. No obvious indications of cladding defects were observed in any of the profilometry traces.

Linear (axial) profilometry traces were run at 0°, 45°, 90°, and 135° orientations on the high burnup rod (AHR) in the region of the eddy current indication and in the 0° orientation over the full rod length. Helical variations

---

(a) This is in sharp contrast to the ovality noted in fuel rods from assemblies G11 and H07 (Pasupathi and Klingensmith 1981). In G11 and H07 rods, the ovality was rather low (less than 0.10 mm or 0.004 in.). The nominal diametral gap (i.e., cladding ID minus pellet diameter) for S004, G11, and H07 fuel rods was 0.14 mm (0.0055 in.). S004 fuel densified about the same amount as G11 fuel but swelled at a lower rate.

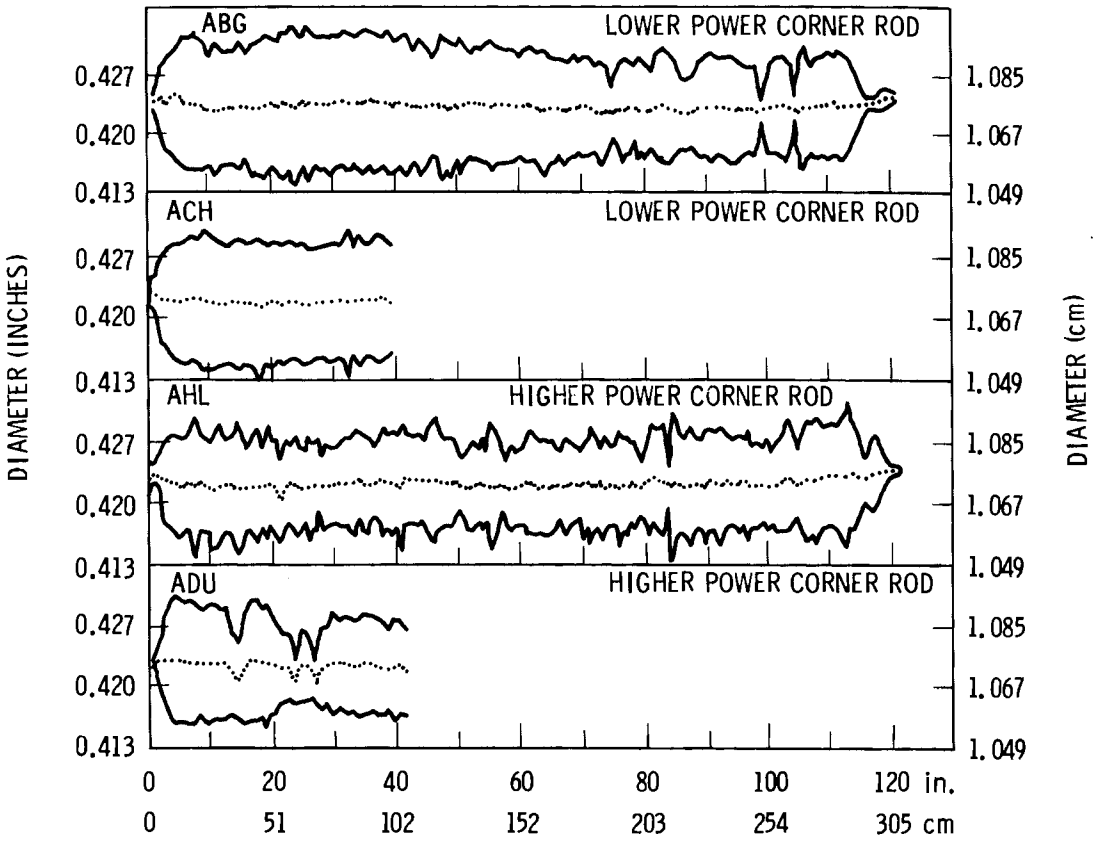

FIGURE 20. Spiral Profilometry Data for Corner Rods ABG, ACH, AHL, and ADU from Assembly S004 Showing the Envelope of Maximum and Minimum Cladding Diameters Along the Rod Axis. (Only the bottom portions of Rods ACH and ADU were measured. Note similarity of profiles of rods from symmetrical power/burnup positions within the assembly, i.e., ABG/ACH and AHL/ADU.)

in the cladding ovality were observed when comparing the traces of the spiral and linear profilometry scans for rod AHR in the fourth span (Figure 22). The change in orientation of the cladding ovality over the length of the rod is difficult to determine from the spiral profilometry without the corresponding linear trace.

The "bulge" suggested in the poolside examination now appears to have been an optical illusion. The impression of a bulge in the cladding could result if a cladding section with high ovality disposed helically along the

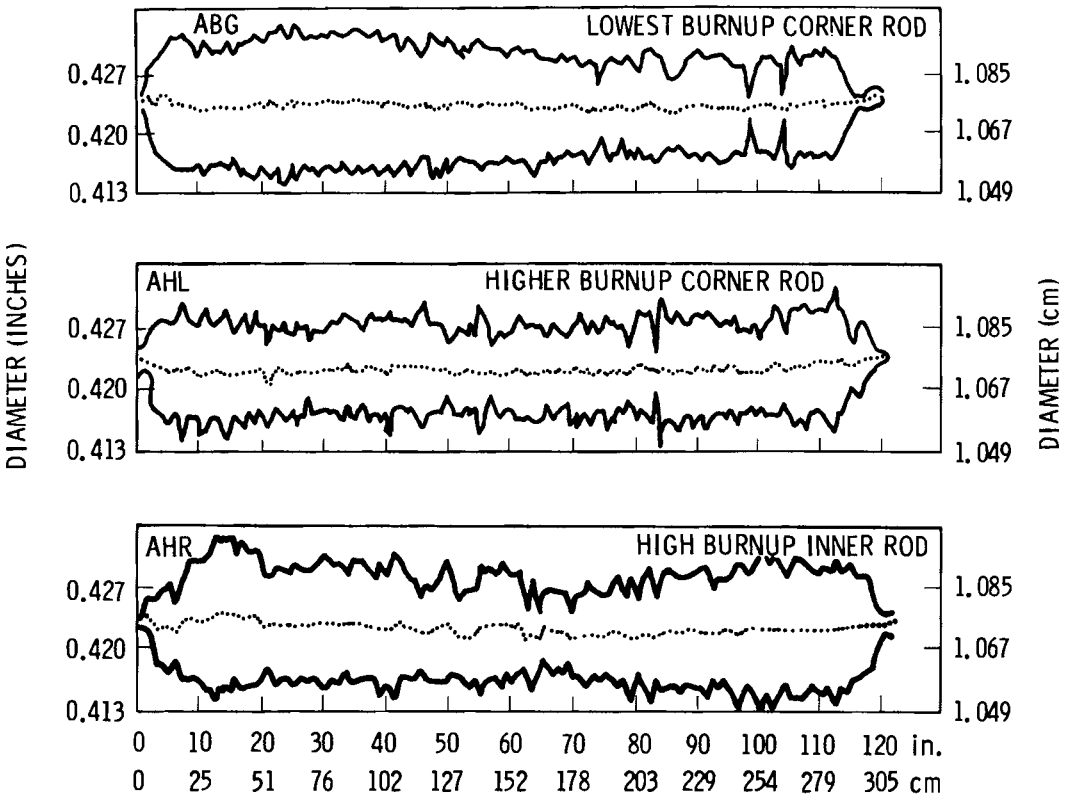

FIGURE 21. Spiral Profilometry Data for Rods ABG, AHL, and AHR from Assembly S004 Showing the Envelope of Maximum and Minimum Cladding Diameters and the Mean Cladding Diameter Along the Rod Length

rod axis is viewed from a point where the maximum cladding diameter is perpendicular to the line of sight and then rapidly changes orientation above and below the apparent maximum. However, the cladding profilometry has shown no bulges. Also, the dimensional envelopes of each of the four corner rods in S004 do not intrude significantly into the coolant channels and do not constitute any operational problem that might be associated with a cladding bulge obstructing the flow of coolant.

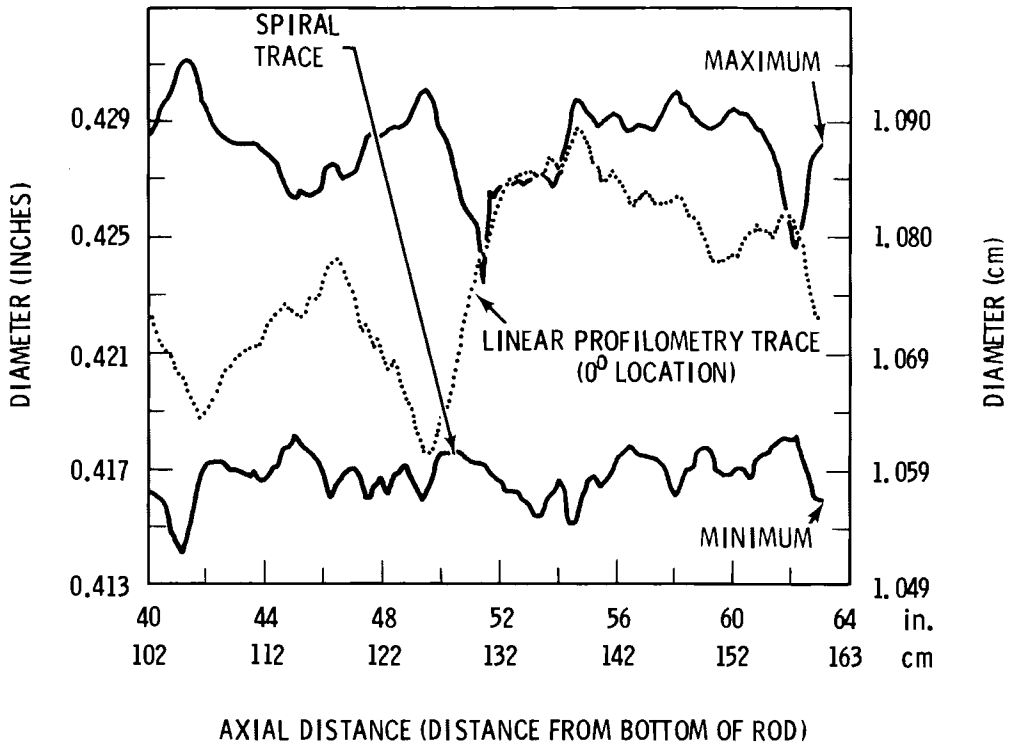

FIGURE 22. Overlay of Spiral and Linear Profilometry Traces Showing the Precession of Maximum Ovality Around the Axis of Rod AHR

Gamma Scan

Five rods were gamma scanned along their entire lengths to determine the relative burnup and time-averaged power generation of the fuel. The gamma scans were also used to determine if axial separations between fuel pellets or wide transverse pellet cracks had developed in the fuel column. No unusual axial separations were observed. There was no gross ^{137}Cs axial migration.

Each scan was made by moving the vertically positioned rod at a constant rate of 2 in./min past a collimating slit-detector arrangement and continuously measuring and recording the gamma radiation intensity from the section of the rod passing the collimator. All energies greater than 0.5 MeV were measured with a Ge(Li) crystal and recorded for the gross gamma scan. A malfunction of the instrument channel which measures the gross gamma radiation resulted in gross gamma measurements being made on only two out of the five rods. The ^{137}Cs isotopic gamma scan measured all energies from 0.63 to 0.68 MeV and was completed for all five rods. Collimators and slits were adjusted to maintain

a counting rate sufficiently low to avoid dead-time losses. The scanning apparatus was capable of determining the axial rod location to within ±1/32 in. (0.0794 cm); the minimum detectable axial gap in the fuel column was 20 mils (0.0509 cm).

The ^{137}Cs isotopic gamma activity traces were used in this investigation because of the correlation of ^{137}Cs activity with fuel burnup reported by others (Phillips et al. 1980). Table 15 lists the fuel stack lengths and the ^{137}Cs activity normalized to the activity of the rod with the highest calculated burnup (rod AHR). Figure 23 shows the normalized value correlated with the calculated rod burnup. The value for average burnup calculated for AHR agreed well with the analytically determined (^{148}Nd) value of a sample from the high power region from AHR when the calculated average value was multiplied by a 1.2 peaking factor. By normalizing to the analytically determined value of the burnup sample, the burnup of other rods was estimated, thereby improving the confidence in the estimate of the burnup obtained from the physics calculations.

The gamma activity traces clearly showed the pellet-to-pellet interface locations characteristic of fuel columns composed of dished pellets. The pellet interface locations are shown particularly well on the gross gamma scans as well as on the ^{137}Cs isotopic gamma scans (Figure 24). However, the pellet interfaces are not apparent in the high burnup rod (Figure 25) that operated at high power (the higher fuel temperature can result in migration of ^{137}Cs).

Figure 26 shows the pellet dish area at the 77-in. (196-cm) location on fuel rod 595A10 from G11. Figure 27a shows the gamma scan for the same area. Fuel pellet interfaces are not clearly defined on this trace as they are in the gamma scans of another rod from G11 and one from H07 (Figures 27b and 27c). Figure 25 shows the gamma scan traces of two corner rods (AHL and ABG) from S004, as well as the pellet interface locations. Figure 25 also shows the gamma scan from rod AHR, a high power, high burnup, interior rod from S004. Pellet interfaces are much less distinct in this case than in traces of

TABLE 15. Cesium-137 Gamma Scan Measurements for Selected Fuel Rods from Assembly S004

Rod Designation	Rod Location	Fuel Stack Length (in.)	Fuel Stack Length (cm)	Average Burnup (MWd/MTU)	Average $[^{137}Cs(x)/^{137}Cs(AHR)]$	Peak Burnup (MWd/MTU)	Peak $\left[\frac{^{137}Cs(x)}{^{137}Cs(AHR)}\right]$
AHR	F12	120-7/16	305.9	34470	1.00	41400	1.00
AJQ	K12	120-13/16	306.9	34470	0.98	41400	0.99
AHL	R15	121	307.3	29890	0.94	35900	0.98
AEK	F04	121-3/16	307.8	32160	0.90	38600	0.95
ABG	R01	120-7/8	307.0	24750	0.86	29700	0.90

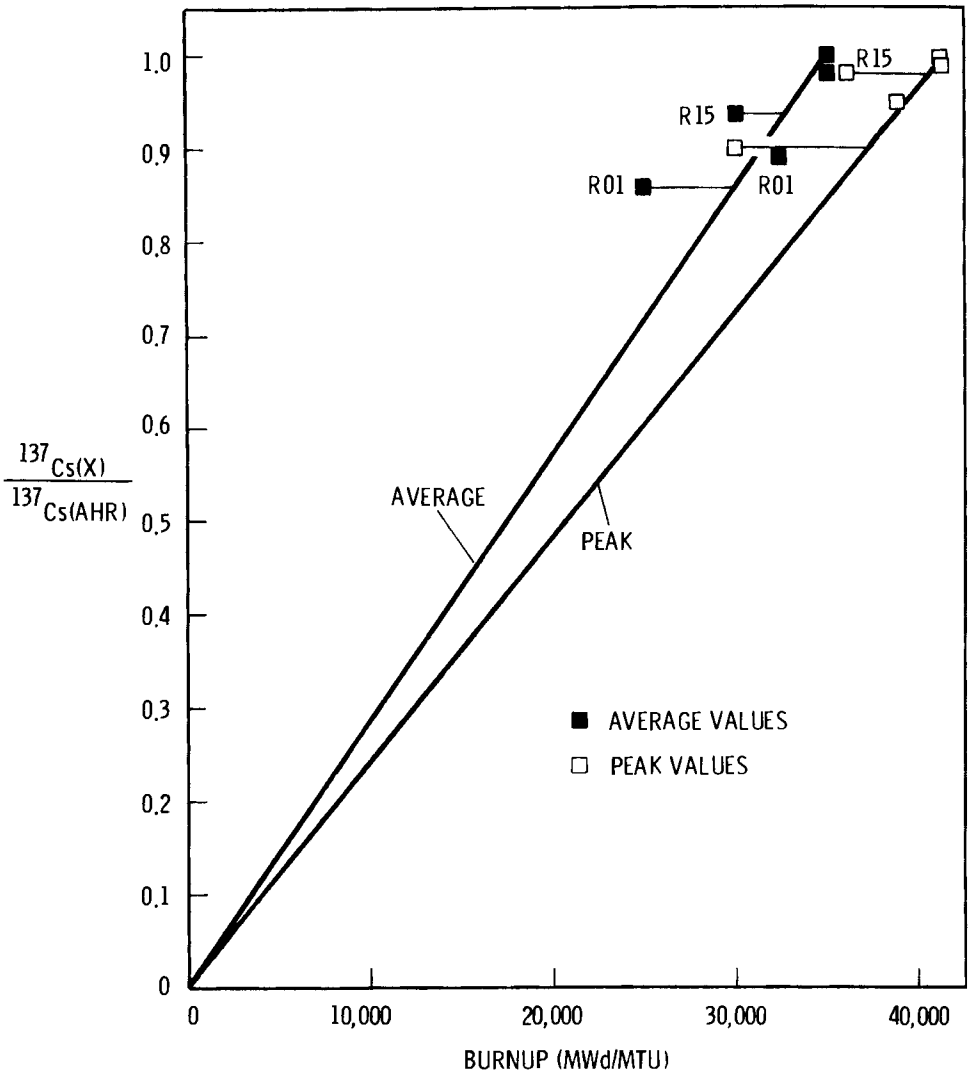

FIGURE 23. Correlation of the Measured ^{137}Cs Gamma Activities (Normalized) With the Calculated Burnup Values for Fuel Rods R01 and R15 From Assembly S004

the corner rods. The gamma scan traces for the other interior rods (AEK and AJQ) from assembly S004 also show indistinct pellet interface locations. Figure 65 (see section on ceramography) is a photograph of the fuel from rod AHR at the 56 in. (142 cm) location and shows a discontinuous change in fuel grain size across a crack. The temperature increase across the gap is the most likely cause of the grain size increase. This effect is quite common.

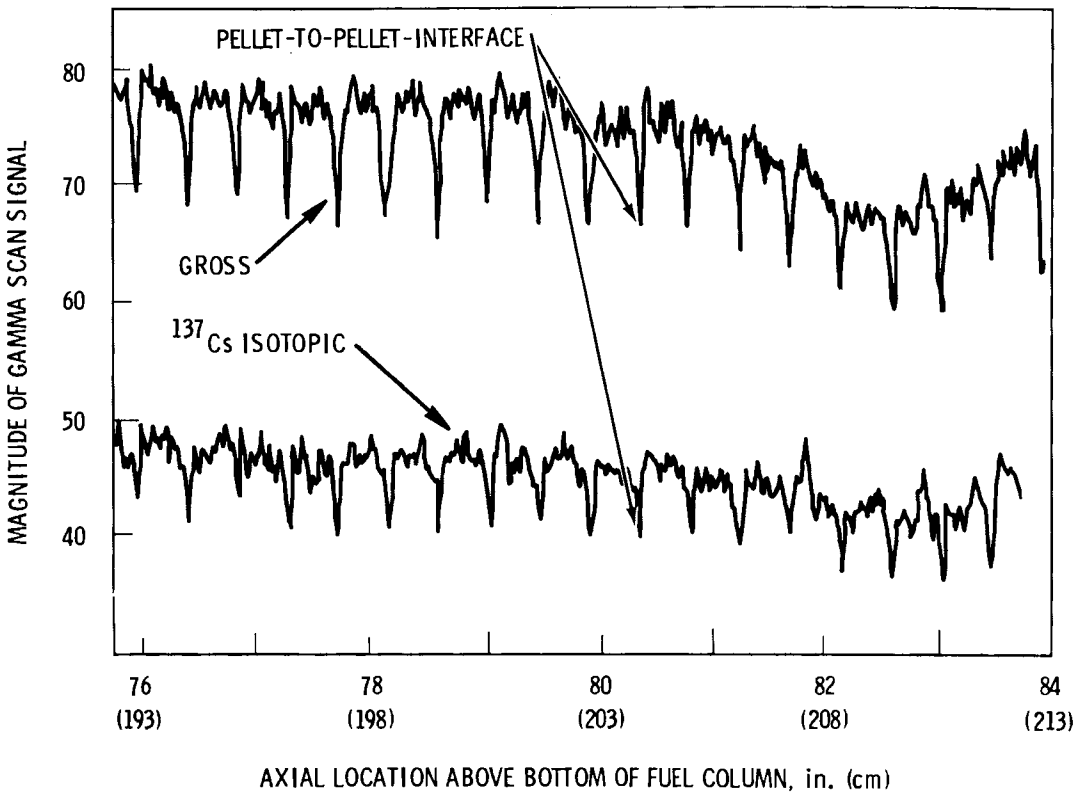

FIGURE 24. Gamma Scan Traces Showing Pellet-to-Pellet Interface Locations in Fuel Column of Rod AHL from Assembly S004

Eddy Current

An encircling coil was used for the eddy current examinations. No strong indications were observed, although a weak indication was observed at 98.5 in. (250 cm) above the bottom end of the high burnup fuel rod (Figure 28). Subsequent destructive examination revealed no evidence of a defect at that location.

Defect indications from traces of the vertical and horizontal components of the eddy current signal and the differential of the horizontal component are qualitative. An indication suggests the possibility of a cladding defect at a given axial location.

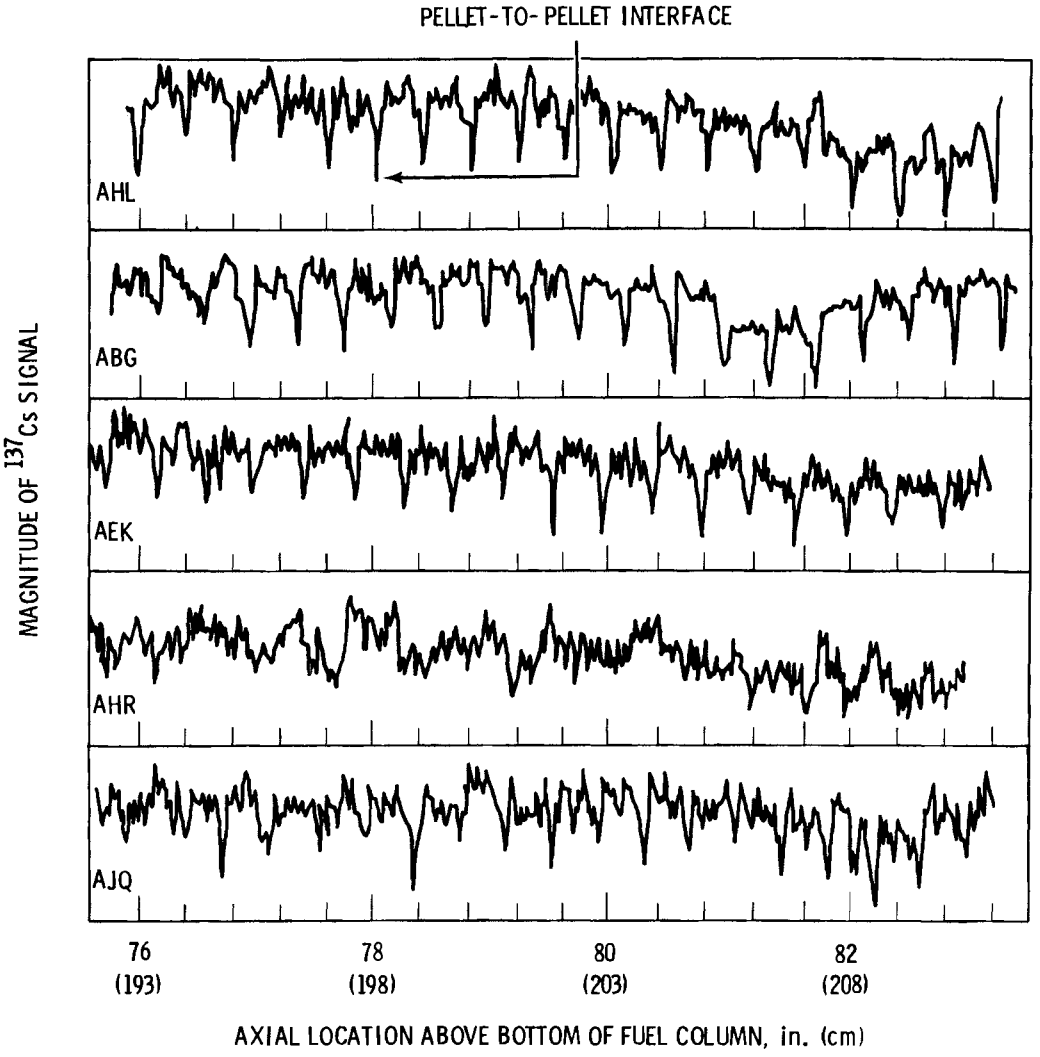

FIGURE 25. Gamma Scan Traces from Five Fuel Rods from Assembly S004 Showing the Pellet-to-Pellet Interfaces Distinctly in Lower Power Rods (e.g., ABG) and Less Distinctly in Higher Power Rods (e.g., AHR)

Temperature

Temperature measurements were made on selected fuel rods because fuel temperature affects rod internal gas pressure calculations and rod dimensional measurements and is used to verify rod decay heat calculations used in fuel storage consideration. The measurements were made to verify that the ambient

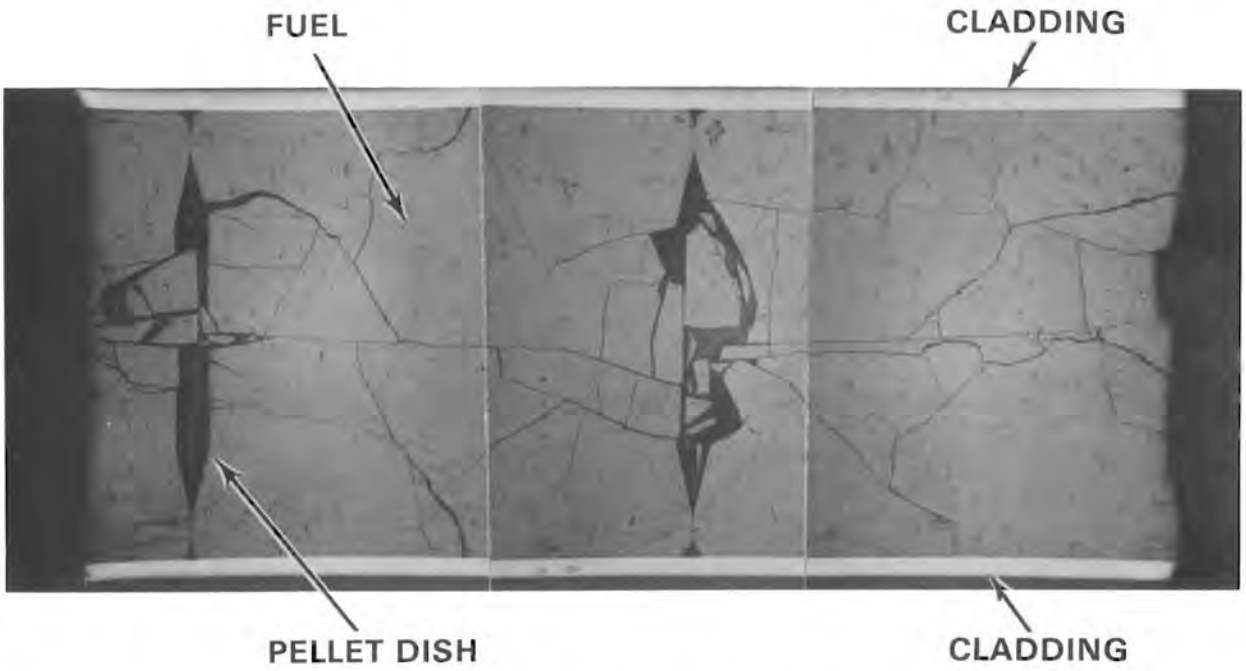

FIGURE 26. Longitudinal Section Showing Pellet Dish Area in Rod 595A10 from Assembly G11 (Figure 33 from Pasupathi and Klingensmith 1981)

cell temperatures would be representative of the gas temperatures in the rods from S004. The results of cladding temperature measurements made on two of the corner rods and four of the interior rods selected for examination are listed in Table 16.

A rod was placed on the visual examination apparatus to prevent heat loss due to contact with a metal surface. The rod was suspended from supports spaced at approximately 30-cm (1-ft) intervals. A probe thermocouple and a Leeds & Northrup 8690-2 millivolt potentiostat were used for the measurements. Ambient air temperature was checked after each measurement. The results showed good agreement between fuel rod surface temperatures (Table 16) and in-cell ambient temperatures (see Table 17 in subsection on fission gas collection and analysis).

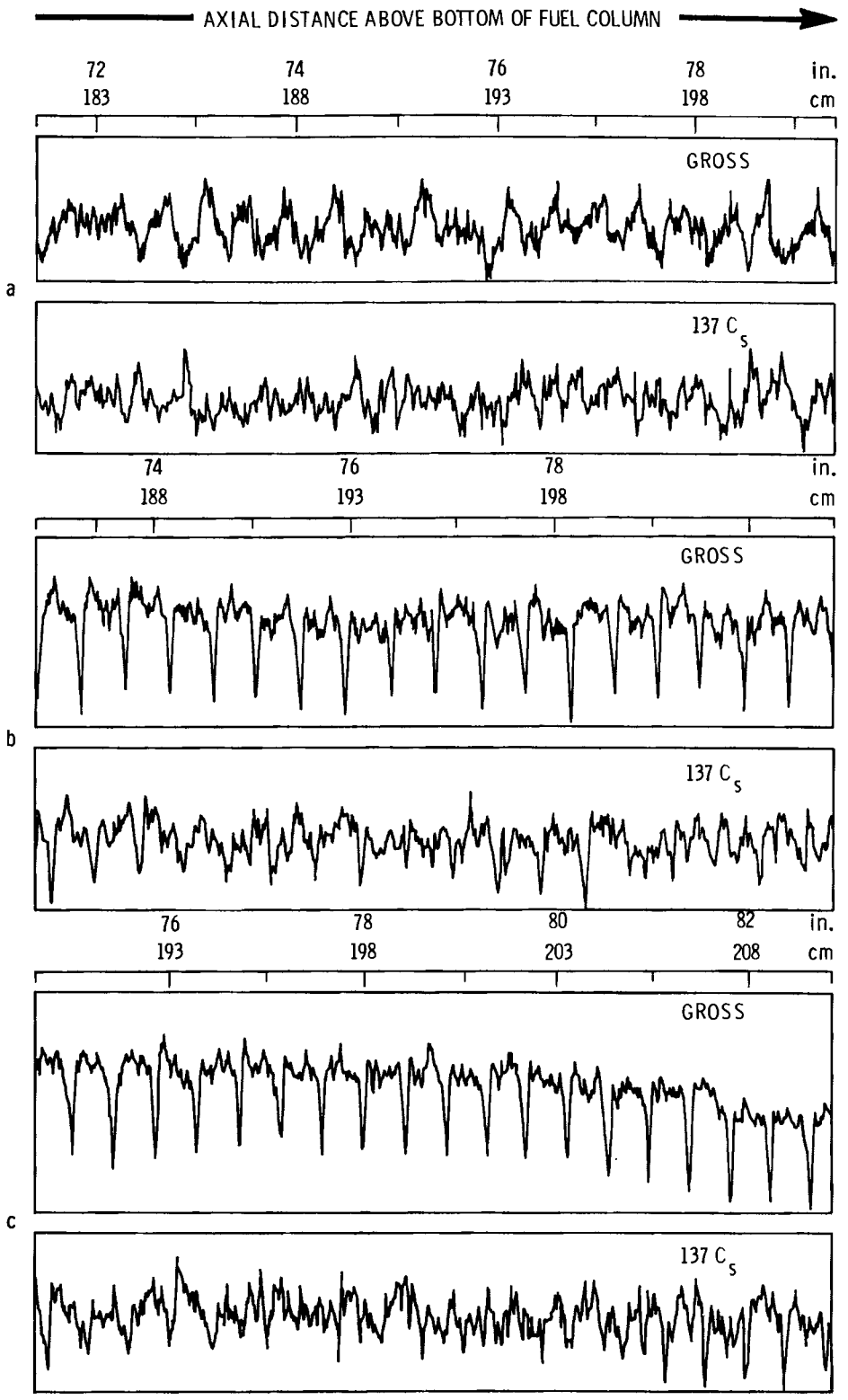

FIGURE 27. Gamma Scan Traces for Selected Fuel Rods from Assemblies G11 and H07 Showing the Pellet-to-Pellet Interfaces Distinctly in (b) G11 Rod 595A01 and (c) H07 Rod 217E02 and Less Distinctly in (a) G11 Rod 595A10

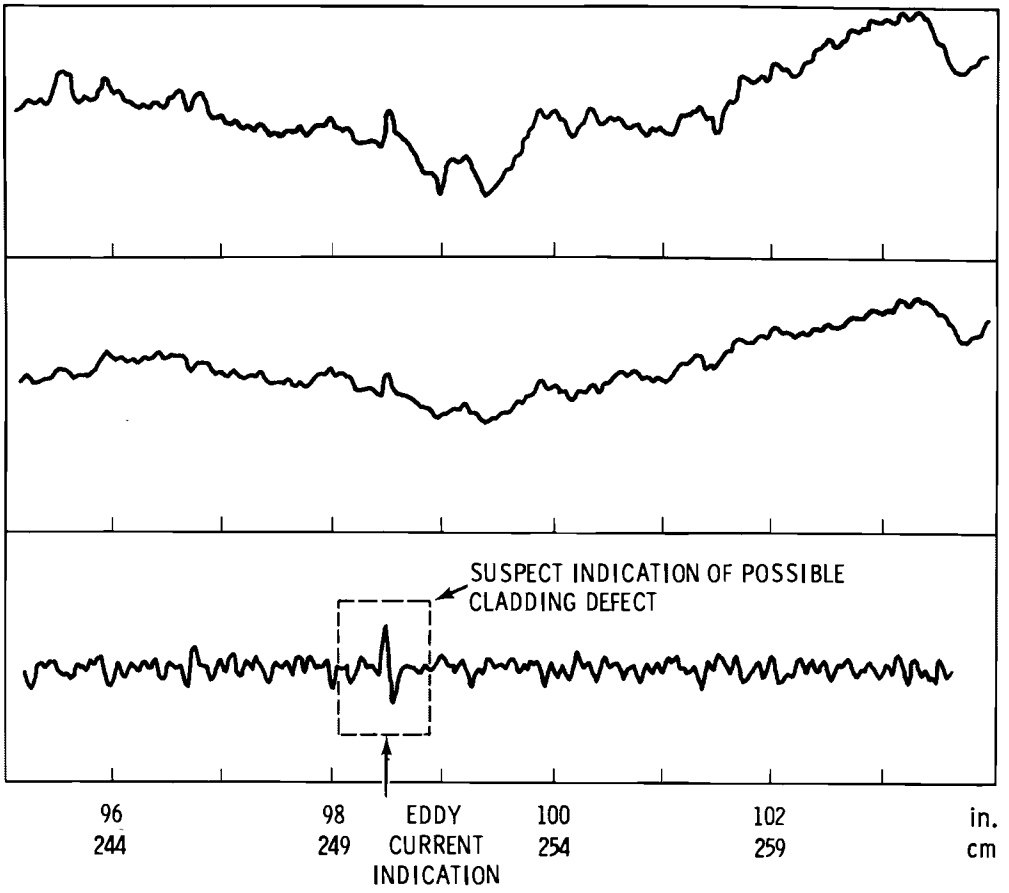

FIGURE 28. Eddy Current Traces of Rod AHR from Assembly S004, Showing Typical Traces and the Area Suspected to Contain a Cladding Defect. Subsequent destructive examination revealed no evidence of a defect in that area.

DESTRUCTIVE EXAMINATIONS OF FUEL RODS FROM ASSEMBLY S004

The objective of the destructive fuel rod examinations was to define the condition of the fuel and the cladding. The examinations and analyses were chosen:

- to determine whether significant cladding or fuel degradation had occurred during reactor residence
- to determine whether significant cladding degradation had occurred during pool residence
- to establish baseline conditions for possible future examinations.

TABLE 16. Temperature Measurements (°F) for Cladding on Irradiated Fuel Rods from S004

Rod Designation	Cladding Temperature at Given Distance from Bottom of Rod °F (°C) 1 in. (2.5 cm)	60 in. (152 cm)	121 in. (307 cm)	Room Temperature, °F (°C)
AGB[a]	76.0 (24.4)	78.5 (25.8)	77.0 (25.0)	75 (24)
AHR[a]	76.0 (24.4)	78.0 (25.6)	77.0 (25.0)	75 (24)
AHL[b]	75.0 (23.9)	76.0 (24.4)	76.0 (24.4)	74 (23)
AJQ	76.0 (24.4)	77.0 (25.0)	76.0 (24.4)	75 (24)
AEK	76.0 (24.4)	77.0 (25.0)	76.0 (24.4)	75 (24)
AAP	76.0 (24.4)	78.0 (25.6)	76.5 (24.7)	75 (24)

(a) Rod lying in air approximately 1/2 hr before temperature measured.
(b) Rod lying in air approximately 1/4 hr before temperature measured.

The specific examinations included fission gas collection and analysis, void volume determination, metallographic examination of the fuel and cladding, burnup analysis, autoradiography, fuel density, and cladding mechanical property testing.

Fission Gas Collection and Analysis

The gas inside the fuel rods (fission gas plus helium fill gas) was collected from four S004 rods, three H07 rods (Pasupathi and Klingensmith 1981) and one[a] G11 rod (Pasupathi and Klingensmith 1981) to determine the fission gas release. For each rod, the rod void volume was measured, the prepuncture rod pressure was calculated, and the collected gas was analyzed. The values for the increase in measured gas pressure in the rods over the fill gas pressure (1 atm) fell into two distinct groups: those with negligible pressure increase and those with a definite measurable pressure increase.

Figure 29 shows the fission gas collection system, which consists of an evacuable sleeve that contains a mechanical punch and fits over the plenum region of the rod; a series of calibrated expansion volumes that contain

(a) Another rod from assembly G11 was subsequently punctured to obtain additional fission gas release data.

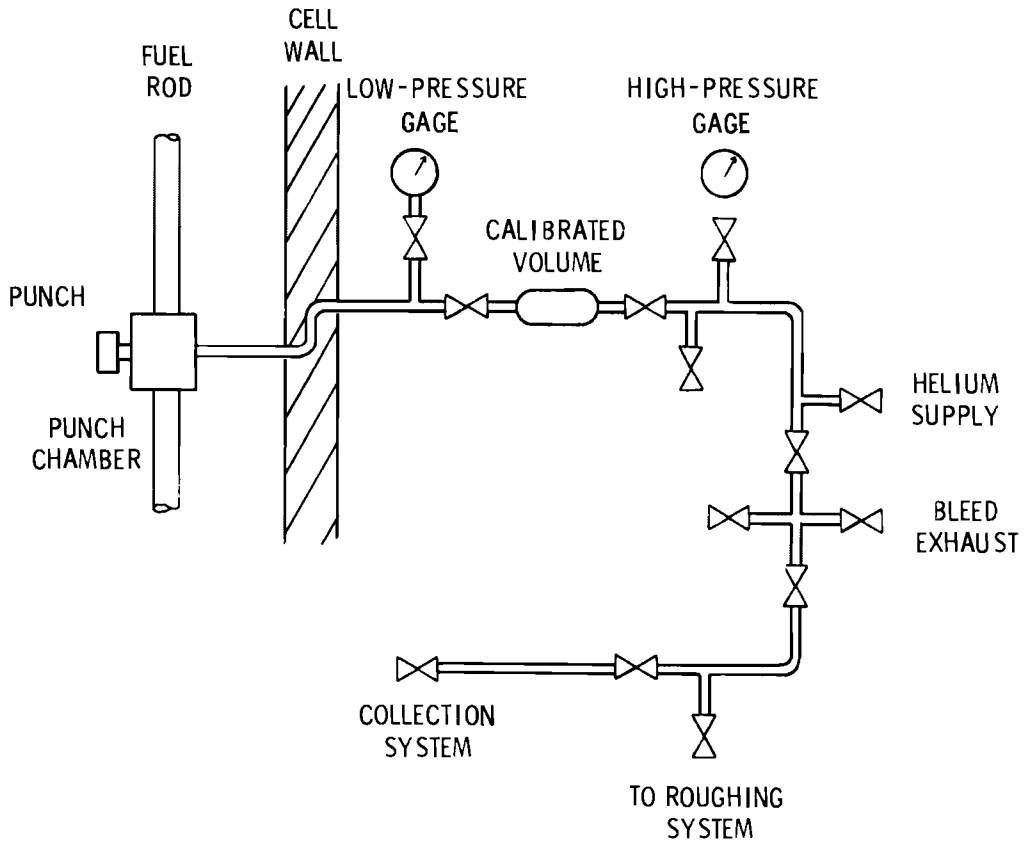

FIGURE 29. Schematic Diagram of the Fission Gas Collection System Used at the Hot-Cell Facility at Battelle Columbus Laboratories

low-range (0 to 15 psi) and high-range (0 to 199 psi) pressure gages; a collection system with a Toepler pump; and an evacuation system. The collection procedure is to insert the rod and seal the punch chamber. The entire system (punch chamber, expansion system, pressure gauges, and collection system) is evacuated to a few microns pressure. The prepunch system volume (V_s) is measured by pressurizing the punch chamber to about 80 psi (0.55 MPa) with helium and then expanding it into a known volume. The system volume (V_s) is calculated by the pressure drop. This step is repeated 10 times. The system is evacuated to less than 50 μm and the pressure and the hot-cell, collection system, and collection vial temperatures are recorded.

When the rod is punctured, pressure readings are recorded on puncturing, at a 2-min interval and subsequent 5-min intervals until the system equilibrates. The total system and rod void volumes (V_t) are measured. The rod

gas is expanded into the collection system and then Toepler-pumped into two vials. These vials are removed from the system. One is sent for mass spectrometric analysis; the other is held as a backup. The total system and rod void volumes (V_t) are then measured by again pressurizing the punch chamber to about 80 psi with helium and expanding it into a known volume. This step is repeated 10 times. From these data, the rod void volume, the prepuncture rod pressure, and the amount of gas contained in the rod are calculated.

The high (AHR) and low (ABG) burnup fuel rods from assembly S004 were the first to be selected and punctured for fission gas collection and analysis. Rods ADT and AGD were selected for supplemental analysis after an order of magnitude difference in prepuncture rod pressures and fission gas release was indicated for AHR and ABG. Hydrogen was present in the gases collected from all the S004 rods; negligible hydrogen was measured in fuel rods from assemblies H07 and G11. The Xe/Kr ratios for the four rods showed no burnup dependence in the range of burnups measured. The fission gas releases fell into two ranges and correlated more with fuel temperature during irradiation, as estimated from the appearance of the microstructure, than with rod power or burnup. It should be noted that the fuel rods from assembly S004 were not of the prepressurized type. S004 fuel densified about the same amount as G11 fuel but swelled at a lower rate than G11 fuel. Results from a study by Belgonucleaire (Bouffioux and De Meulemeester 1979) and from an EPRI-sponsored program (Fuhrman et al. 1976) show that large variations in fission gas release can occur in two fuel rod groups with nominally the same power history because of densification of the fuel and thermal feedback effects. The densification and thermal feedback result in a larger gap between the fuel and cladding, higher temperature, and higher gas release.

The prior studies of fission gas release versus fuel temperature (Bouffioux and De Meulemeester 1979; Fuhrman et al. 1976) indicated that gas releases in rods from assembly S004 would not be expected to occur while the rods were in pool storage at low temperatures. The void volumes determined for these rods ranged from 21.35 cm^3 to 24.71 cm^3 with an average value for the four rods of 22.78 cm^3. Table 17 lists the temperature, pressure, and volume measurements. Table 18 gives rod gas composition and fuel burnup information.

TABLE 17. Measurements for Gases Collected from Connecticut Yankee Fuel Rods

Assembly-Fuel Rod Designation	Report Date	Total System Volume, V_T (cm^3)	Initial System Volume, V_S (cm^3)	Rod Void Volume, V_R (cm^3)	Expanded Pressure in V_T (psi)	Expanded Pressure in V_T (Pa)	Temperature (°C) System	Temperature (°C) In-Cell
S004-ABG	8/26/80	497.24	472.53	24.71	1.07	7,380	22.0	24.0
-ADT	2/25/81	495.34	473.99	21.35	1.19	8,210	21.5	25.5
-AHR	8/25/80	495.56	473.01	22.55	6.91	47,600	22.0	23.5
-AGD	2/25/81	496.05	473.54	22.51	10.57	72,600	23.0	25.0
H07-157ED1	6/19/80	493.32	474.66	18.66	1.19	8,210	23.0	24.8
-062E12	6/18/80	493.02	472.16	20.86	1.25	8,620	22.0	25.0
-217E02	6/20/80	492.64	472.34	20.30	1.46	10,100	22.5	25.5
G11-595A10	10/8/80	494.50	473.57	20.93	4.60	31,700	22.0	24.0

TABLE 18. Compositions of Collected Gases and Calculated Fuel Burnups for Selected Connecticut Yankee Fuel Rods

Assembly-Fuel Rod Designation	Report Date	Fuel Burnup (MWd/MTU)	Sample Volume (cm^3), STP[a]	Gases Collected (Vol%)										Ratio, Xe/Kr
				He	Kr	Xe	A	O_2	N_2	CO_2	H_2O	CH_4	H_2	
S004-ABG	8/29/80	24,750	10.2	77.4	1.10	19.0	0.01	0.02	0.17	<0.01	<0.1	<0.01	12.2	8.3
-ADT	3/06/81	34,470	10.1	71.5	2.14	18.4	0.03	0.01	0.12	0.04	<0.1	<0.01	7.71	8.6
-AHR	8/29/80	34,470	66.6	18.4	9.35	70.9	0.02	<0.01	<0.01	-	<0.1	<0.01	1.30	7.6
-AGD	3/02/81	30,880	88.7	13.6	9.88	75.7	0.01	<0.01	0.07	0.06	<0.1	<0.01	0.72	7.7
H07-157E01	6/26/80	36,740	11.8	50.9	3.90	34.9	10.3	<0.01	<0.01	<0.01	<0.1	<0.01	<0.01	9.0
-062E12	6/26/80	36,670	12.7	54.0	3.47	31.3	11.2	<0.01	<0.01	<0.01	<0.1	<0.01	<0.01	9.0
-217E02	6/26/80	36,740	14.0	46.5	4.44	40.3	8.74	<0.01	<0.01	<0.01	<0.1	<0.01	<0.01	9.1
G11-595A10	10/10/80	38,060	46.4	29.3	7.79	61.4	1.43	<0.01	<0.01	<0.01	<0.1	<0.01	0.04	7.9

(a) STP = standard temperature and pressure.

Table 19 lists the prepuncture rod pressures computed for Connecticut Yankee fuel rods. The gas pressures were computed using ratios derived from the Ideal Gas Law, assuming that the number of moles of gas was constant. Isothermal (23°C) conditions were assumed because the system and in-cell temperatures only varied from 21°C to 26°C. The helium and argon pressures are included to point out that additional helium was generated and released during irradiation if the original rod filling pressure was 1 atm. The helium and argon pressures were calculated by multiplying the gas pressure (P_r) by the volume fractions of helium and argon in the collected gases (see Table 18).

The percent of fission gas released during irradiation was calculated by determining the total moles of Xe and Kr in the collected gas and dividing that number by the total moles of Xe and Kr generated based on a calculation that considered the fuel stack weight and the fuel burnup (see Table 20). The calculated value for burnup agreed well with the measured burnup value for rods AHR and AJQ. The largest difference between calculated burnup and a value estimated from the ^{137}Cs correlation (see Figure 23) for burnup was for rod ABG; the calculated value was about 17% below the ^{137}Cs correlation value. The calculated values for burnup were used in the calculation of fission gas release.

The moles of Xe and Kr in the collected gases were determined by Amagat's Law of partial volumes:

$$n = \frac{P_s V_s}{RT} (Xe + Kr)$$

where n = number of moles of Xe + Kr

P_s = system pressure after rod puncture, i.e., expand (volume atm)

V_s = total system volume after rod puncture (ℓ)

T = collection system temperature (K)

R = 0.08206 ℓ-atm/K-mole

Xe,Kr = Xe and Kr composition of collected gas (vol. fraction).

The moles of H_2 in the collected gases were computed similarly. Table 21 lists the results for the moles of fission gas, i.e., Xe and Kr, generated during

TABLE 19. Gas Pressures in Connecticut Yankee Fuel Rods

Assembly-Fuel Rod Designation	Total System Volume, V_T (cm^3)	Rod Void Volume, V_R (cm^3)	Expanded System Pressure, P_T (psi)	(atm)	Total Pressure in Rod P_R (psi)	P_R (atm)	Helium P_{He} (atm)	Argon P_{Ar} (atm)
S004-ABG	499.24	24.71	1.07	0.072	21.53	1.46	1.03	--
-ADT	495.34	21.35	1.19	0.081	27.61	1.88	1.34	--
-AHR	495.56	22.55	6.91	0.470	151.85	10.33	1.90	--
-AGD	496.05	22.51	10.57	0.719	232.93	15.85	2.16	--
H07-157E01	493.32	18.66	1.19	0.081	31.46	2.14	1.09	0.22
-062E12	493.02	20.86	1.25	0.085	29.54	2.01	1.09	0.225
-217E02	492.64	20.30	1.46	0.099	35.43	2.41	1.12	0.21
G11-595A10	494.50	20.93	4.60	0.313	108.68	7.39	2.17	0.11

TABLE 20. Fission Gas Release in Selected Connecticut Yankee Fuel Rods

Assembly-Fuel Rod Designation	Fuel Stack Weight (kg Oxide)	Fuel Stack Weight (MTU)[b]	Burnup (MWd/MTU)[b]	Moles of Xe + Kr Generated	Moles of Xe + Kr Released	Fission Gas Released (%)
S004-ABG	2.264	1.992×10^{-3}	24750	6.953×10^{-2}	1.525x10-4	0.22
-ADT	2.264[a]	1.992×10^{-3}	34470	9.683×10^{-2}	3.410×1^{-4}	0.35
-AHR	2.258	1.987×10^{-3}	34470	9.657×10^{-2}	77.235×10^{-4}	8.00
-AGD	2.264[a]	1.992×10^{-3}	30880	8.675×10^{-2}	125.670×10^{-4}	14.49
H07-157E01	2.264[a]	1.992×10^{-3}	36740	10.321×10^{-2}	6.383×10^{-4}	0.62
-062E72	2.264[a]	1.992×10^{-3}	36669	10.301×10^{-2}	6.019×10^{-4}	0.58
-217E02	2.264[a]	1.992×10^{-3}	36740	10.321×10^{-2}	9.025×10^{-4}	0.87
G11-595A10	2.264[a]	1.992×10^{-3}	38062	10.692×10^{-2}	44.224×10^{-4}	4.41

(a) Nominal fuel stack weight.
(b) MTU = metric ton of uranium.

TABLE 21. Moles of (Xe + Kr) and H_2 in Selected Connecticut Yankee Fuel Rods

Assembly-Fuel Rod Designation	P_s (atm)	V_s (l)	T (K)	Xe + Kr (Vol. Fraction)	Moles of Xe + Kr Collected	H_2 (Vol. Fraction)	H_2 (moles)	H_2 (grams)	H_2O (ppm)
S004-ABG	0.0728	0.4972	295.0	0.1020	1.525×10^{-4}	0.122	1.82×10^{-4}	3.28×10^{-4}	1.5
-ADT	0.0810	0.4953	294.5	0.2054	3.410x	0.077	1.28×10^{-4}	2.30×10^{-4}	1.0
-AHR	0.4701	0.4956	295.0	0.8025	77.235x	0.013	1.25×10^{-4}	2.25×10^{-4}	1.0
-AGD	0.7190	0.4961	296.0	0.8558	125.670x	0.0072	1.06×10^{-4}	1.90×10^{-4}	0.8
H07-157E01	0.0810	0.4933	296.0	0.3880	6.383x	<0.0001	--	--	--
-062E12	0.0850	0.4930	295.0	0.3477	6.019x	<0.0001	--	--	--
-217E02	0.0993	0.4926	295.5	0.4474	9.025x	<0.0001	--	--	--
G11-595A10	0.3129	0.4945	295.0	0.6919	44.224x	<0.0001	0.06x10-4	0.12	0.05

irradiation and the moles of H_2 in the collected gases and the bulk concentration (ppm) of H_2O in the fuel necessary to yield the amount of H_2 measured.

The moles of fission gas (Xe and Kr) generated by fuel fissions during irradiation are calculated by the following expression:

$$N_o = (1.41 \times 10^{-3})(BU)(W)$$

where N_o = number of moles of (Xe + Kr)
BU = fuel burnup (MWd/MTU)
W = fuel stack weight (MTU)

Rod Marking and Sectioning

The objective here was to obtain fuel and cladding samples to characterize the fuel through fuel density measurements, burnup analysis, autoradiography, ceramography, fuel cladding tests, metallography, and mechanical testing while disturbing the fuel and cladding as little as possible.

The axial sample locations, as measured from the bottom end of the fuel rod (see Figures 3 and 13), were established by reference to nondestructive examinations and from calculated values of rod power and fuel burnup (see Figures 7, 8, 9). The locations were indexed on the outer surface of the cladding with a tube cutter, which made circumferential scribe marks with an axial accuracy of $\pm$1/32 in. (0.79 mm). Motor-driven chucks gripped each end of the fuel rod and rotated it during marking. After marking was completed, the rod was removed from the marking tool and placed in the sectioning tool.

A rotating chuck and tubing cutter comprised the sectioning tool. This tool provided cladding sections with crimped ends that were sufficiently deformed to retain individual pellets or large fragments of cracked pellets. The first cuts were made at 42.25 in. (107 cm) and 80.50 in. (204 cm) above the bottom of the rod. The lower two sections were marked at the section top, in line with the 0° reference mark cut in the upper end cap (assembly west direction, as shown in Figures 2 and 12), with a burring tool to identify the azimuthal orientation (for an example see Figure 38 in the Metallography

subsection) and the section top end. The sections were inserted into containers marked with the section identification. The specimens were transferred to the high-level cell for further sectioning.

Further sectioning was accomplished with an abrasive cut-off saw. A flow of water was used to cool the cut area and control contamination. A white paint dot was placed near the top end of each cut piece, in line with the cut mark on the top end of the rod. The cut sections were placed in individual containers marked with the section identification. Each container was listed and stored for retrieval for the desired examinations. Care was taken to prevent loss of fuel fragments. However, the water coolant disturbed the soluble fission products in the samples intended for fuel leach testing. Therefore, fuel leach testing was not included in the examinations. The sample numbers are listed in Tables 22 and 23 along with sample location and the examination requested.

Fuel Burnup Analysis

The burnup sample (No. 8) was taken immediately below the mid-core plane of fuel rod AHR, a high burnup rod from assembly S004. The burnup analysis yielded a value of 4.209 at.% or 40,410 MWd/MTU. This value compares well with the peak burnup of 41,400 MWd/MTU calculated for AHR by multiplying the rod average burnup (34,473 MWd/MTU) times the peaking factor. A value of 1.2 was used for the peaking factor.(a)

The sample was dissolved in the chemistry hot cell by refluxing in 12 N nitric acid. All glassware was new and each piece was cleaned in boiling 8 N HNO_3 prior to use, as required by American Society for Testing and Materials (ASTM) procedure E-267. The dissolved uranium samples were diluted to a concentration of 0.001 gU/ml with 8 N HNO_3. The BCL mass spectrometer laboratory conducted the burnup analysis by the ^{148}Nd method (ASTM E-321). Results of the mass spectrometric analysis are shown in Table 24. The burnup and time-average linear heat generation rates were calculated for each rod by normalizing the gamma scanning data for each rod to the analytically determined burnup values.

(a) For assemblies H07 and G11, a value of 1.15 was used for the peaking factor (see page 3-45 in Pasupathi and Klingensmith 1981).

TABLE 22. Sectioning for Fuel Rod AHR from Assembly S004

Sample No.	Location[b] (in.)	Examination
1 & 1A	0.00 - 1.00	Longitudinal Metallographic (Met.) Sample at Lower End Cap
(a)		
3	1.00 - 1.50	Density
3A	1.50 - 2.00	Density
3B	2.00 - 24.00	Remnant
3C	24.00 - 29.00	Tensile
3D	29.00 - 34.00	Tensile
3E	34.00 - 34.50	Ring Tensile
3F	34.50 - 35.00	Ring Crush
3G	35.00 - 35.50	Ring Tensile
3H	35.50 - 36.00	Ring Crush
4	36.00 - 36.50	Transverse Met. (Top Face)
5	36.50 - 37.50	Leach (Wet Cut)
6	37.50 - 42.25	Remnant
7	42.25 - 43.75	Remnant
7A	43.75 - 48.75	Tensile
7B	48.75 - 49.25	Ring Tensile
7C	49.25 - 49.75	Ring (Save)
7D	49.75 - 50.25	Ring Crush
7E	50.25 - 50.75	Ring (Save)
7F	50.75 - 55.75	Tensile
8	55.75 - 56.25	Burnup
9	56.25 - 56.75	Transverse Met. (Top Face)
10	56.75 - 57.75	Leach (Wet Cut)
11	57.75 - 58.25	Density
12	58.25 - 58.75	Density
12A	58.75 - 59.25	Ring Tensile

(a) There was no Sample No. 2.
(b) Distance from bottom end of fuel rod.

TABLE 22. (Contd)

Sample No.	Location (in.)	Examination
12B	59.25 - 59.75	Ring Crush
12C	59.75 - 60.25	Ring (Save)
12D	60.25 - 65.25	Tensile
12E	65.25 - 65.75	Ring
12F	65.75 - 66.25	Ring
12G	66.25 - 71.25	Tensile
12H	71.25 - 71.75	Ring
(a)		
12J	71.75 - 72.25	Ring
12K	72.25 - 72.75	Ring
12L	72.75 - 73.25	Ring
12M	73.25 - 80.00	Remnant
13	80.00 - 80.50	Transverse Met. (Top Face)
14	80.50 - 83.25	Remnant
15	83.25 - 83.75	Transverse Met. (Top Face) Grid Spacer
16	83.75 - 84.50	Remnant
17	84.50 - 89.50	Tensile
17A	89.50 - 90.00	Ring Tensile
17B	90.00 - 90.50	Ring Crush
17C	90.50 - 91.00	Ring Crush
17D	91.00 - 91.50	Ring Tensile
17E	91.50 - 96.50	Tensile
17F	96.50 - 98.25	Remnant
18	98.25 - 98.75	Transverse Met. (Bottom Face Eddy Current Indication)
19	98.75 - 125.75	Remnant
20 & 21	125.75 - 126.66	Longitudinal Met. Upper End Cap

(a) No Sample 12i.

TABLE 23. Sectioning for Fuel Rod ABG from Assembly S004

Sample No.	Location [a] (in.)	Examination
1 & 1A	0.00 - 1.00	Longitudinal Metallographic (Met.) Samples at Lower End Cap
2	1.00 - 41.00	Remnant
3	41.00 - 41.50	Transverse Met. (Top Face Grid Spacer)
4	41.50 - 42.25	Remnant
5	42.25 - 56.25	Remnant
6	56.25 - 56.75	Transverse Met. (Top Face)
7	56.75 - 84.50	Remnant
8	84.50 - 125.75	Remnant
9 & 9A	125.75 - 126.75	Longitudinal Met. Upper End Cap

(a) Distance from bottom end of fuel rod.

Fuel Density

Fuel densities were determined for irradiated samples from rod AHR in the hot cell by using a mercury pycnometer technique. Pairs of samples were evaluated: two from near the lower end cap in a low burnup region and two from just below the core mid-plane, near the burnup sample in a high burnup, high power

TABLE 24. Mass Spectrometric Analysis of Fuel Burnup Sample AHR-8[a]

Isotope	Atom Percent	Isotope	Atom Percent
^{234}U	0.026	^{240}Pu	23.100
^{235}U	1.101	^{241}Pu	11.201
^{236}U	0.588	^{242}Pu	5.457
^{238}U	98.285	$^{148}Nd/^{238}U$	7.594×10^{-4}
^{238}Pu	2.501	$^{239}Pu/^{238}U$	6.516×10^{3}
^{239}Pu	57.740		

(a) The burnup of the sample was 40,410 MWd/MTU (4.209 at.%).

region. The results indicated that the fuel underwent a densification of almost 2%, but the net density change in the high power, high burnup region was almost nil.

The results of the fuel density measurements are given in Table 25. The original mean as-sintered fuel density was 10.215 g/cm^3 or 93.20% of theoretical density.

Metallography

Metallographic specimens were examined for evidence of surface crud and/or oxide layers, corrosive attack, and cracking. Other goals were to document the microstructure of the cladding, end caps, and weld areas, as well as the geometry of the cladding ovality and fuel-cladding gap. The specimens were cut with an abrasive cut-off wheel. Again, water was used for cooling the sample and controlling dust. The cut specimen was placed in a stainless steel sleeve to reduce edge rounding during polishing. The specimen was oriented so that the prepared metallographic surface would either be transverse or parallel with the rod axis. The sample and sleeve were then positioned in a bakelite holder with markers to denote the rod 0° azimuthal orientation. The entire assembly was placed in a bell jar; the jar was evacuated and a cold-setting epoxy resin was

TABLE 25. Measured Fuel Densities for Rod AHR from Assembly S004

Sample No.	Axial Location[a] (in. above bottom of fuel rod)	Fuel Density (g/cm^3)	Fuel Density % TD[b]
3	1.00 - 1.50	10.435	95.21
3A	1.50 - 2.00	10.438	95.24
11	57.75 - 58.25	10.233	93.37
12	58.25 - 58.75	10.255	93.57

(a) The average burnup for rod AHR was 34,473 MWd/MTU and maximum burnup (see section on fuel burnup analysis) was 40,410 MWd/MTU.

(b) Theoretical density (TD) of UO_2 is 10.96 g/cm^3. The as-fabricated mean pellet density was 10.215 g/cm^3 (93.20% TD).

poured over the sample to fill the cavity. This process was repeated until satisfactory impregnation of the mount was obtained. The resin required a 12-hr curing time.

The metallographic specimens were ground with silicon carbide abrasive papers (120 through 600 grit) and polished with a slurry of Linde A alumina in a 2% chromic acid solution. The specimens were examined in both as-polished and etched conditions. Two etchants were used: a) 50 parts HCl/10 parts HNO_3 and b) 10% oxalic acid with electrolytic etching.

The metallurgical structure of the base material was essentially equiaxed with twinning and slip band formations present. Figure 30 shows archive material; Figure 31 shows irradiated material for comparison. Figure 32 illustrates that the grain size did not change significantly through the wall of the cladding. The grain size in the seam weld heat-affected zone (HAZ) was very similar in the rods from the three fuel assemblies (S004, G11, H07). The inclusion population was divided into two categories, similar to results reported by Babcock and Wilcox (1979)[(a)] for cladding used in the G11 and H07 assemblies. The inclusions were either of the elongated or fragmented stringer type or of the small, isolated type.

The etched samples showed microstructures typical of stainless steel cladding, welds, and end caps. The archive and irradiated materials in Figures 30 and 31 show that the thermo-mechanical history of the tube seam weld has resulted in a uniform, wrought microstructure with a finer grain size than the unwelded metal in the cladding. Figures 33 and 34 show selected microstructures typical of the irradiated stainless steel cladding, weld, end cap, and HAZ material examined. The irradiated material appears to have fewer carbides and twins than the archive material. This may be due to specimen preparation. Again, even in the high magnification photographs of the weld areas, no oxide or crud layers, corrosion attack, or cracking are evident.

The end cap welds showed a dendritic structure characteristic of rapidly quenched austenitic weld metal. Surface flaws on the cladding ID were

---

(a) "Examination of Connecticut Yankee Archive Cladding ID Surface." Letter Report LR:79:6861-01:1, Babcock and Wilcox Company, Lynchburg Research Center, Lynchburg, Virginia, May 30, 1979.

reported (Babcock and Wilcox 1979) for archive fuel cladding. Pre-existing flaws of this type are probably present in the SO04 cladding and explain some of the observed surface roughness that cannot be attributed to fuel handling or machining operations.

Two etchants were used for the cladding. Micrographs with negative numbers up to HC50381 represent surfaces etched with 50HCl-10 HNO_3. Micrographs with negative numbers of HC50381 or greater show surfaces electrolytically etched with 10% oxalic acid. The etchant was changed because of excessive pitting encountered with the 50HCl-10 HNO_3 etchant. Figure 35 shows examples of surfaces prepared with each etchant. The variation in oxalic acid etching characteristics is illustrated in Figures 36 and 37. Over-etching occurred in the cladding away from the weld area.

Generally, oxides and crud were not discernible on OD cladding surfaces at magnification up to 500X. Oxides also were not detected on the ID surfaces (see Figures 38 through 41), in contrast to Zircaloy-clad fuel. However, observation of very thin surface layers, such as the crud or oxide layers that could be present on this cladding, is strongly dependent on the sample preparation and the optical resolution limits of the metallograph. Sample preparation with specimen edge retention of the caliber required to show thin surface films is very difficult, especially when the work is being performed in a hot cell. Some OD areas showed gouging (Figure 42) typical of handling marks and the axial scratches inflicted by grid-spacer springs when the rods are inserted into or withdrawn from the fuel assembly (Figure 16). Corrosive attack or cracking was not evident in the cladding. Examination of cladding seam and end cap welds and weld heat-affected zones showed no evidence of intergranular corrosion or stress-corrosion cracking.

The cladding surface condition was generally very smooth with no measurable surface layers in the fuel rods examined from the three assemblies (Figures 43 through 47). However, the light brown cladding surface appearance suggested the presence of a thin surface oxide. There were no apparent differences in corrosion between the cladding or base material, the weld area, and the weld heat-affected zone.

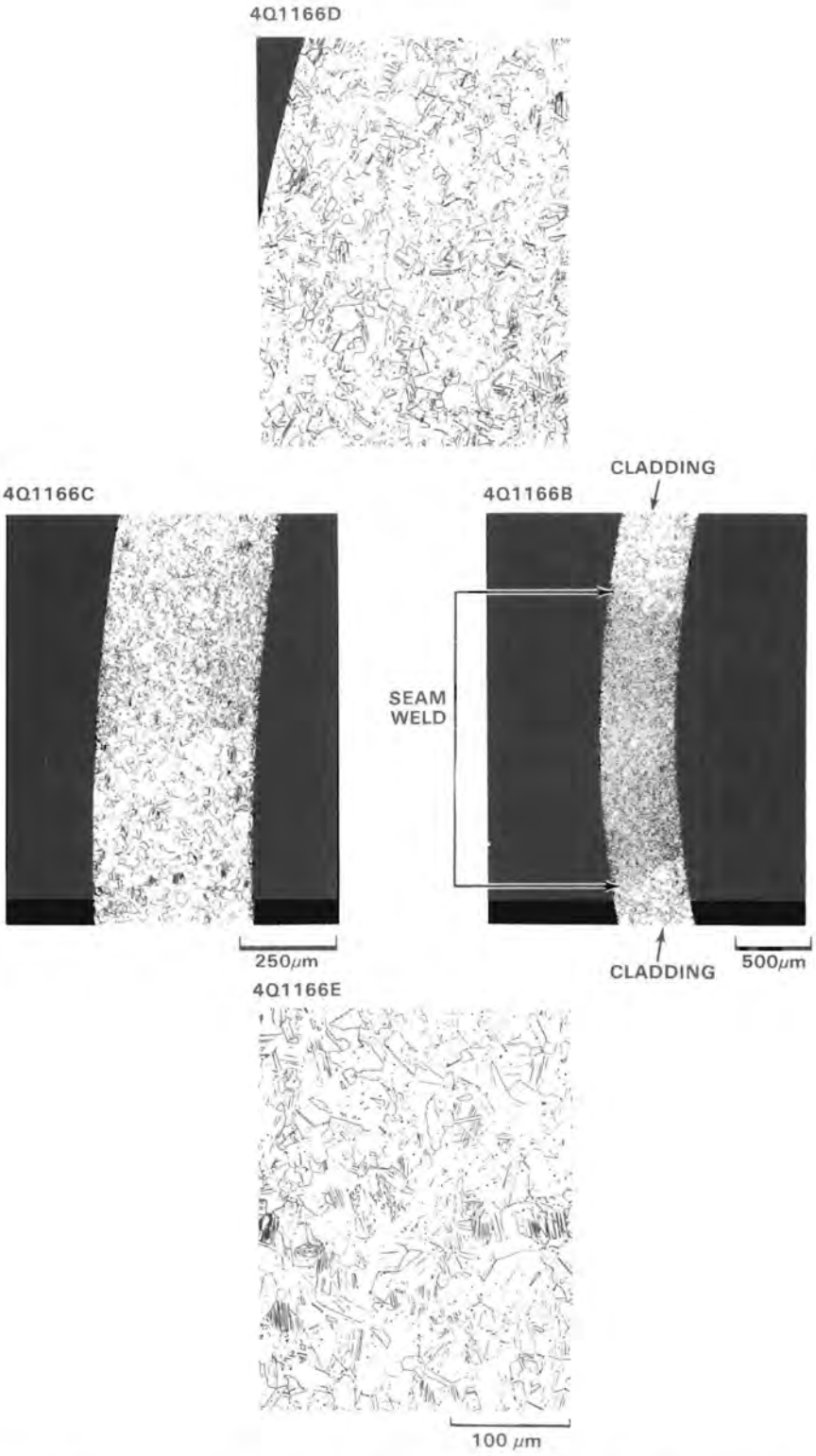

FIGURE 30. Metallography of Archive 304L Stainless Steel Cladding for Fuel Rods in the S004 Assembly (Oxalic Acid Etchant). See Table 2 for fabrication method.

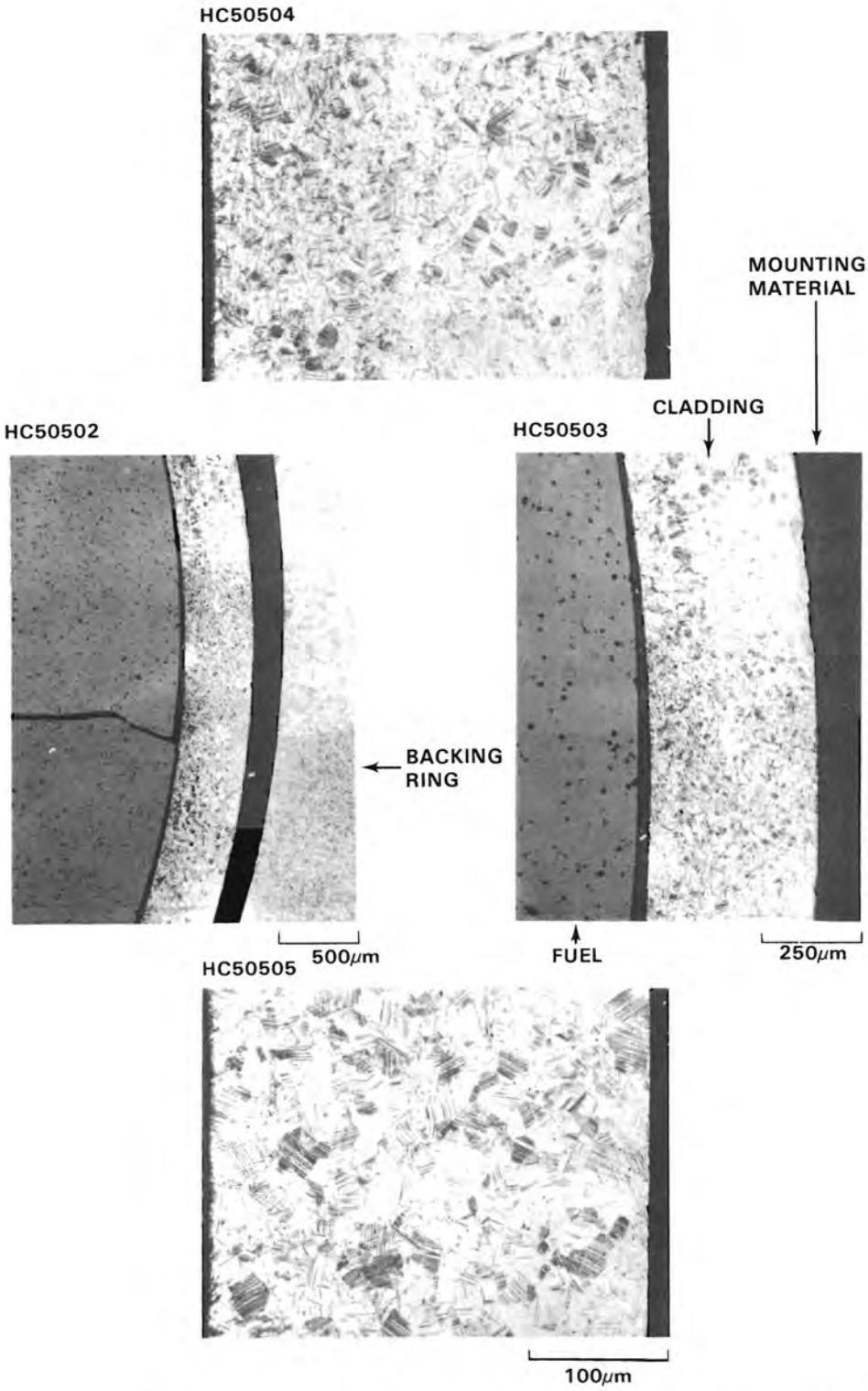

FIGURE 31. Metallography of Cladding from S004 Fuel Rod ABG, 56.75 in. (144 cm) Above Rod Bottom (Oxalic Acid Etchant)

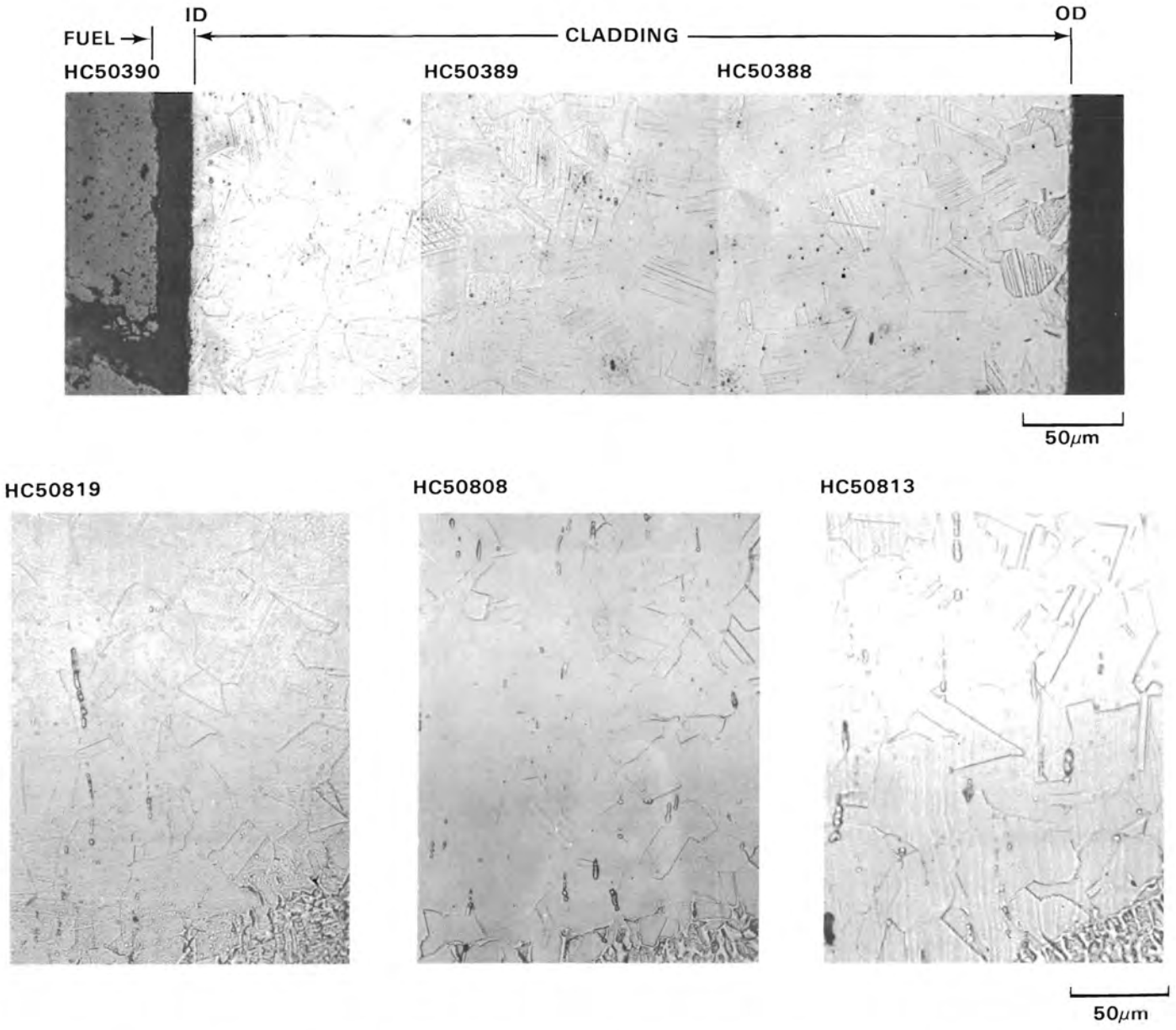

FIGURE 32. Metallography of Cladding from Connecticut Yankee Fuel Rods

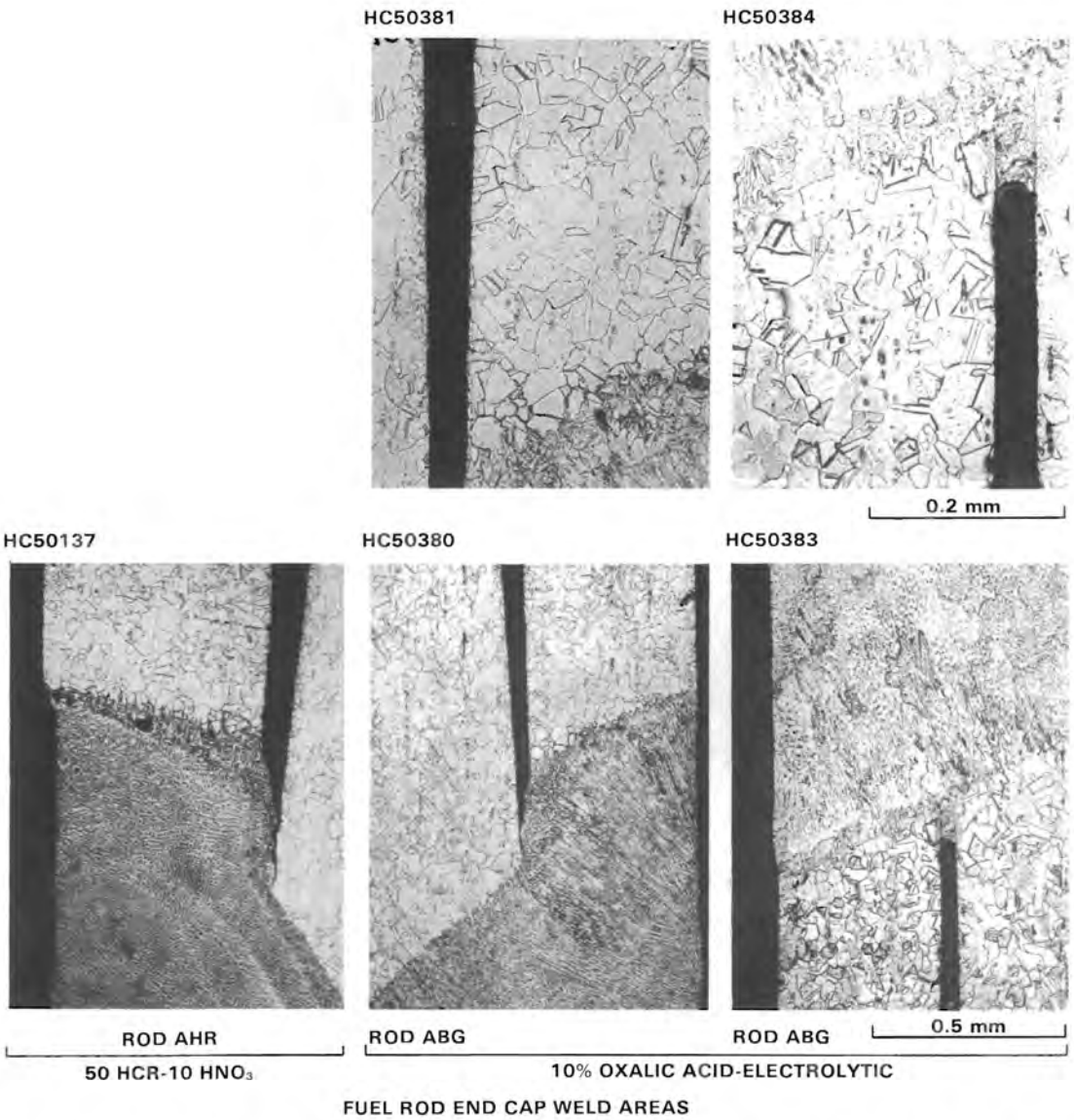

FIGURE 33. Metallography Showing the Heat-Affected Zone of End Cap Weld Areas from Connecticut Yankee Fuel Rods (Longitudinal Section; Etched Condition)

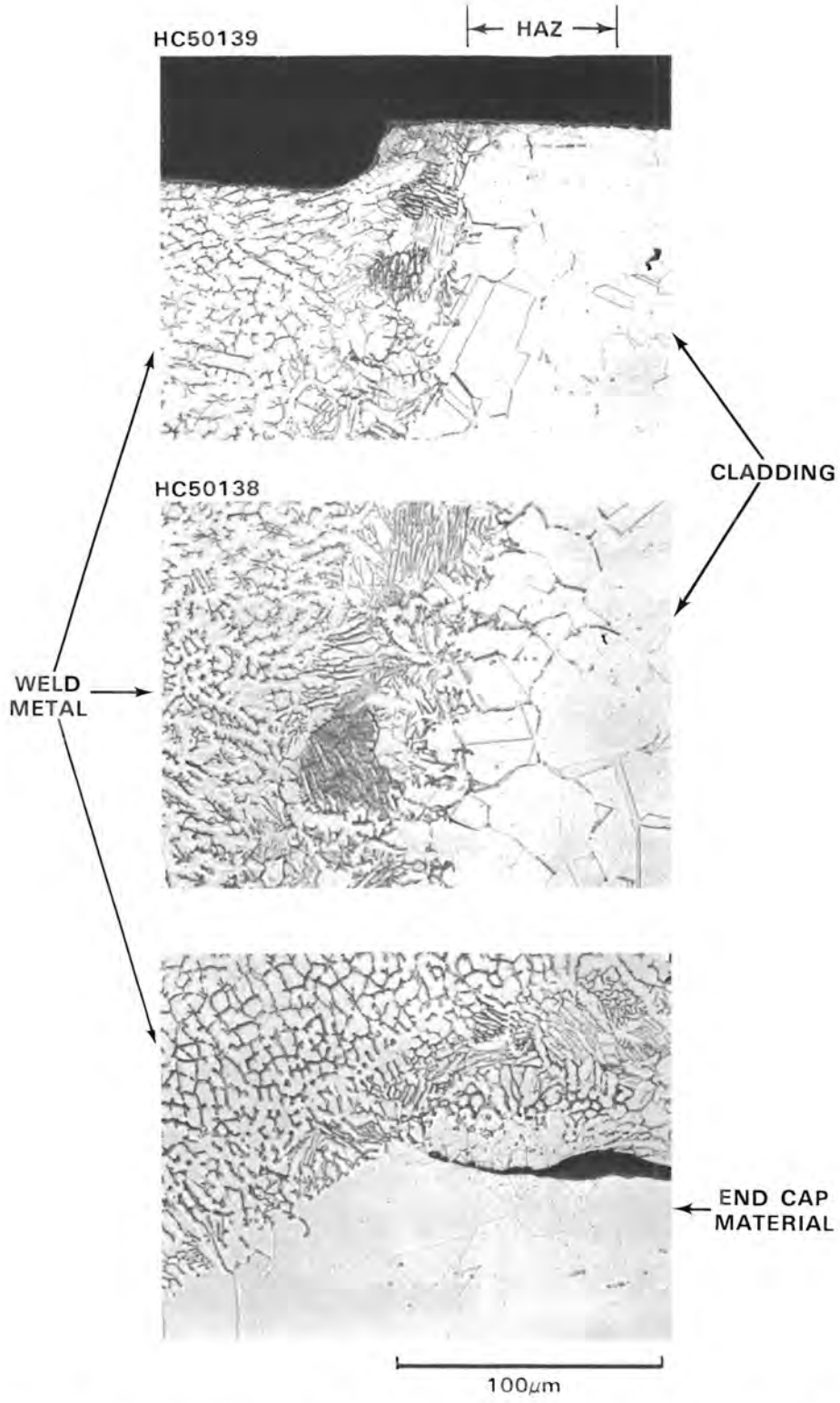

FIGURE 34. Metallography of Weld Heat-Affected Zone (HAZ) from the Lower End Cap, Fuel Rod AHR, Assembly S004 (Longitudinal Section; Etchant 50 HCl-10 HNO_3)

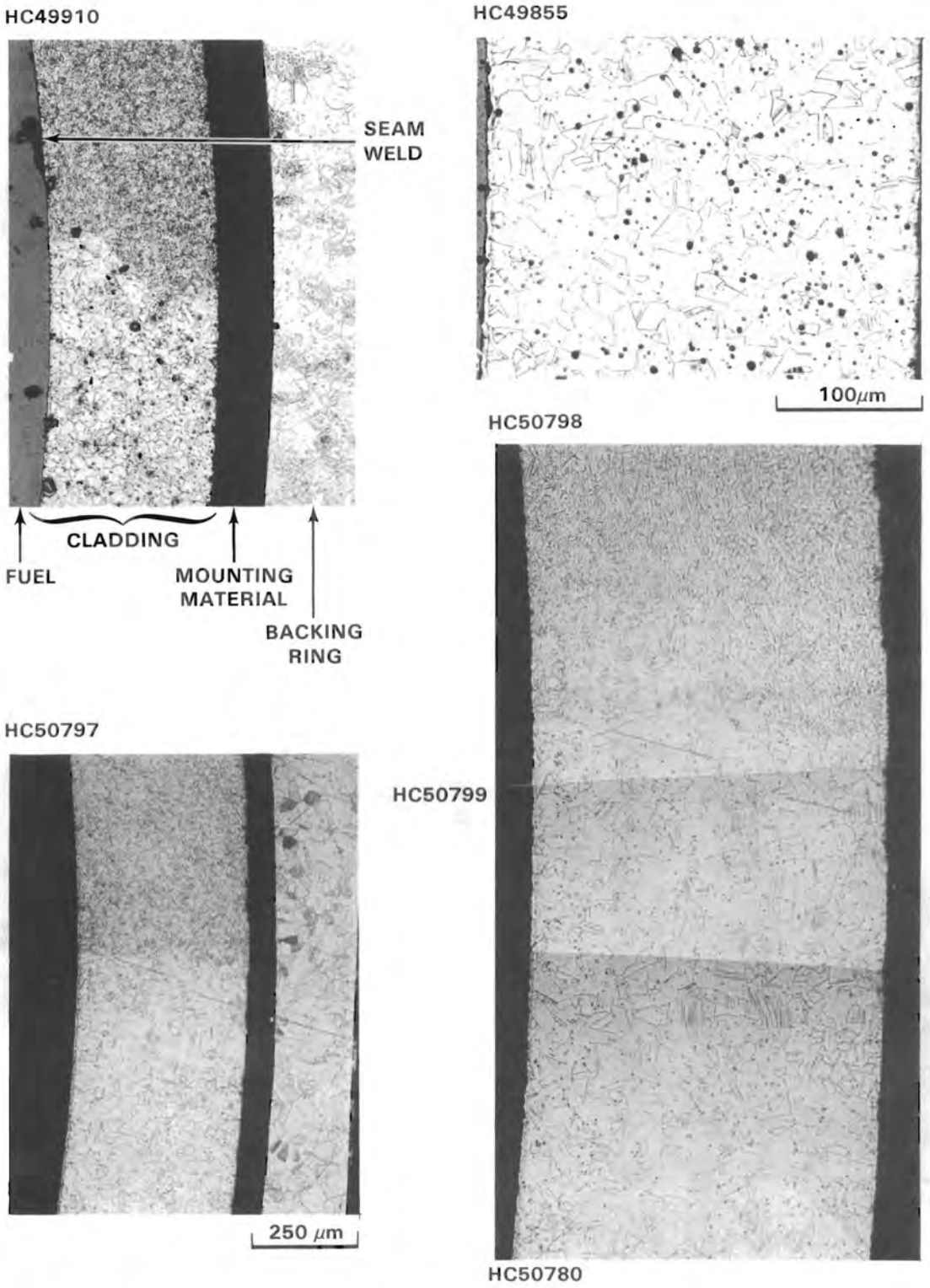

FIGURE 35. Metallography of Surface Condition of Fuel Rods from Connecticut Yankee Fuel Assemblies G11 and H07 (Transverse Sections; Oxalic Acid Etchant)

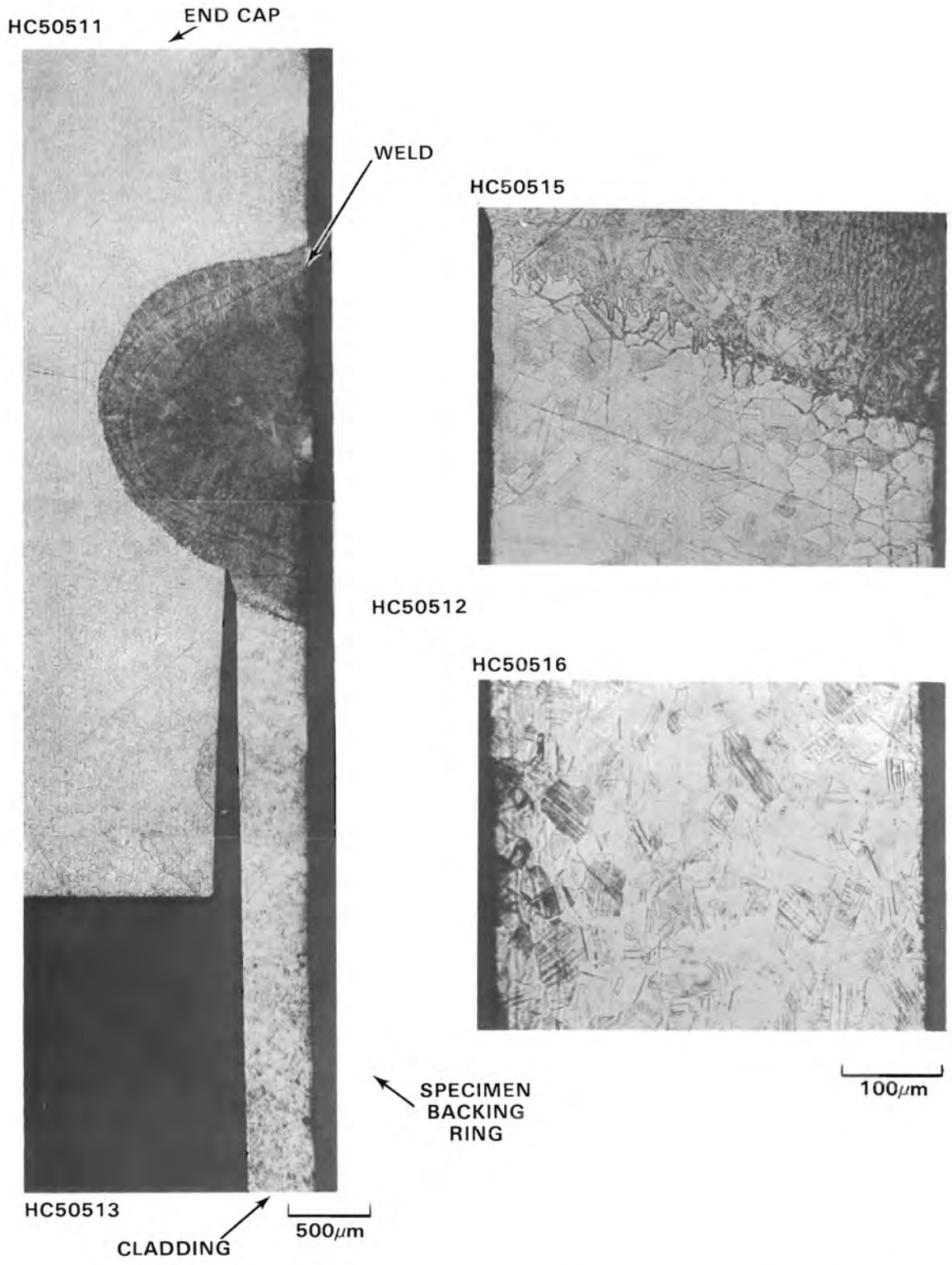

FIGURE 36. Metallography of Weld Area of Upper End Cap from S004 Fuel Rod ABG (Longitudinal Section; Oxalic Acid Etchant)

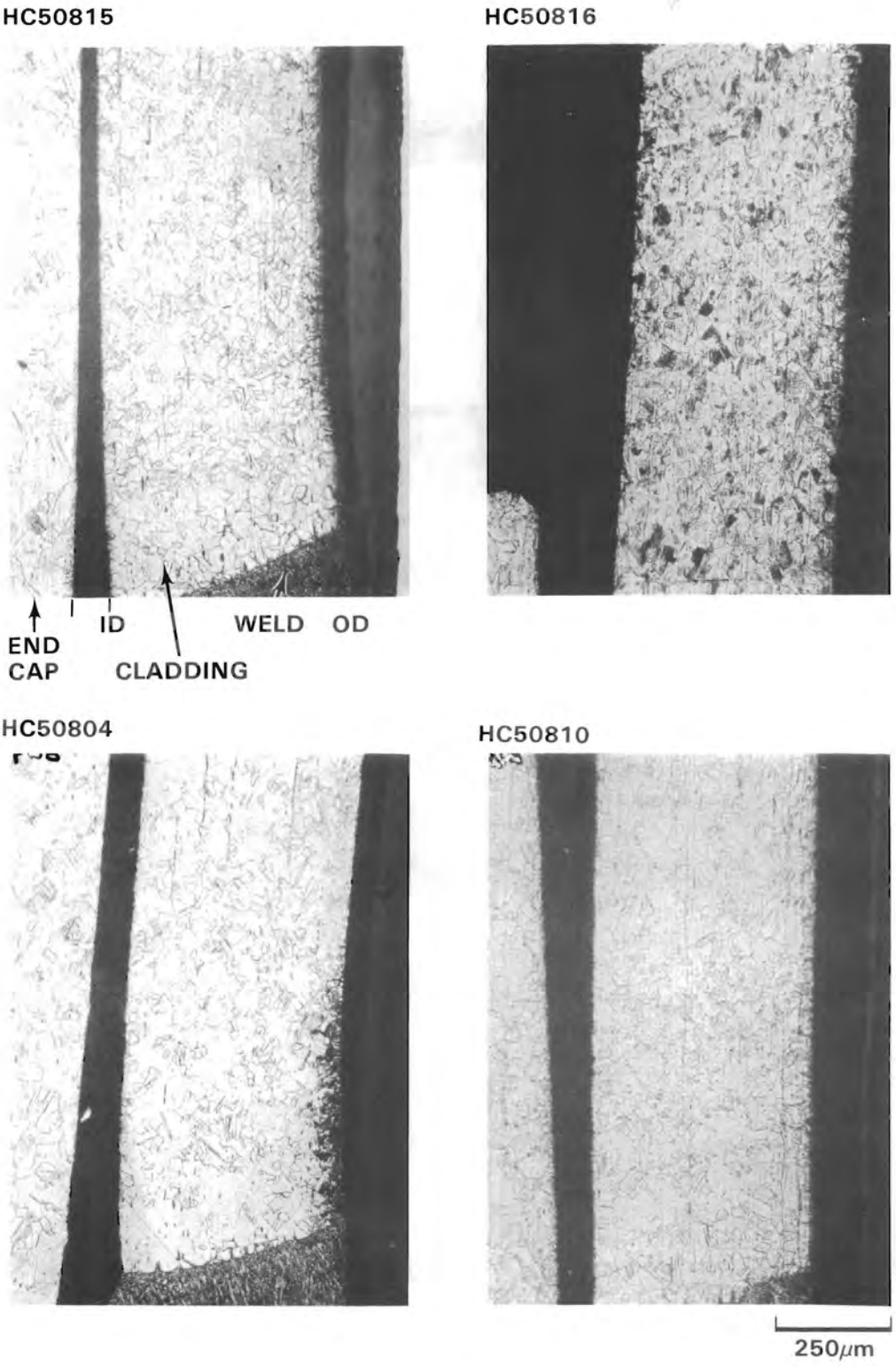

FIGURE 37. Metallography of Cladding Adjacent to Lower End Cap Welds from Connecticut Yankee Fuel Rods (Longitudinal Section; Oxalic Acid Etchant)

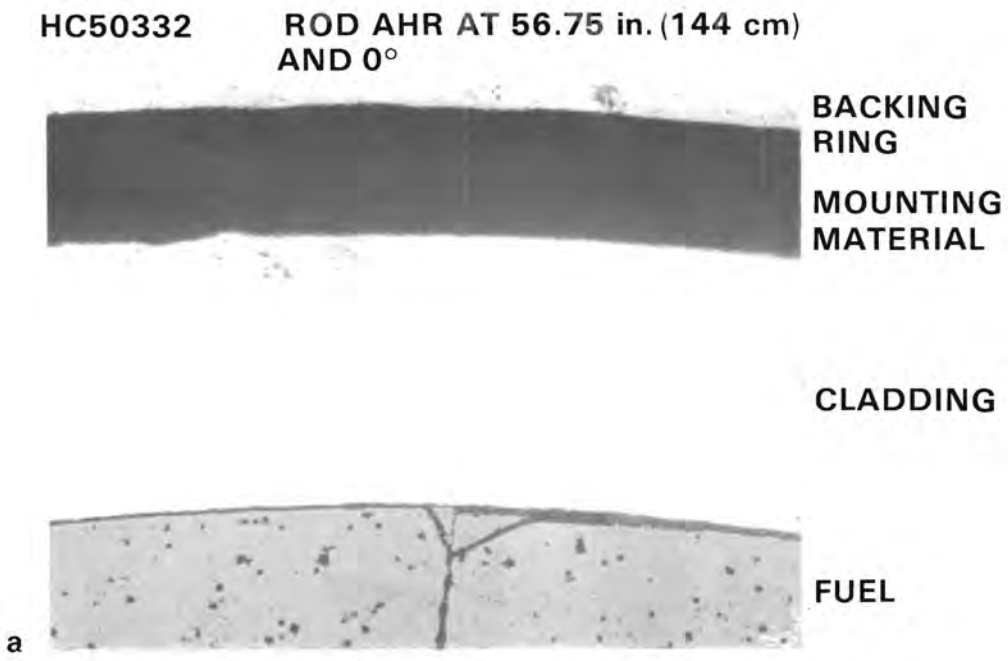

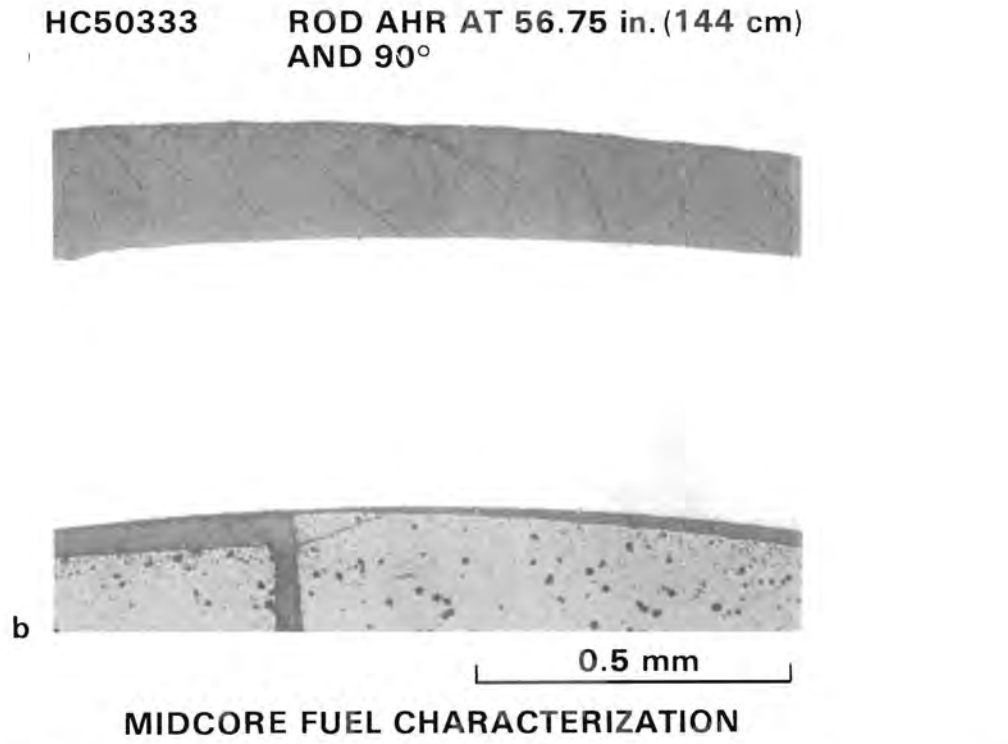

FIGURE 38. Typical As-Polished Transverse Sections of Cladding and Fuel from Rod AHR Showing the Clean Cladding Interior and Exterior Surfaces, i.e., Free of Measurable Crud or Oxide (or Other Reaction) Layers

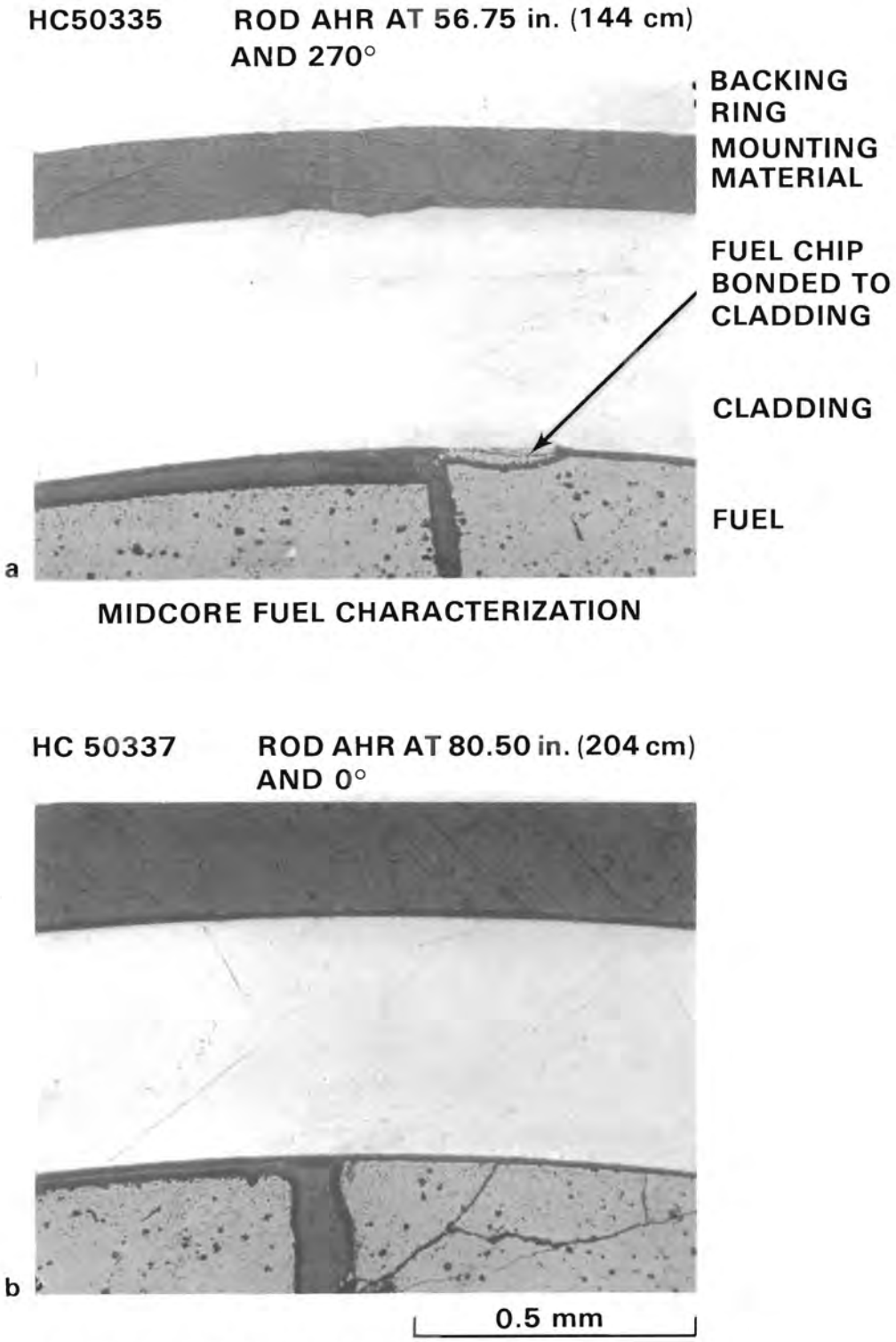

FIGURE 39. Typical As-Polished Transverse Sections of Cladding and Fuel from Rod AHR Showing the Clean Cladding Interior and Exterior Surfaces, i.e., Free of Measurable Crud or Oxide (or Other Reaction) Layers

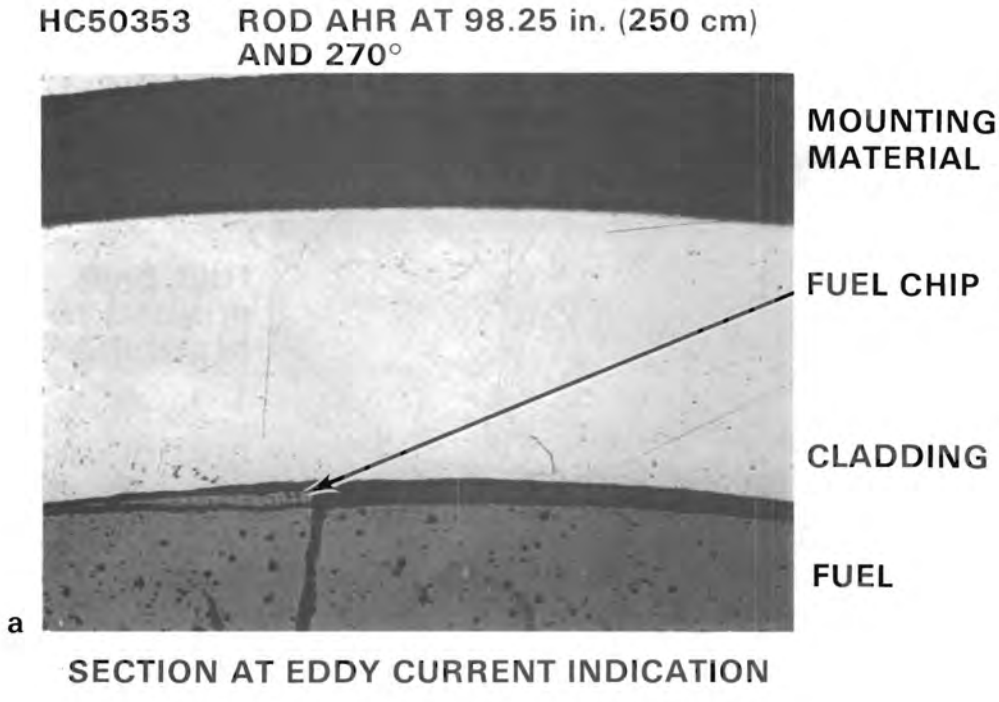

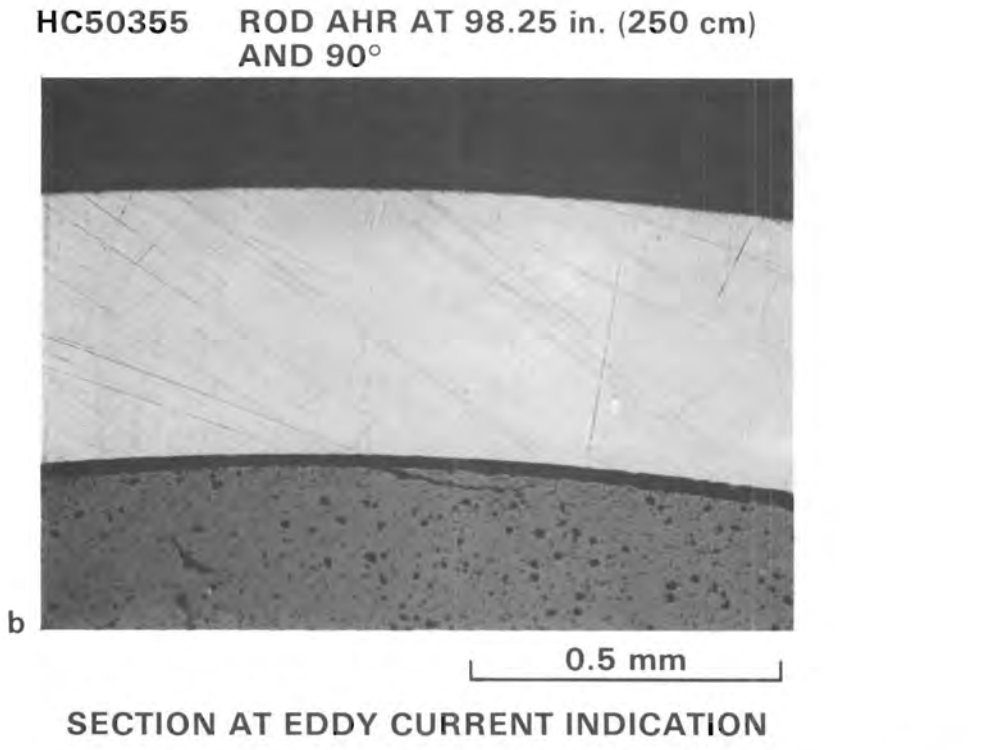

FIGURE 40. Typical As-Polished Transverse Sections of Cladding and Fuel from Rod AHR Showing the Clean Cladding Interior and Exterior Surfaces, i.e., Free of Measurable Crud or Oxide (or Other Reaction) Layers. The fuel chip in the upper photograph is much smaller than the chips observed in fuel rods from assembly H07.

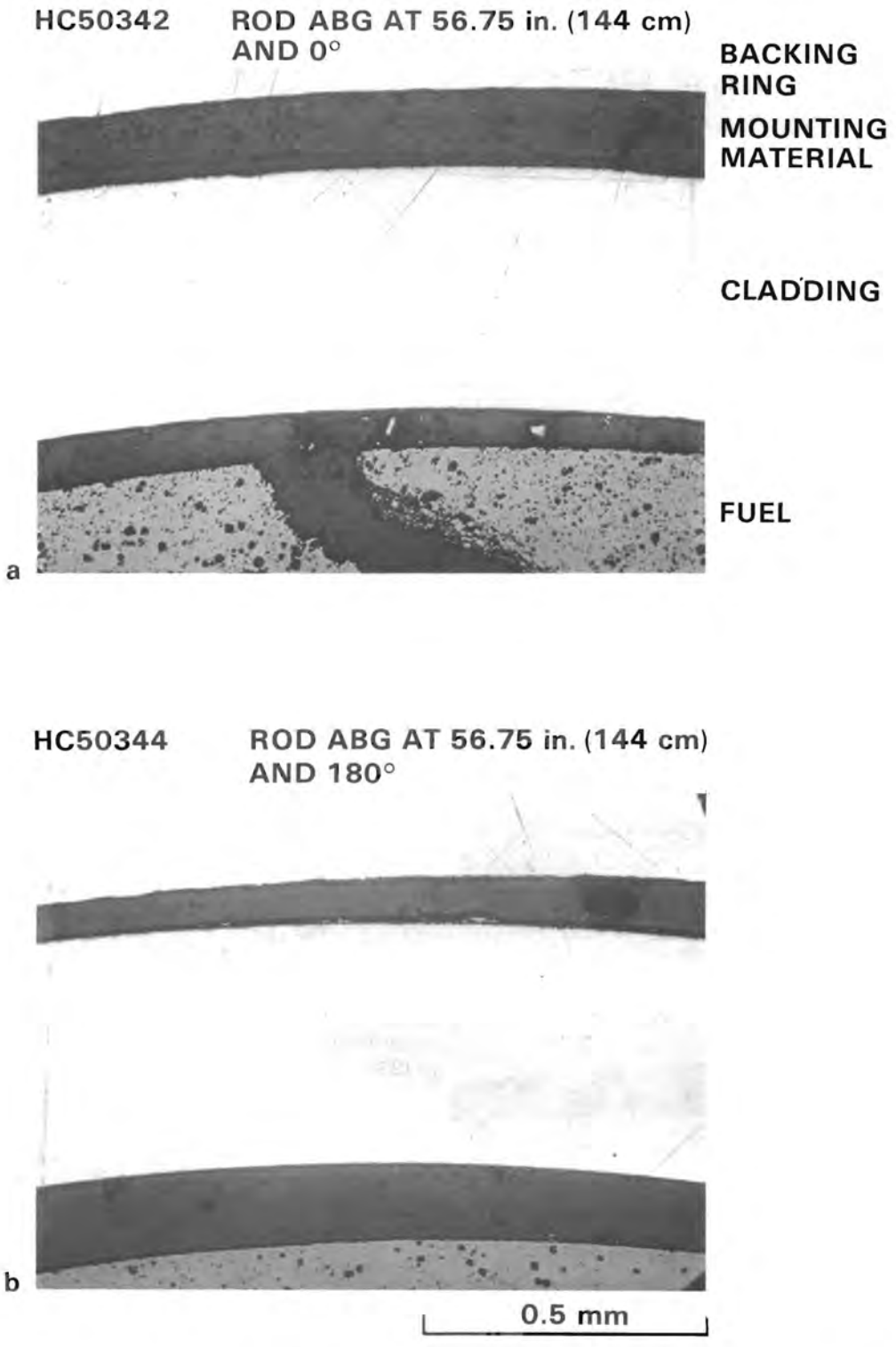

FIGURE 41. Typical As-Polished Transverse Metallographic Sections of Cladding and Fuel from Rod ABG Showing the Essentially Clean Cladding Interior and Exterior Surfaces, i.e., Free of Measurable Crud or Oxide Layers

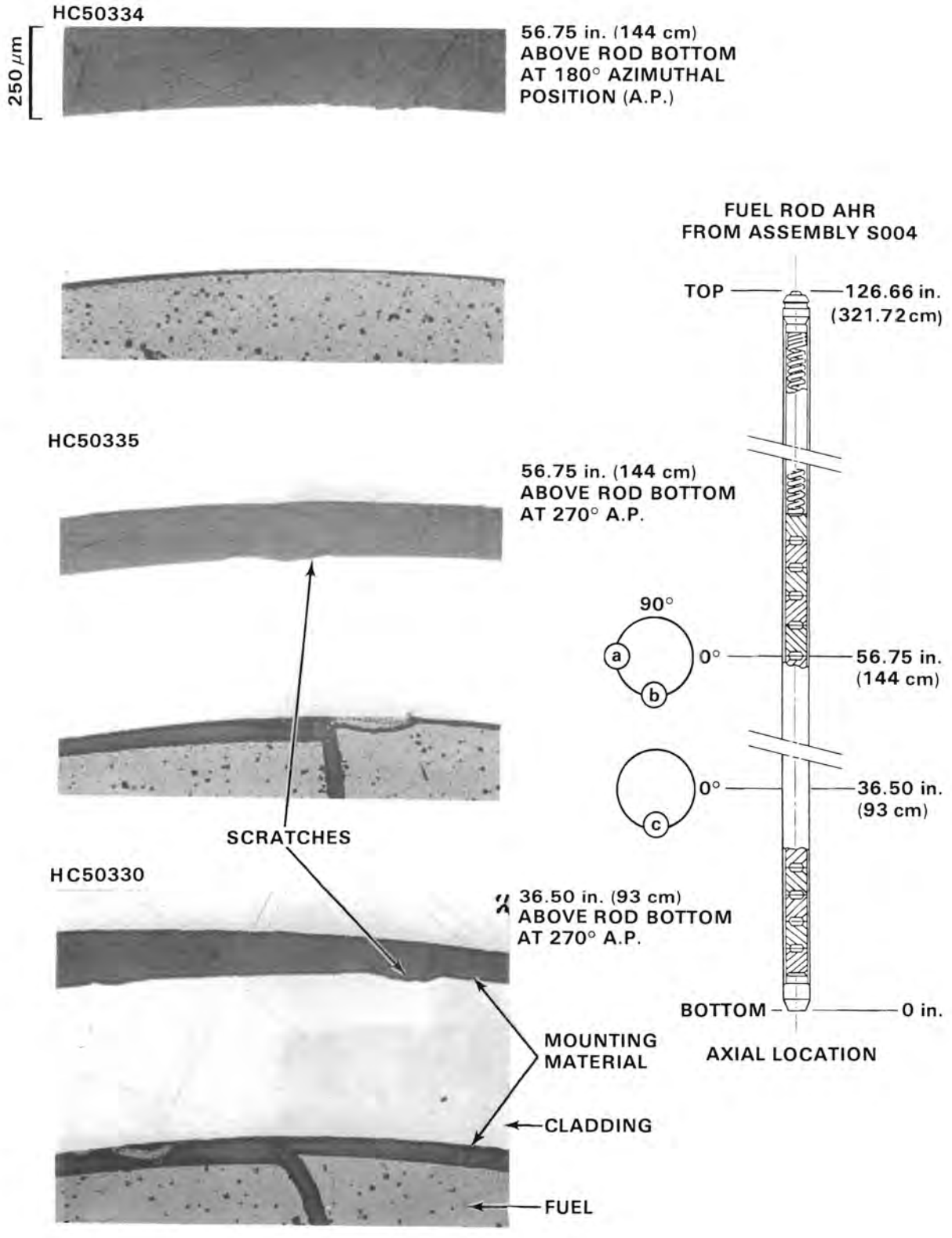

FIGURE 42. As-Polished Transverse Metallographic Sections of Fuel Rod AHR from Assembly S004 Showing Axial Scratches

FIGURE 43. Metallography of ID and OD Surface Condition of Cladding from Connecticut Yankee Fuel Rods

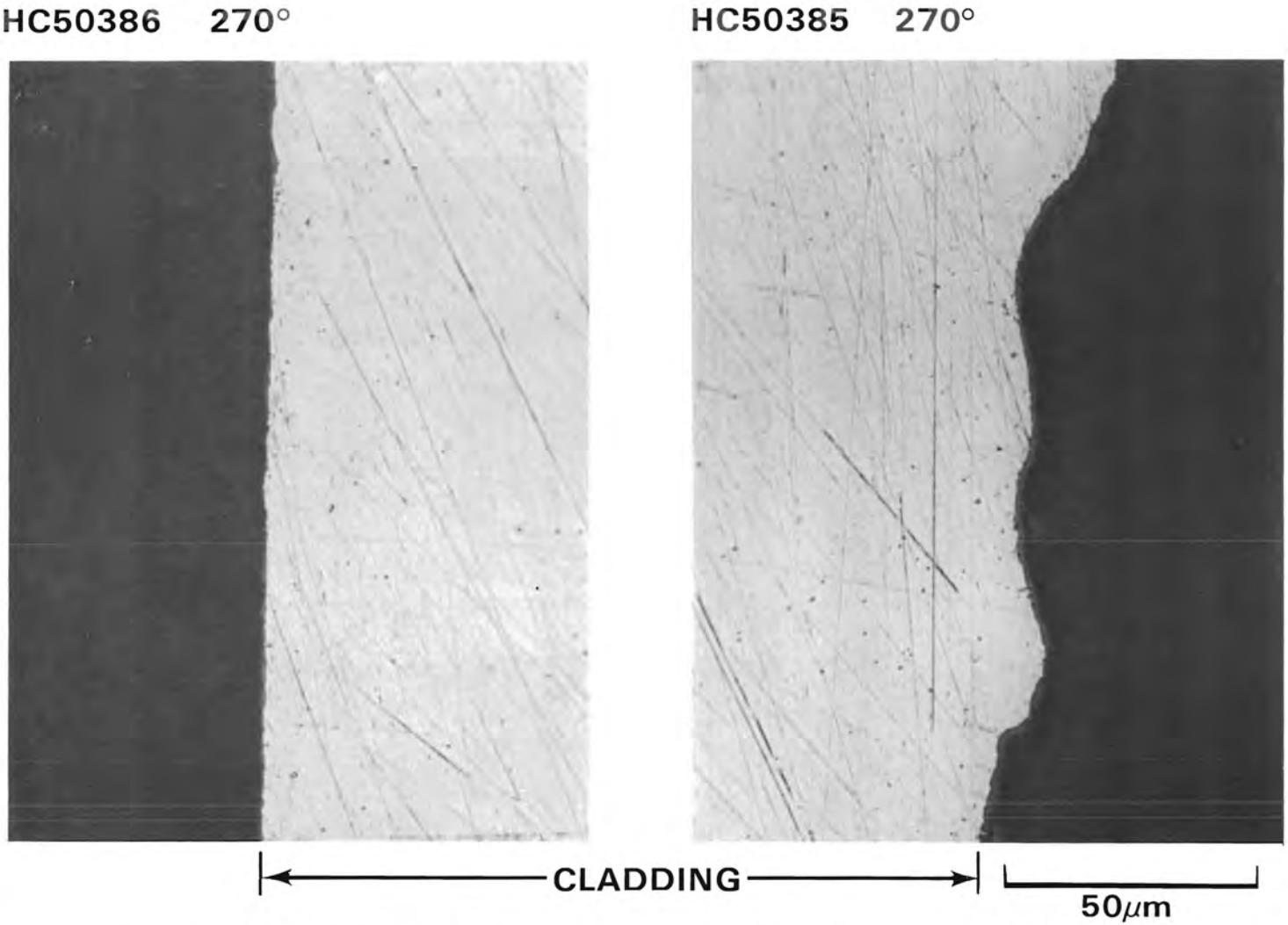

FIGURE 44. Surface Condition of Cladding OD from S004 Fuel Rod ABG at 41.50 in. (105 cm) Above the Bottom of the Rod. (a) Typical cladding exterior surface, smooth, free of surface layers. (b) Gouged area, typical of handling marks or the axial scratches caused by grid-spacer springs when rods are inserted into or withdrawn from the fuel assembly.

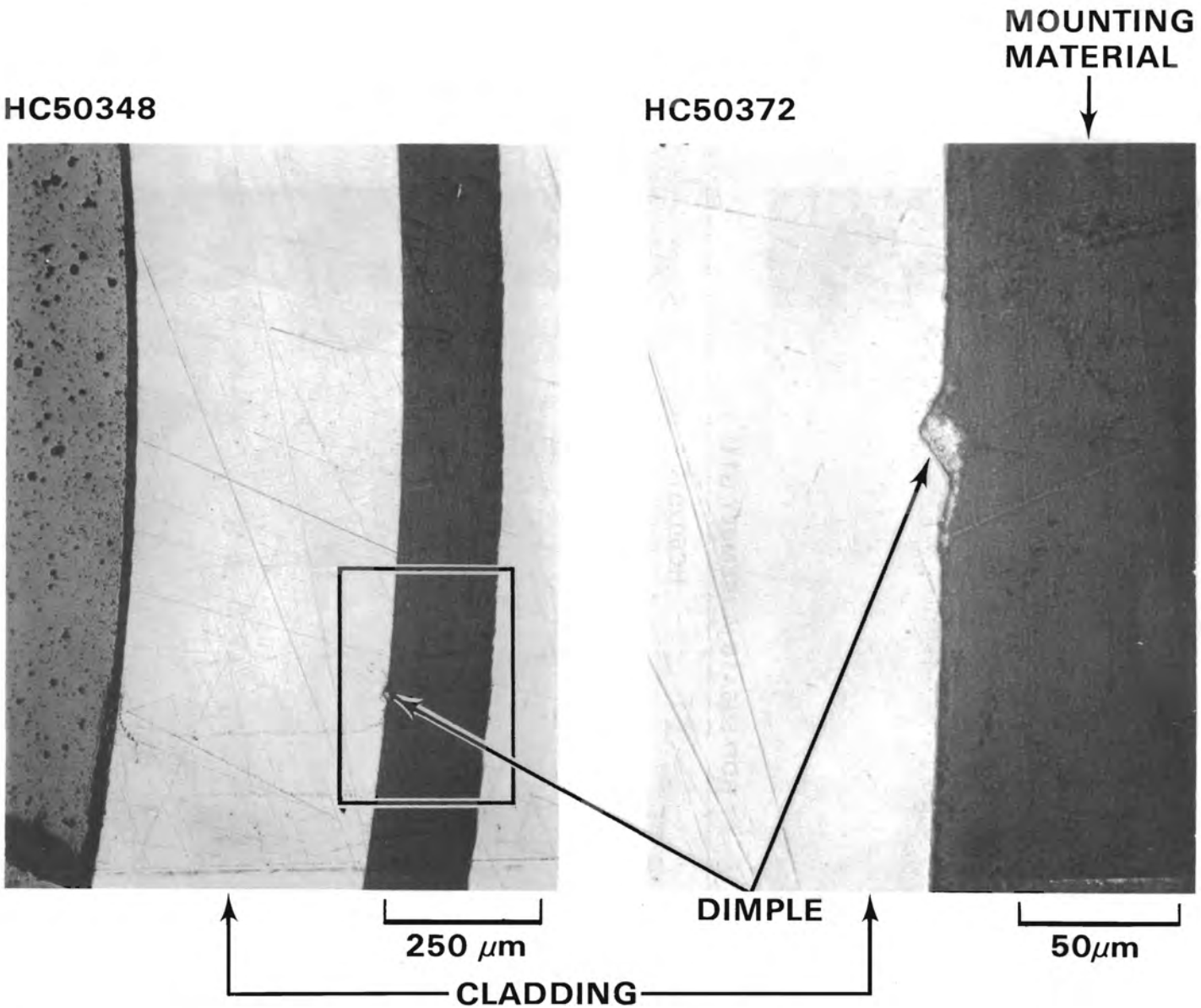

FIGURE 45. Metallography of Grid Spacer Dimple on Cladding OD from S004 Fuel Rod AHR. This transverse section was 83.75 in. (213) cm above rod bottom at 90° azimuthal position.

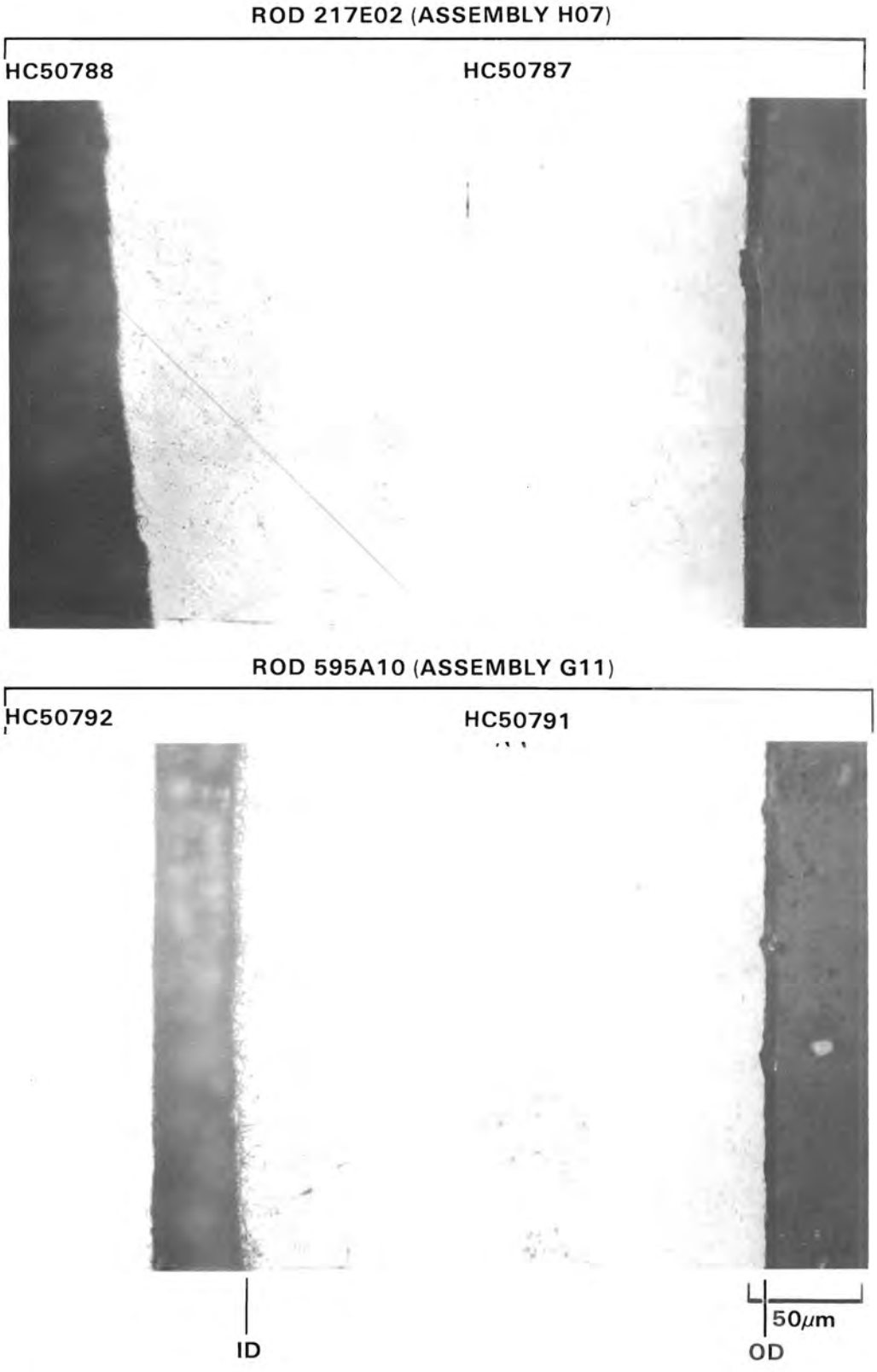

FIGURE 46. Metallography of ID and OD Surface Condition of Cladding from Connecticut Yankee Fuel Rods Near the Lower End Cap

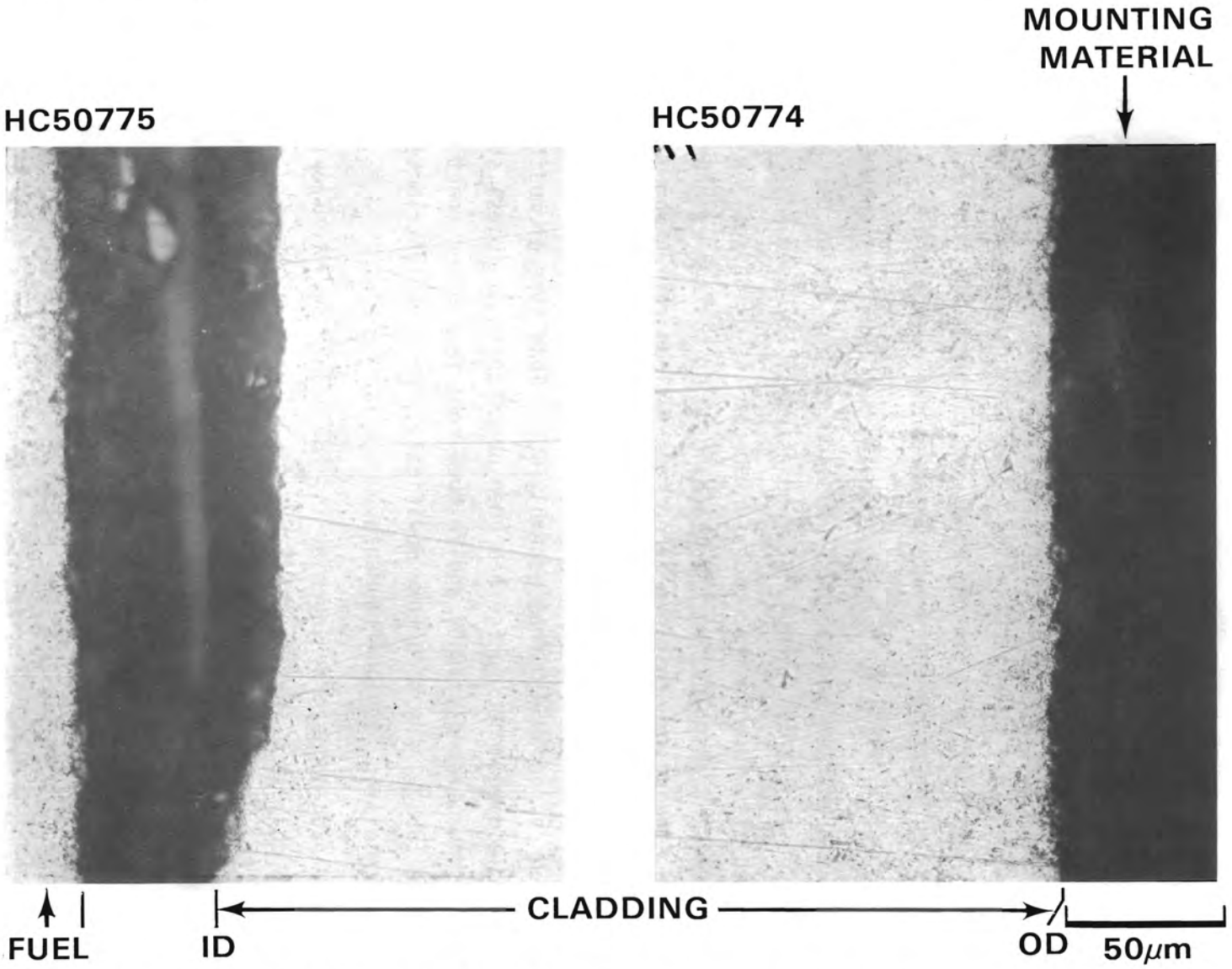

FIGURE 47. Metallography of Surface Condition of Cladding Near Lower End Cap on S004 Fuel Rod AHR

Metallography also revealed two distinct and unrelated types of surface layers on a few samples (Table 26). A darker gray layer occurred on the OD of some samples in the as-polished condition. A metallic layer of the same color as the cladding but with a different microstructure occurred on the cladding ID of a few samples in the etched condition. Another gray layer was detected at the fuel-cladding interface in a failed fuel rod that contained water.

Photomicrographs showed continuous layers of a darker gray substance on the cladding OD in a few local areas on S004 rods AHR (Figures 44 and 48) and ABG (Figures 34 and 45). Figure 49 shows surface layers in a region where a surface deposit was visible during the visual examination in the 270° orientation (see Figure 50). One area in the lower end cap from H07 rod 217E02 (Figure 46) showed an intermittent surface layer on the cladding ID.

The interior surfaces of the cladding from the two S004 rods were clean, i.e., no apparent degradation was caused by fission product attack or by oxidation. However, fuel rods from assembly G11 and assembly H07 (see Figure 35) did show a modified structure on the inner surface of the cladding. As in Figure 35(d), that modified structure on the cladding inner surface extends over the seam weld area, indicating that the effects of environment on the weld metal are metallurgically similar to the effects the base metal. Figure 51 is a view of the modified structure at higher magnification. A similar modified structure was noted in rod 595A10 from assembly G11. This type of modified structure on the cladding inner surfce has been observed in stainless steel-clad BWR fuel (Rosenbaum et al. 1966) and in fuel rods from other reactors (Barney and Wenple 1958). The structure modification has been attributed to damage caused by recoiling fission fragments.

The H07 rod 013E03 had a gray layer at the fuel-cladding interface. The layer was observed only in a fuel rod that had failed and had absorbed water. It is likely that the gray layer is a reaction product layer associated with the presence of water. The metallic and gray layers appeared only in the high-power regions in the fuel rods examined.

TABLE 26. Information on the Metallographic Examination of Fuel Rods from Connecticut Yankee Fuel Assemblies S004, H07, and G11

Thickness of Layer on Cladding OD (μm)	Fuel Assembly No.	Fuel Rod No.	Location (in.)[a]	Face on Metallographic Specimen	Magnification	Specimen Surface Condition	Comments	Negative No.
0.5	S004	AHR	LEC[b]	first	500X	Etched	Layer on cladding OD	HC50139
1-3	S004	AHR	LEC	second	500X	AP[c]	Layer on cladding OD	HC50776
0.5	S004	AHR	83-3/4	first	500X	AP	Layer on cladding OD	HC50372
3-5	S004	ABG	LEC	first	250X	AP	Layer on cladding OD	HC50366-69
3-5	S004	ABG	41-1/2	first	750X	AP	Layer on cladding OD	HC50385
--[d]	H07	013E03	--	--	--	--	No layer on cladding OD was evident	--
--	H07	157E01	--	--	--	--	No layer on cladding OD was evident	--
1	H07	217E02	LEC	--	500X	AP	--	HC50787
--	G11	595A10	--	--	--	--	No layer on cladding OD was evident	--
Thickness of Layer on Cladding ID, (μm)								
--	S004	AHR	--	--	--	--	No layer on cladding ID was evident	--
--	S004	ABG	--	--	--	--	No layer on cladding ID was evident	--
--	H07	013E03	27	--	500X	Etched	Gray layer on fuel OD	HC50454
--	H07	013E03	78-1/4	--	7X	AP	Thin gray layer part way around circumference of fuel pellet.	HC50248
--	H07	013E03	79	--	7X	AP		HC50287
6	H07	157E01	35-13/16	--	250X	Etched	Cladding ID had modified structure (thin)	HC49855
5	H07	157E01	64-1/16	--	100X	Etched	Cladding ID had modified structure (thin)	HC49910
--	H07	217E02	LEC	--	--	--	No longer on cladding ID was evident	--
--	H07	217E02	45-1/2	--	7X	AP	Modified structure on cladding ID	HC50793
--	H07	217E02	45-1/2	--	100X	Ap	Intermittent voids in layer at fuel-cladding interface	HC50794

(a) Inches above bottom end of fuel rod.
(b) Lower end cap (LEC).
(c) As-polished (AP).
(d) No entry.

TABLE 26. (contd)

Thickness of Layer on Cladding ID (μm)	Fuel Assembly No.	Fuel Rod No.	Location (in.)[a]	Face on Metallographic Specimen	Magnification	Specimen Surface Condition	Comments	Negative No.
3	H07	217E02	45-1/2	--	500X	AP	Intermittent voids in layer at fuel-cladding interface	HC50796
3	H07	217E02	45-1/2	--	100X	Etched	Cladding ID had modified structure that continued through weld area.	HC50797
1-2	H07	217E02	45-1/2	--	200X	Etched	Cladding ID had modified structure	HC50798-800
3	H07	217E02	45-1/2	--	500X	Etched	Cladding ID had modified structure	HC50801
--	G11	595A10	LEC	--	--	--	No layer on ID was evident	--
--	G11	595A10	44-3/4	--	100X	Etched	Modified structure on cladding ID	HC50820
--	G11	595A10	44-2/4	--	500X	Etched	Modified structure on cladding ID	HC50824
Fuel Chips Adhering to Cladding ID								
Yes	S004	AHR	56-3/4	--	7X	AP	--	HC50331
Yes	S004	AHR	56-3/4	--	100X	AP	--	HC50335
Yes	S004	AHR	80-1/2	--	7X	Ap	--	HC50336
No	S004	ABG	--	--	--	--	--	--
No	H07	013E03	--	--	--	--	--	--
No	H07	157E01	35-13/16	--	100X	AP	--	HC49887
No	H07	217E02	--	--	--	--	--	--
Yes	G11	595A10	44-3/4	--	500X	AP	--	HC50400
Yes	G11	595A10	44-3/4	--	500X	Etched	--	HC50430
Circumferential Cracking of UO_2 Fuel								
Only noted in in high power regions of fuel rods	--	--	--	--	--	--	Circumferential cracking of UO_2 noted mostly in H07 fuel rods, observed to a limited extent in G11 fuel rods, and not seen in S004 fuel rods.	--

FIGURE 48. Metallography of Surface Layer on Cladding from S004 Fuel Rod AHR

Surface roughness occurred in localized areas on cladding outer surfaces and was attributed to the effects of fabrication or to fuel handling operations. The rough surfaces shown in Figure 49 occurred at or below the lower end cap weld, an area that had been machined to remove the weld flash. The rough surface shown in Figure 44 is associated with a surface scratch,

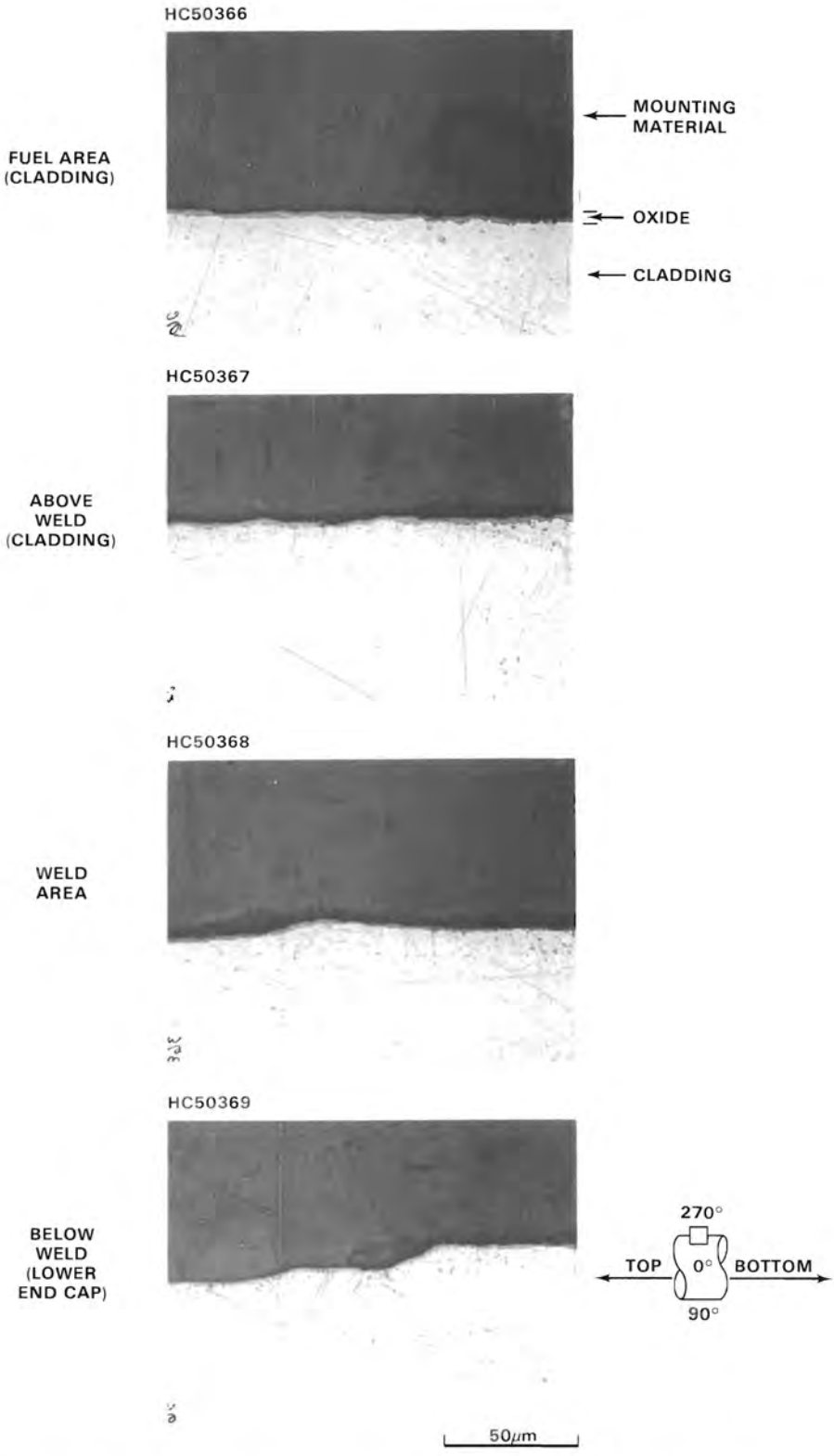

FIGURE 49. Metallography of Surface Layers at 270° Near the Lower End Cap on the Cladding from Fuel Rod ABG from Assembly S004

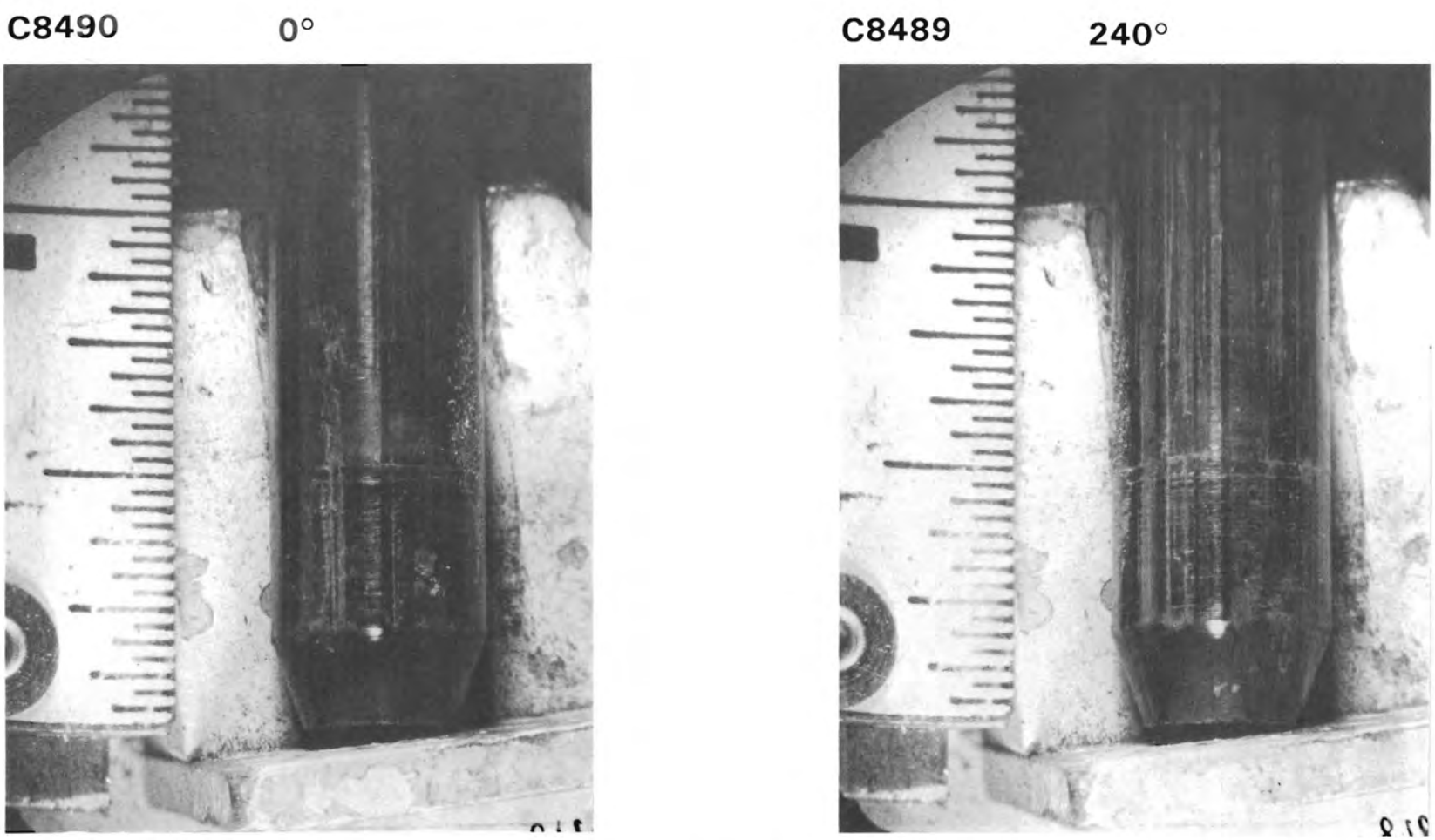

FIGURE 50. Surface Appearance of Lower End Cap Area of Fuel Rod ABG from Assembly S004

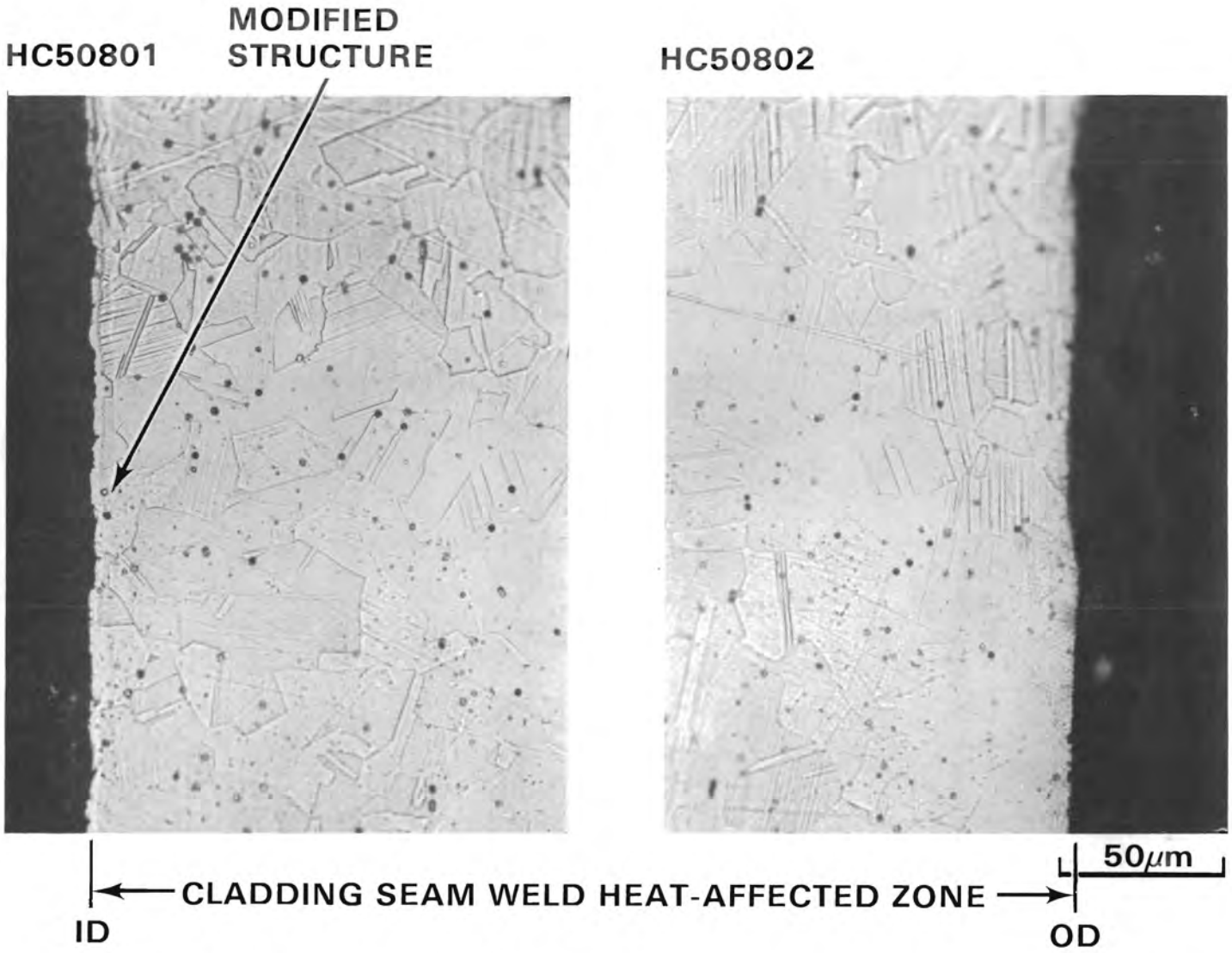

FIGURE 51. Surface Condition of Cladding from Connecticut Yankee Fuel Rod 217E02 from Assembly H07 Including the Detail of Modified Structure on the Cladding ID. Transverse section, 45.50 in. (116 cm) above the bottom of the rod. Oxalic acid etchant used.

probably a handling mark. In Figure 45, note a dimple formed in the cladding at a spacer grid spring contact apparently by fretting corrosion (see Figure 18 for visual examination results of a similar area). This is the extreme example observed of cladding surface damage caused by grid spacer contact. The depth of this dimple ($\sim$10 μm) was less than that of many handling marks.

The cladding thickness measurements in Table 27 were made from photographs of cladding in the as-polished condition at 100X magnification. The photographs were taken at 90° intervals. Three measurements were made from each photograph. No significant reduction in cladding thickness was discernible compared to the original cladding thickness.

The weld area of S004 rod ABG at the upper end cap was seen earlier in Figure 36. Areas of recrystallization occur adjacent to the weld in the end cap material and in the cladding. This figure also showed the weld metal, heat-affected zone, and base metal structures at higher magnification. Figure 37 showed the similarity of the microstructure of the cladding from the three fuel assemblies, as well as the difference in etching behavior between the cladding in the weld HAZ and the more remote base metal. The difference in lower end cap weld geometry between the S004 rods and the G11 rods is evident in Figure 52.

All structural and microstructural aspects of the welds in rods from the H07 and G11 assemblies are similar except for the appearance of the HAZ in the G11 rod, which does not appear to have the intergranular weld metal penetration seen in the H07 and S004 rods (see Figures 32, 33, and 37). The lower end cap welds in the S004 and H07 assemblies may have been made with a higher welding heat input resulting in some intergranular melting. Figure 34 illustrated the metallographic detail of the HAZ of rod AHR through the cladding thickness. Figure 33 showed HAZ metallographic detail for other S004 fuel rods.

The dendritic structure generally characteristic of the end cap welds in the fuel rods is shown in Figure 53. From the limited data available, the welds in the three assemblies appear very similar. This similarity is not unexpected since the welding processes and practice used in the nuclear fuel fabrication industry are closely controlled.

TABLE 27. S004 Cladding Thickness Measurements

Specimen	Neg No.	Magnification (Nominal)	Measured Thickness (in. x 10^{-3})	Cladding Thickness, Average of Group (in.) At 100X	Cladding Thickness, Average of Group (in.) With Calibration Correction (x 1.015)
Archive (Etched)	PNL	100X	1.67		
			1.61		
			1.66	0.01663	0.01688[a]
AHR 56.75 in. (A.P.)[b]	BCL-332	100X	1.63		
		"	1.64		
	BCL-333	100X	1.66		
		"	1.66		
		"	1.66		
	BCL-334	100X	1.66		
		"	1.65		
		"	1.66		
	BCL-335	100X	1.63		
		"	1.62		
			1.64		
				0.01647 ±0.00014	0.01672[a]
ABG 56.75 in.	BCL-342	100X	1.63		
		"	1.64		
		"	1.64		
	BCL-343	100X	1.65		
		"	1.65		
		"	1.65		
	BCL-344	100X	1.65		
		"	1.65		
		"	1.65		
	BCL-345	100X	1.64		
		"	1.64		
		"	1.64		
				0.01644 ±0.00007	0.01669[a]
Archive[c] (A.P.)	PNL -0° (weld)	100X	1.66		
		"	1.66		
		"	1.66		
	PNL-90°	100X	1.68		
		"	1.68		
		"	1.68		
	PNL-180°	100X	1.68		
		"	1.68		
		"	1.68		
	PNL-270°	100X	1.65		
		"	1.66		
		"	1.65	0.01668 ±0.00013	0.01675[d]

(a) Calibration correction factor was 1.015
(b) A.P. = as polished
(c) Specimen reworked on February 17, 1981.
(d) Calibration correction factor was 1.004.

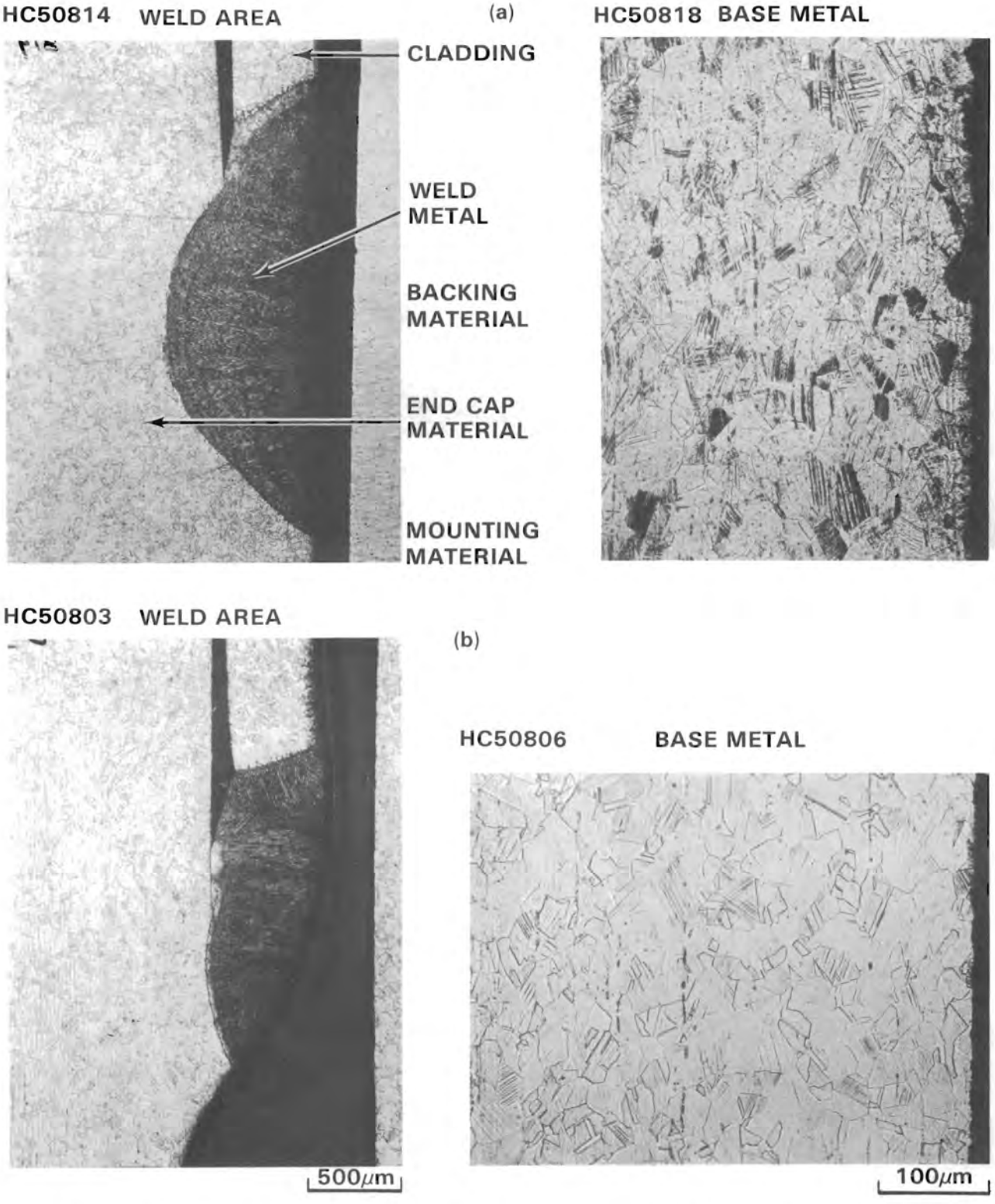

FIGURE 52. Metallography of Weld Area and Base Metal Near Lower End Cap Weld Areas of Fuel Rods (a) AHR from Assembly S004 and (b) 217E02 from Assembly H07

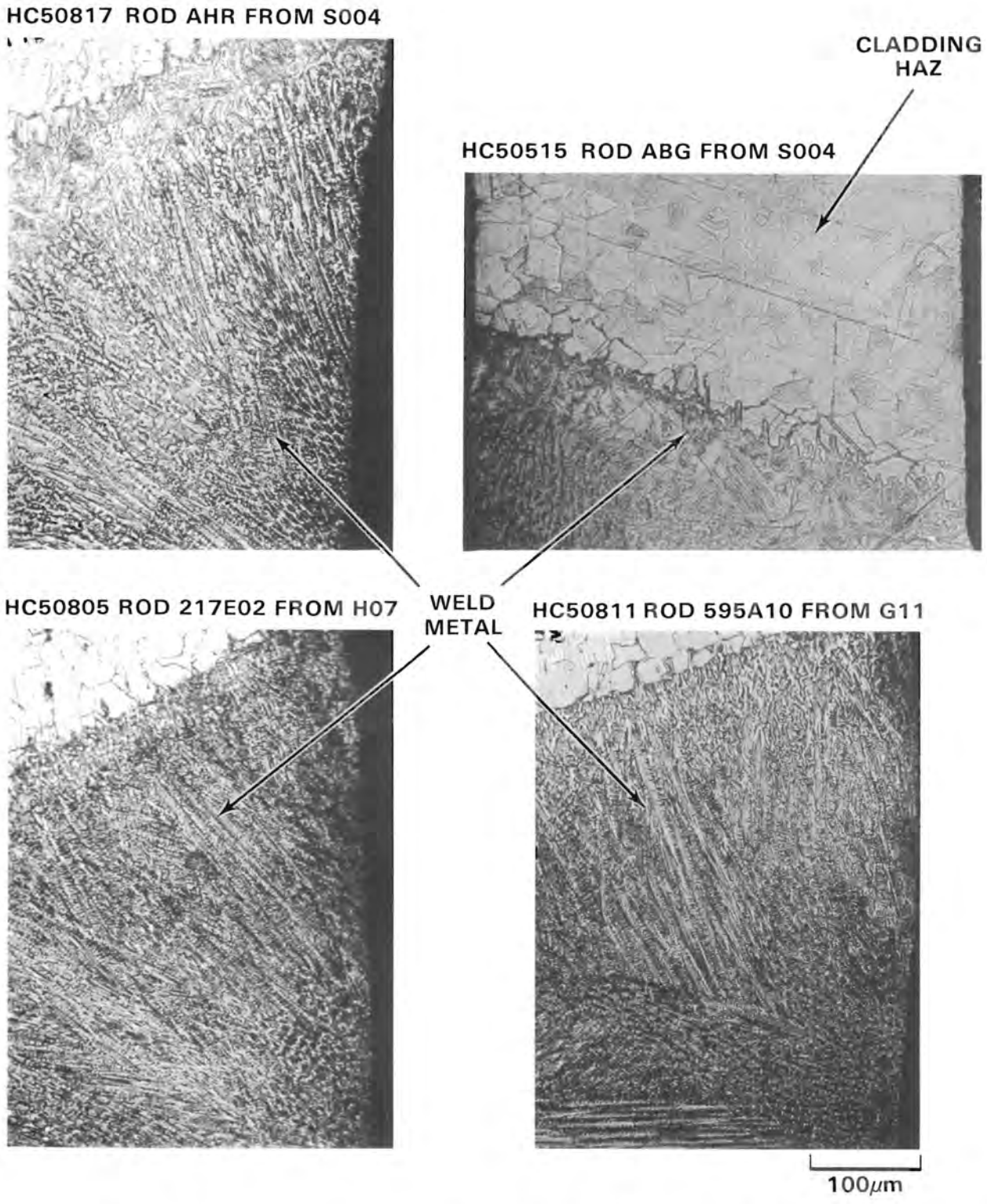

FIGURE 53. Metallography of Weld Metal from End Cap Welds from Connecticut Yankee Fuel Rods (HAZ = heat-affected zone)

Cladding ovality was evident in the macrographs shown in Figures 54 through 60, especially in the sections at 56.75 in. (144 cm) above the bottom of the rod in both ABG and AHR. The fuel-cladding gap was larger in rod ABG than in AHR. The fuel-cladding gap was very small in the G11 rod and essentially nil in the H07 rods.

Fuel rods from both S004 and G11 showed some cases of fuel chips adhering to the cladding ID. No adherent fuel chips were observed in the H07 rods.

Circumferential fuel cracking was observed in fuel rods from the H07 assembly. Circumferential cracks were less pronounced and fewer in rods from the G11 assembly, and none were observed in rods from the S004 assembly. The circumferential cracking occurred only in high-power regions of the fuel rod.

Ceramography

Ceramographic specimens were examined to document fuel pellet cracking and chipping and such fuel microstructural features as porosity, grain size, and metallic fission product inclusion formation.[a] Specimen preparation was identical to that for metallography specimens through the polishing operation. Ceramography specimens were examined in both as-polished and etched conditions. The etchant used for examination of fuel microstructure consisted of 85 parts H_2O_2 and 15 parts concentrated H_2SO_4. The macrographs of the as-polished fuel clearly show pellet cracking (Figures 55 through 60). Radial cracks are the most pronounced, but there is not circumferential cracking comparable to that seen in the high-power regions of the fuel rods from assemblies G11 and H07. Figures 38 through 40 showed that there were pellet chips in S004 fuel rods. However, no fuel pellet chips were found lodged in the fuel-cladding gap. Pellet chips were found lodged in the fuel-cladding gap in the G11 and H07 fuel

(a) The term "metallic fission product inclusions" is typically used with light-water reactor fuels (Garzarolli and Manzel 1979). The term "metallic fission product ingots" is typically used with fast reactor fuels (Zhou and Olander 1981).

HC50326

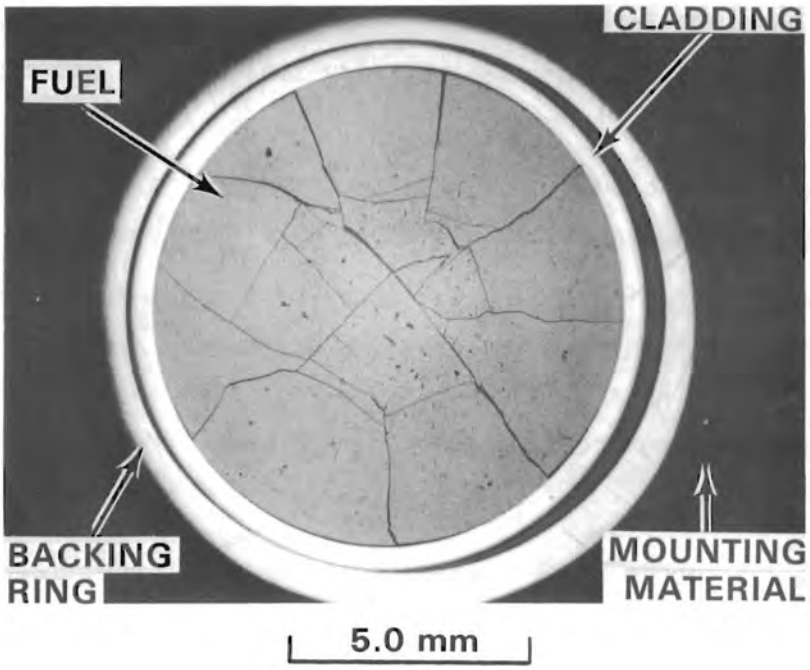

FIGURE 54. As-Polished Macrograph of Rod AHR at 36.50 in. (93 cm) from Bottom End

HC50331

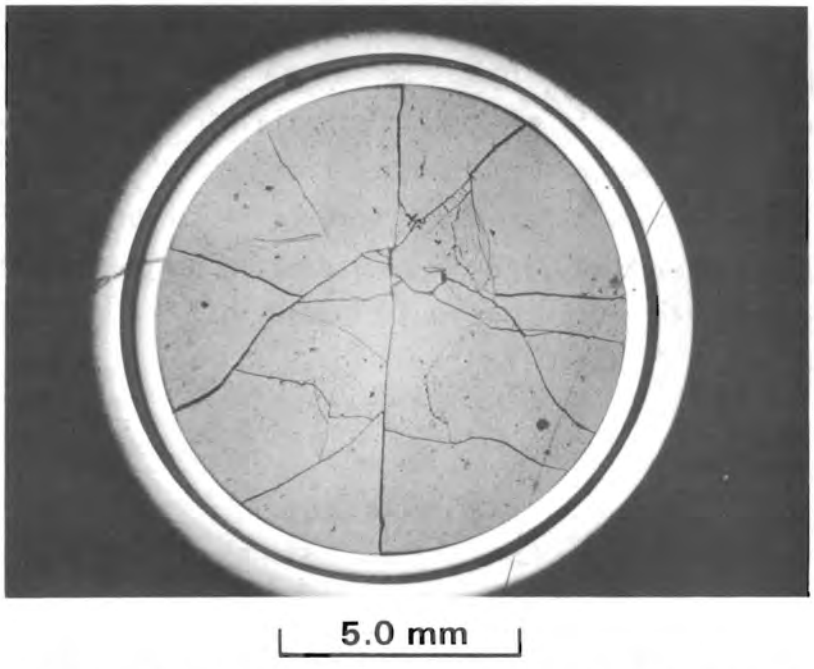

FIGURE 55. As-Polished Macrograph of Rod AHR at 56.75 in. (144 cm) from Bottom End

HC50336

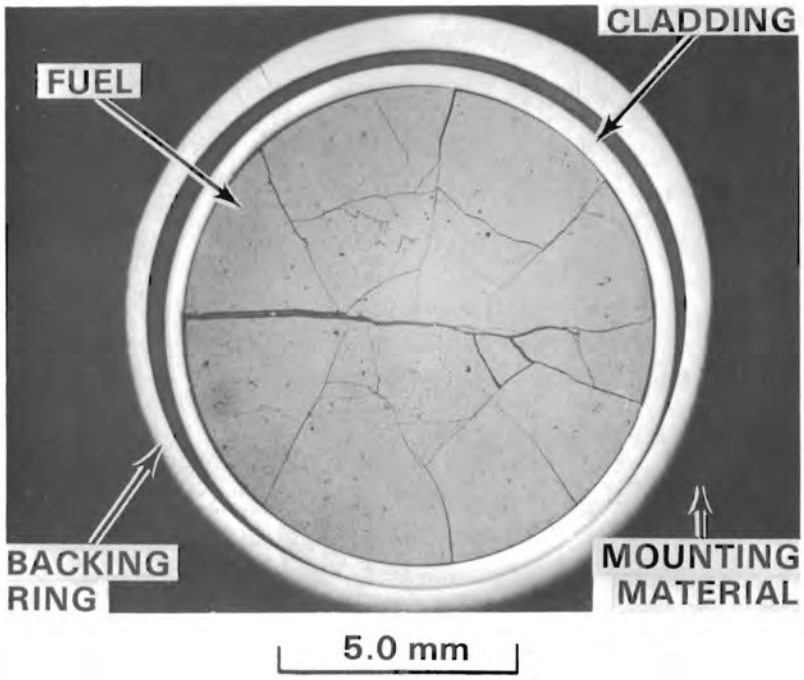

FIGURE 56. As-Polished Macrograph of Rod AHR at 80.50 in. (204 cm) from Bottom End

HC50346

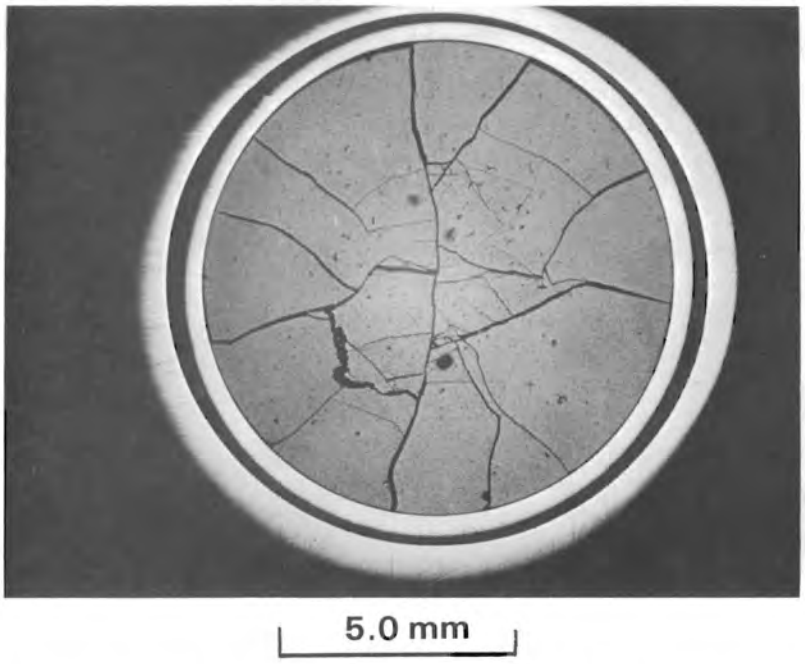

FIGURE 57. As-Polished Macrograph of Rod AHR at 83.75 in. (213 cm) from Bottom End

HC50351

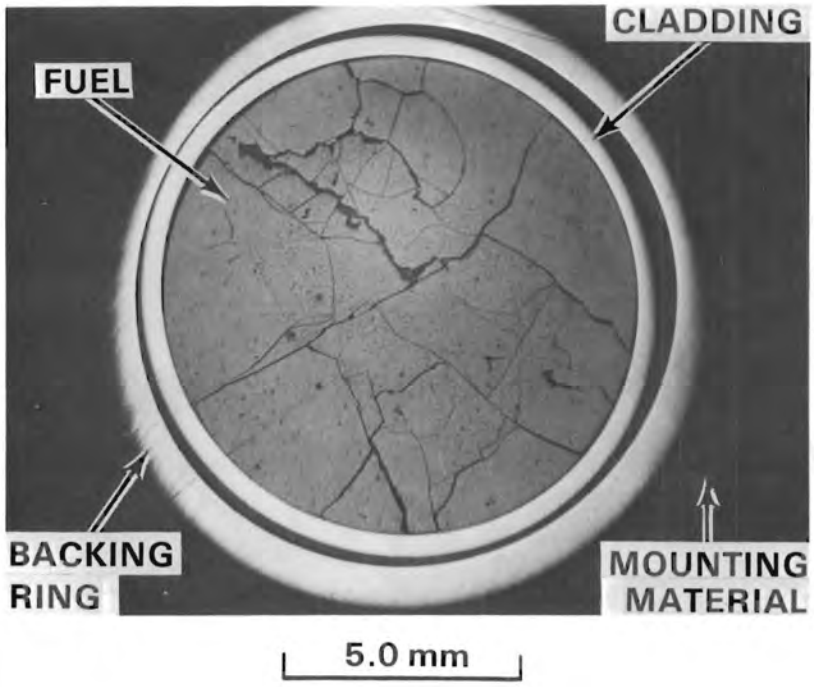

FIGURE 58. As-Polished Macrograph of Rod AHR at 98.25 in. (250 cm) from Bottom End

HC50356

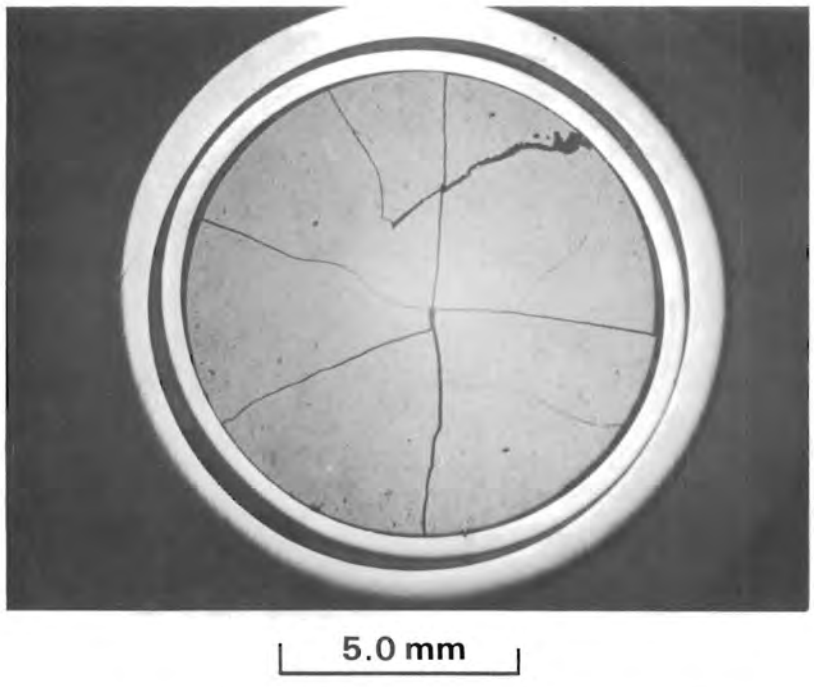

FIGURE 59. As-Polished Macrograph of Rod ABG at 41.50 in. (105 cm) from Bottom End

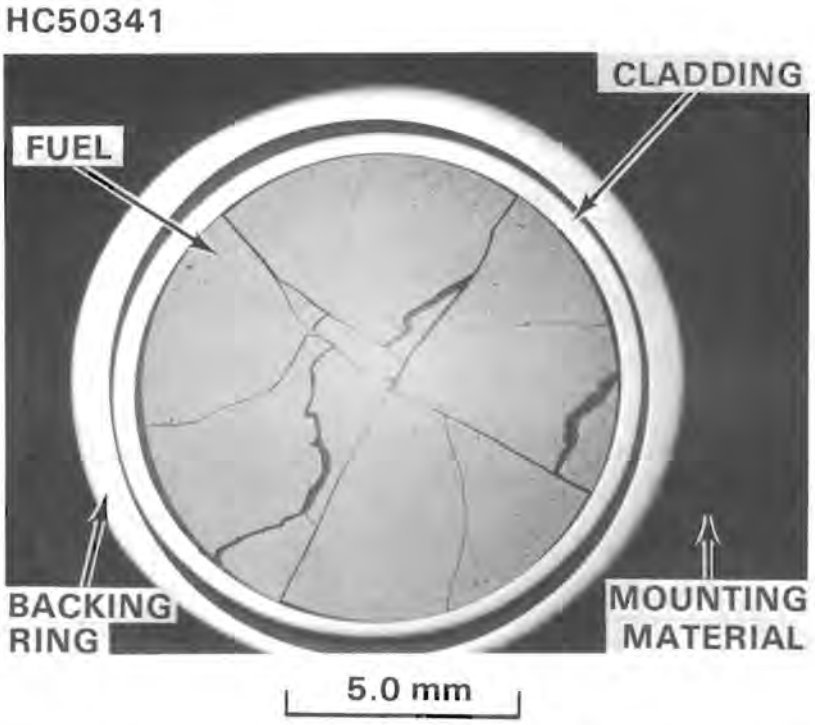

FIGURE 60. As-Polished Macrograph of Rod ABG at 56.75 in. (144 cm) from Bottom End

rods, and were consistently associated with cladding cracks that developed in the reactor, probably due to high local stresses at the chips.(a)

The reader should be cautious about forming opinions regarding fuel porosity from the ceramography. A significant number of small fuel particles can inadvertantly be pulled out of the pellet surface during specimen preparation.

The etched fuel specimens showed a minimal increase in grain size in rod ABG (Figure 61) and a small increase in grain size in rod AHR (Figure 62). Figure 63 is a macrograph of a transverse section of AHR located 56.75 in. (144 cm) above the bottom of the rod. The fuel areas shown enlarged in Figure 64 are summarized in Figure 63. One feature noted in rod AHR in Figure 63 is that the grain size gradient in areas #1 and #4 is perpendicular to the fuel

(a) The pellet chips in the S004 rods were much smaller than the chips in H07 and G11 rods. The pellet chips in H07 and G11 rods were generated during the fabrication process. The nominal diametral gap (i.e., cladding ID minus pellet diameter) for S004, G11, and H07 fuel rods was 0.14 mm (0.0055 in.). S004 fuel densified about the same amount as G11 fuel but swelled at a lower rate.

FUEL

HC 50604 HC 50603 HC 50602 HC 50601 HC 50600 HC 50599 HC 5059

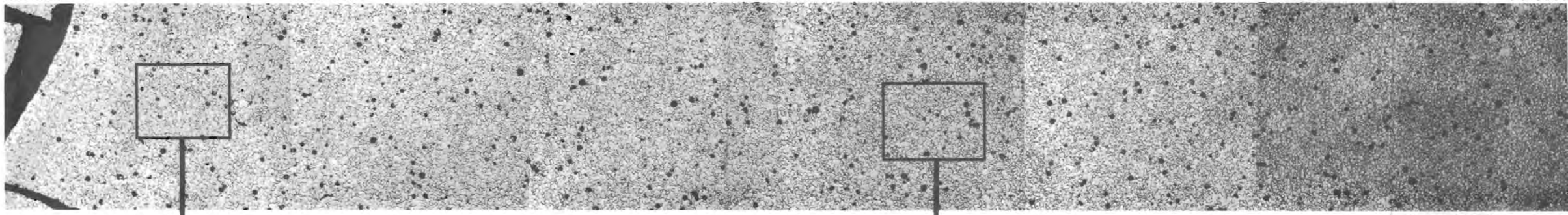

ETCHED 150

HC 50605

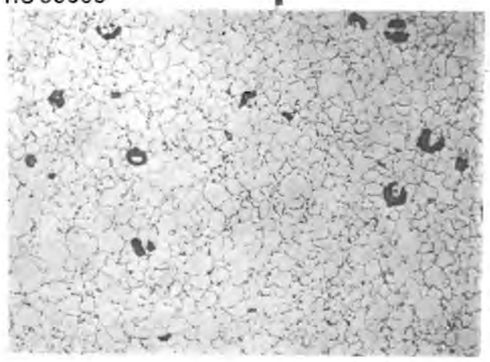

HC 50606

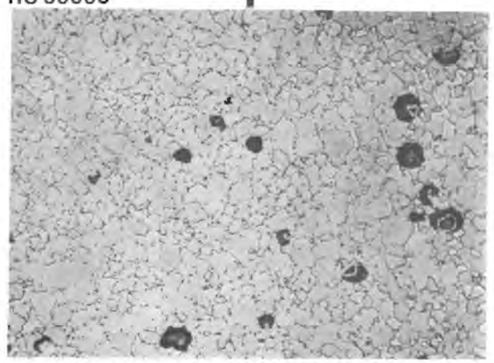

ETCHED 500X

FIGURE 61. Radial Strip of an Etched Transverse Metallographic Section from Low-Power Fuel Rod ABG from Assembly S004 at 56.75 in. (144 cm) Above the Bottom of the Rod Showing the Fuel Microstructure Typical of the High-Power Region

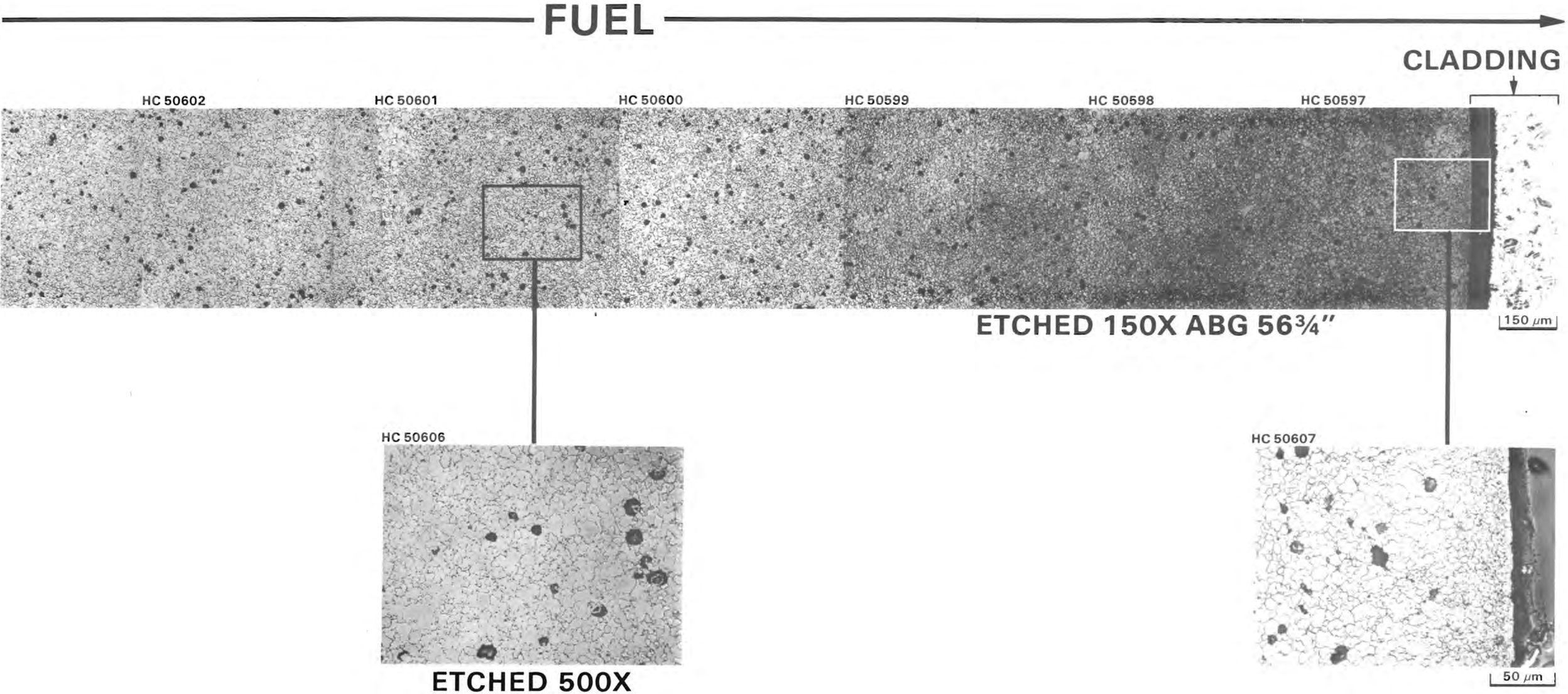

FIGURE 61. Radial Strip of an Etched Transverse Metallographic Section from Low-Power Fuel Rod ABG from Assembly S004 at 56.75 in. (144 cm) Above the Bottom of the Rod Showing the Fuel Microstructure Typical of the High-Power Region

FUEL

HC 50619 HC 50618 HC 50617 HC 50616 HC 50615 HC 50614 HC 50613

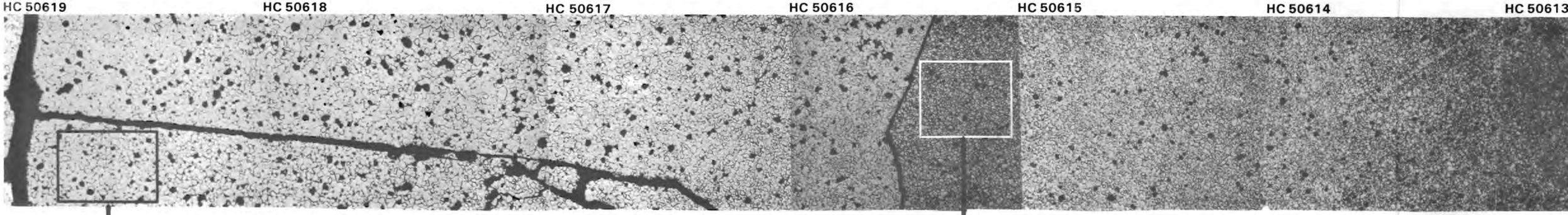

ETCHED 1

HC 50609

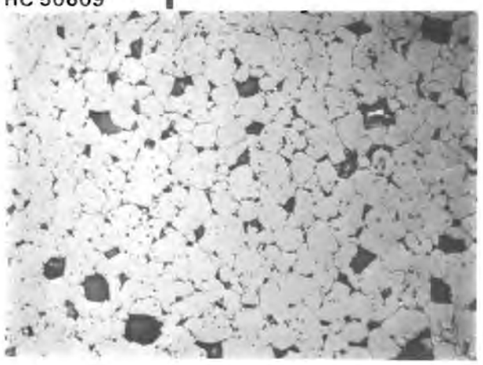

HC 50610

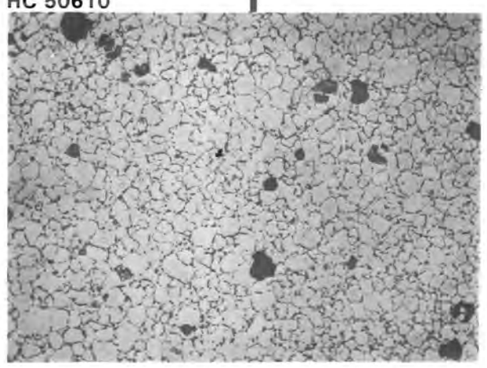

ETCHED 500X

FIGURE 62. Radial Strip of an Etched Transverse Metallographic Section from High-Power Fuel Rod AHR from Assembly S004 at 56.75 in. (144 cm) Above the Bottom of the Rod Showing the Fuel Microstructure Typical of the High-Power Region

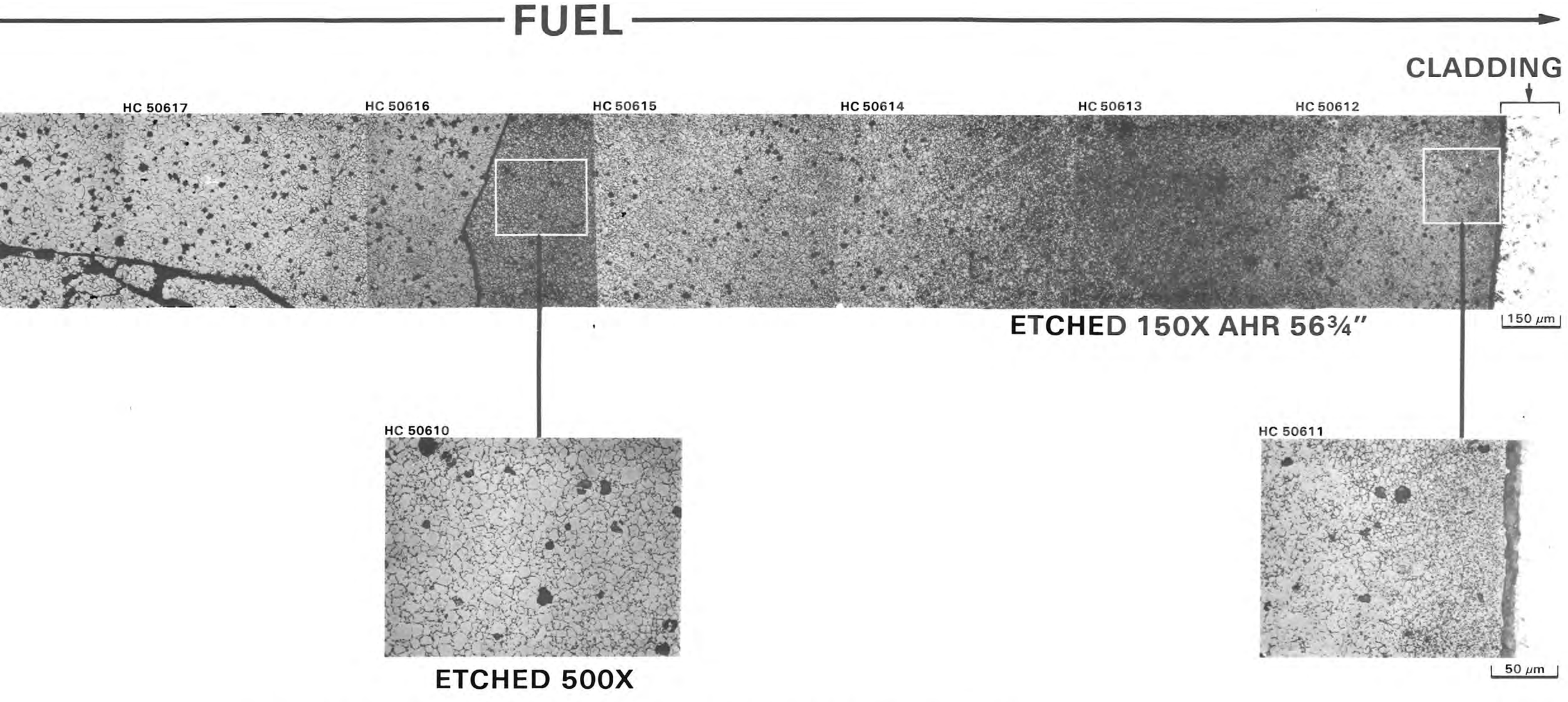

FIGURE 62. Radial Strip of an Etched Transverse Metallographic Section from High-Power Fuel Rod AHR from Assembly S004 at 56.75 in. (144 cm) Above the Bottom of the Rod Showing the Fuel Microstructure Typical of the High-Power Region

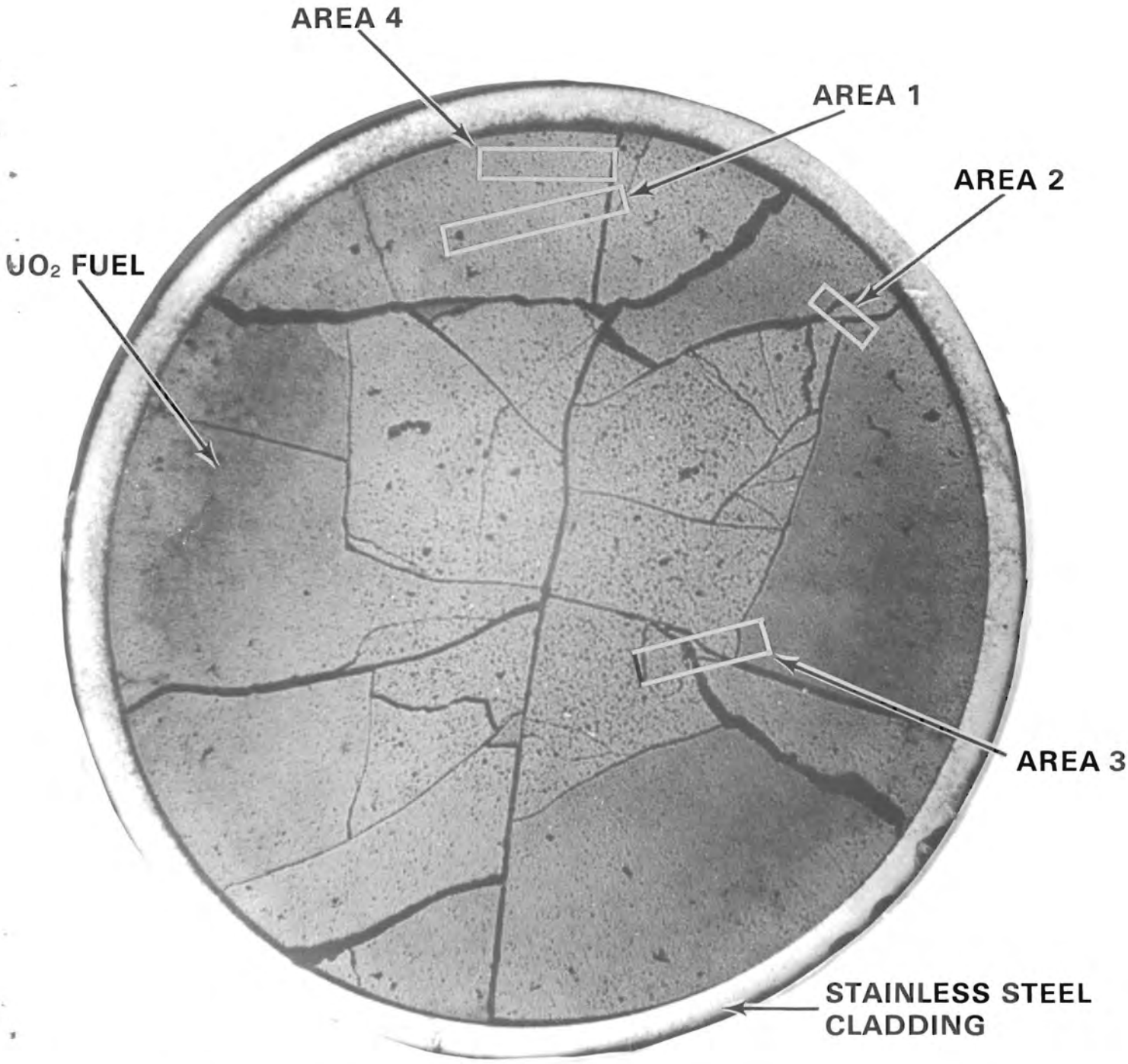

FIGURE 63. Macrograph of an Etched Transverse Metallographic Section from Rod AHR from Assembly S004 at 56.75 in. (144 cm) Above the Bottom of the Rod Showing the Locations of Photo Composite Strips of the Fuel (see Figure 64)

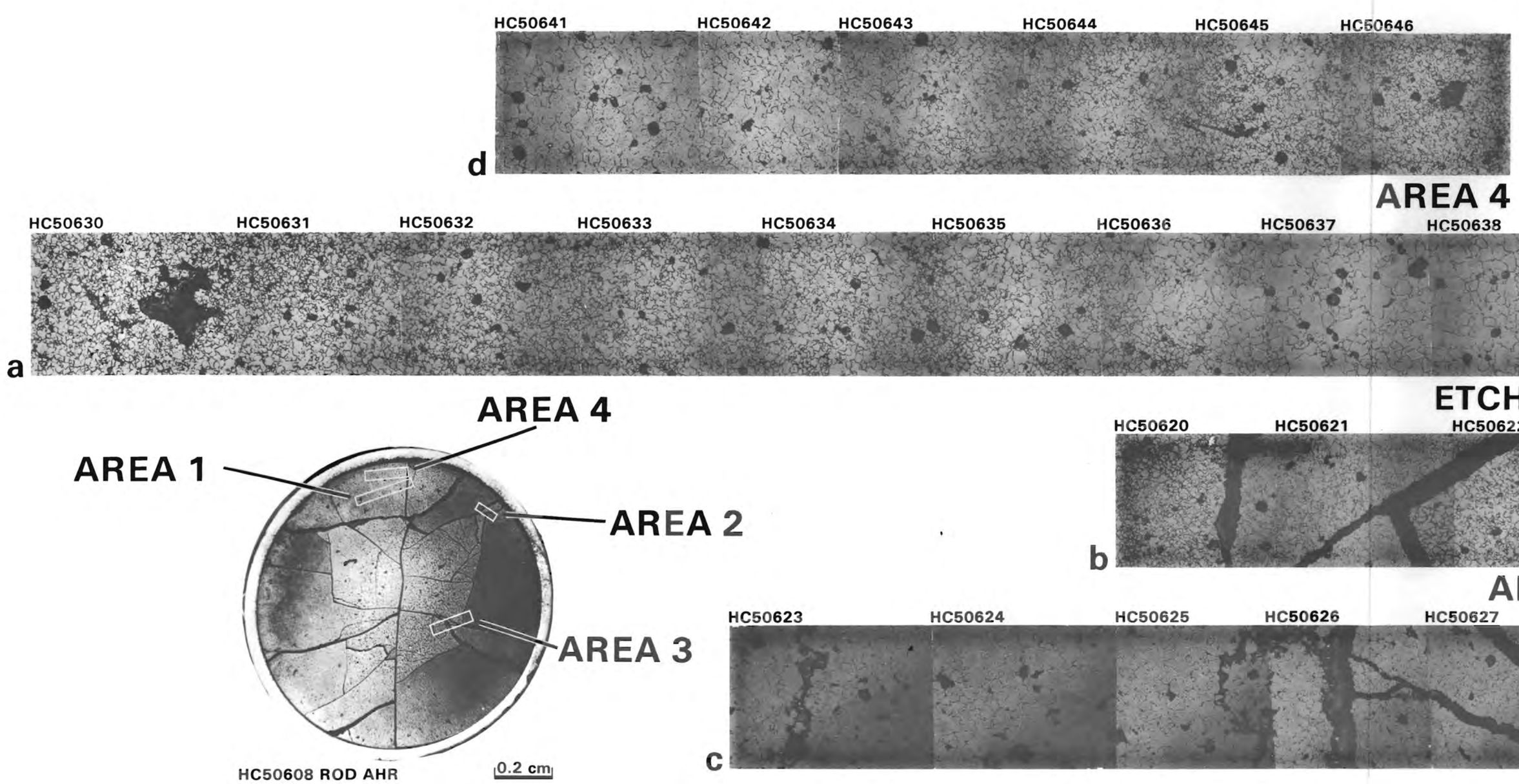

FIGURE 64. Photo Composite of (a) Area #1, (b) Area #2, (c) Area #3, (d) Area #4 from Figure 63 Showing Details of the Fuel Microstructure. Etched transverse metallographic section from S004 Rod AHR at 56.75 in. (144 cm) above the bottom of the rod.

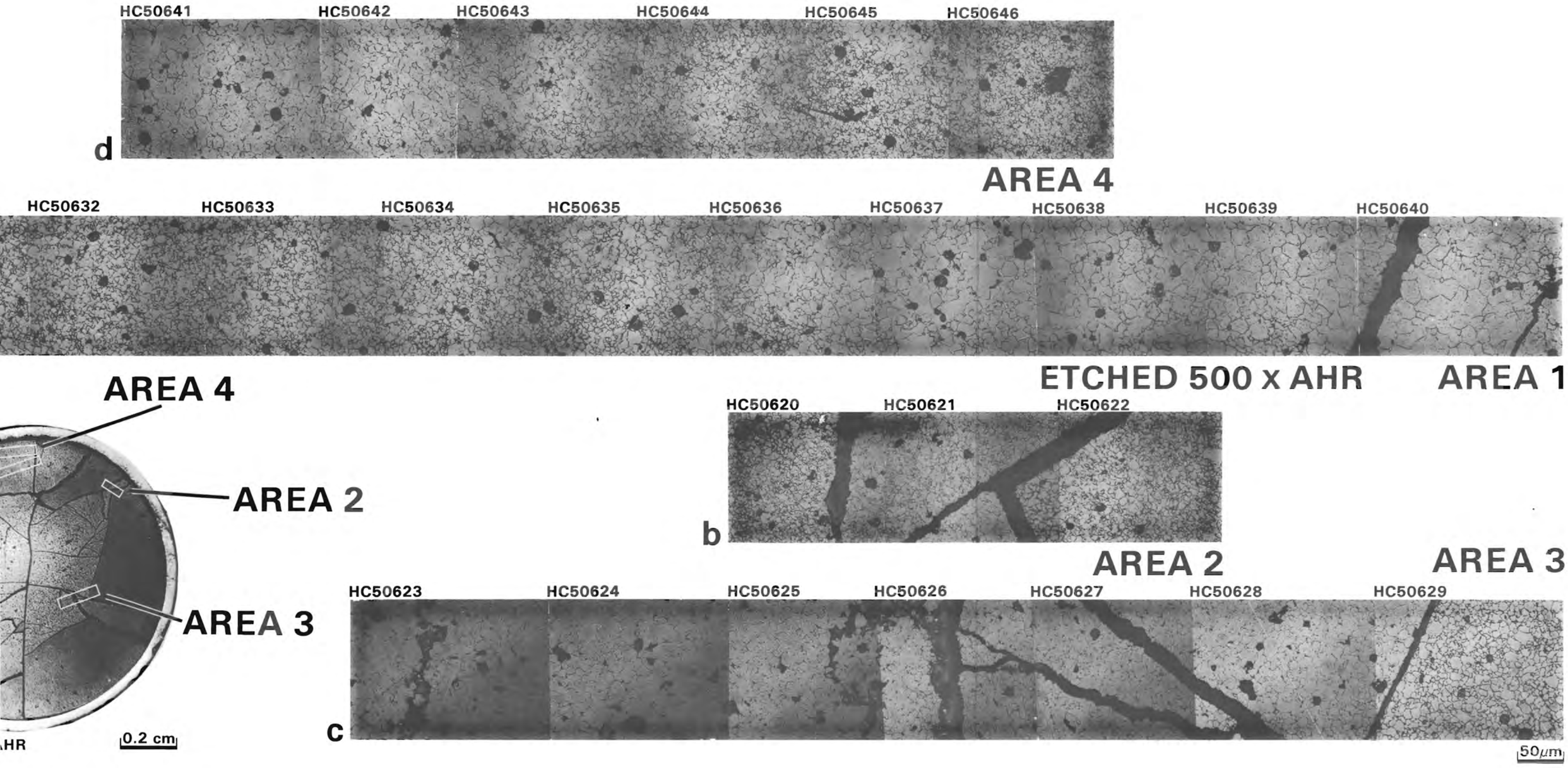

FIGURE 64. Photo Composite of (a) Area #1, (b) Area #2, (c) Area #3, (d) Area #4 from Figure 63 Showing Details of the Fuel Microstructure. Etched transverse metallographic section from S004 Rod AHR at 56.75 in. (144 cm) above the bottom of the rod.

radius and that the change in grain size is discontinuous across a crack interface, as shown in Figure 65 and area #3 of Figure 64c.[a] Figure 66 illustrates the range of grain sizes observed in rods ABG and AHR.

Metallic fission product inclusions (i.e., the small bright spots seen in the center of the AHR fuel in Figure 66) are not observed in rod ABG. Higher operational fuel temperatures are indicated in fuels with metallic fission product inclusions than in similar fuels without visible inclusions.

Autoradiography

The purpose of alpha and beta-gamma autoradiography is to show the relative distributions of alpha and beta-gamma emitting nuclides in an irradiated fuel specimen. The principal alpha emitters are plutonium and the transuranics, e.g., Np, Am, and Cm. The beta and gamma emitters are uranium and the fission products.

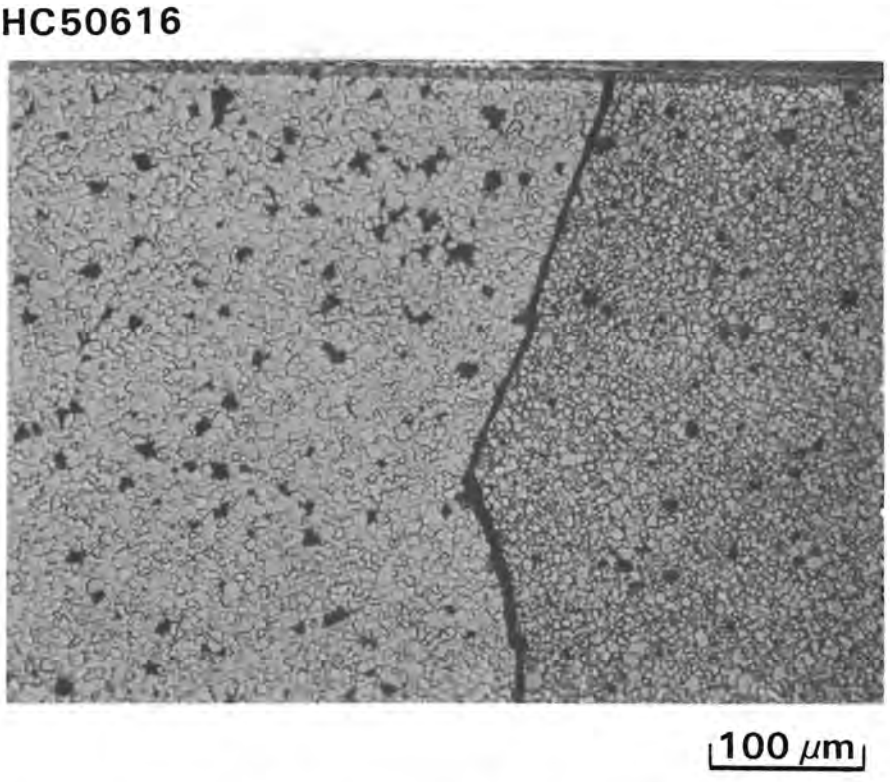

FIGURE 65. Photomicrograph Showing Grain Size Discontinuity Across a Crack Interface from the Area #3 Location in Rod AHR (see Figure 64)

(a) The grain size increase is most likely caused by the temperature increase across the interface(s). This effect is quite common.

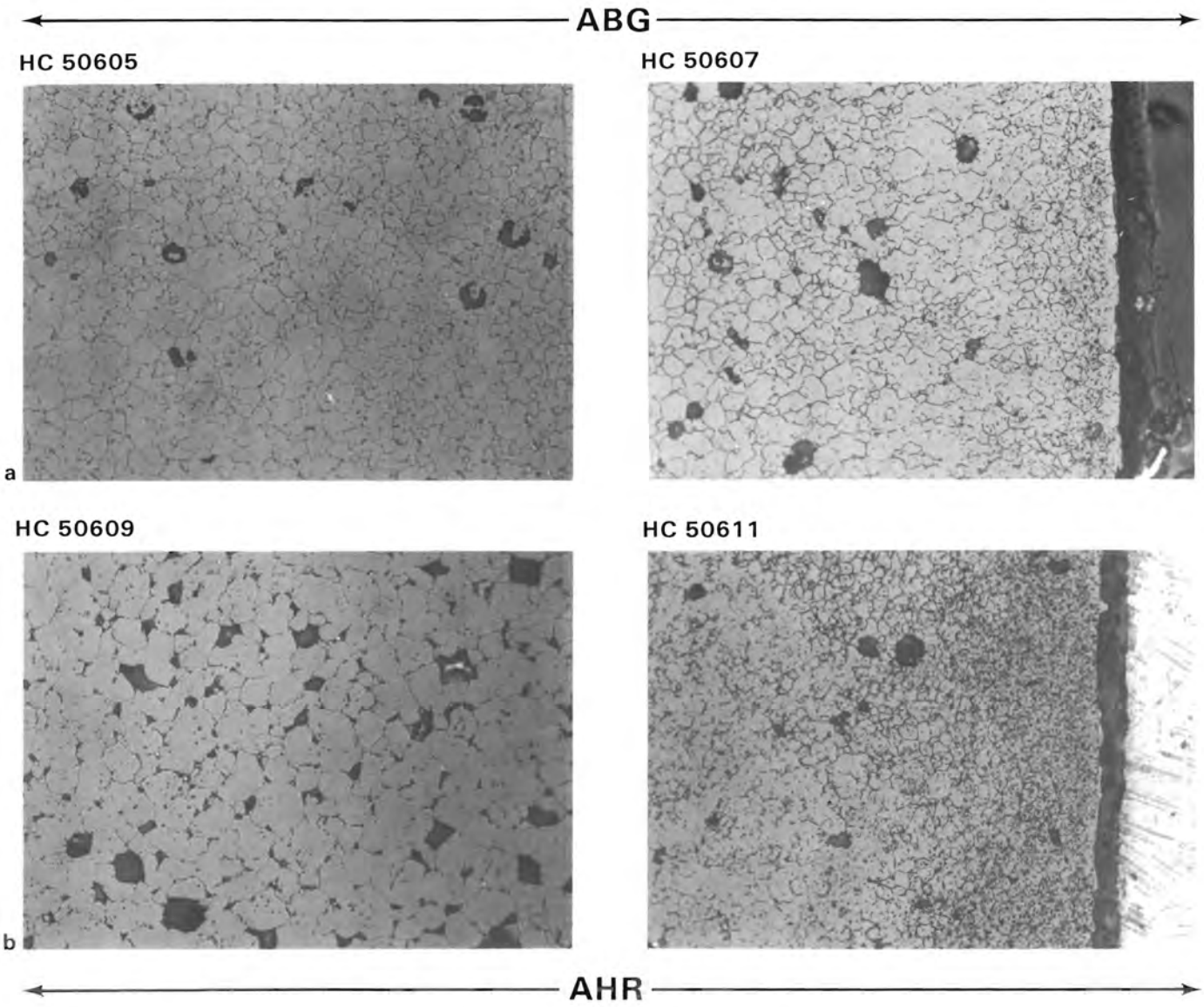

FIGURE 66. Photomicrograph of Etched Fuel Showing Range of Grain Sizes Between (a) Rod ABG and (b) Rod AHR

An autoradiograph is made by exposing film to the specimen radiation, the film being held flat against the specimen surface. The specimen surface prepared for metallogaphic examination is in the as-polished condition. Specimen No. 9 from rod AHR was placed topside down on the film to obtain the exposure.

Alpha autoradiography uses a special cellulose nitrate film. After exposure, the alpha tracks in the film are brought out by etching in a 6 N NaOH solution. Enlargements are obtained by standard photographic techniques. Beta-gamma autoradiography uses high resolution photographic plates. The plate is developed and reversed by contact printing. Enlargements are obtained by standard photographic techniques. A light gray color on the auto-radiograph indicates emitters; black indicates that no emitters were detected.

The alpha autoradiograph (Figure 67) shows an increase in alpha emitter concentration over a very small distance around the periphery of the fuels; the cladding appears to be free of alpha emitters. The beta-gamma autoradiograph (Figure 68) also shows a steep increase in emitter concentration around the fuel periphery, along cracks, and at some voids. A comparison of the optical macrograph in Figure 69 with the autoradiograph shows coincidence between cracks and some pores in the fuel. A radiation shine effect occurs in such void areas, thereby enhancing the images of those areas on the autoradiograph.

Cladding Mechanical Properties Testing

Cladding mechanical properties were measured to determine mechanical deformation behavior (ring crush tests), as well as strength and ductility (tensile tests). Tests to characterize cladding mechanical behavior were conducted because of the mechanical stresses that can develop during handling and transport of the spent fuel assembly. The tests focused on the cladding because it constitutes the first barrier for containment of actinides, nuclides, and fission products.

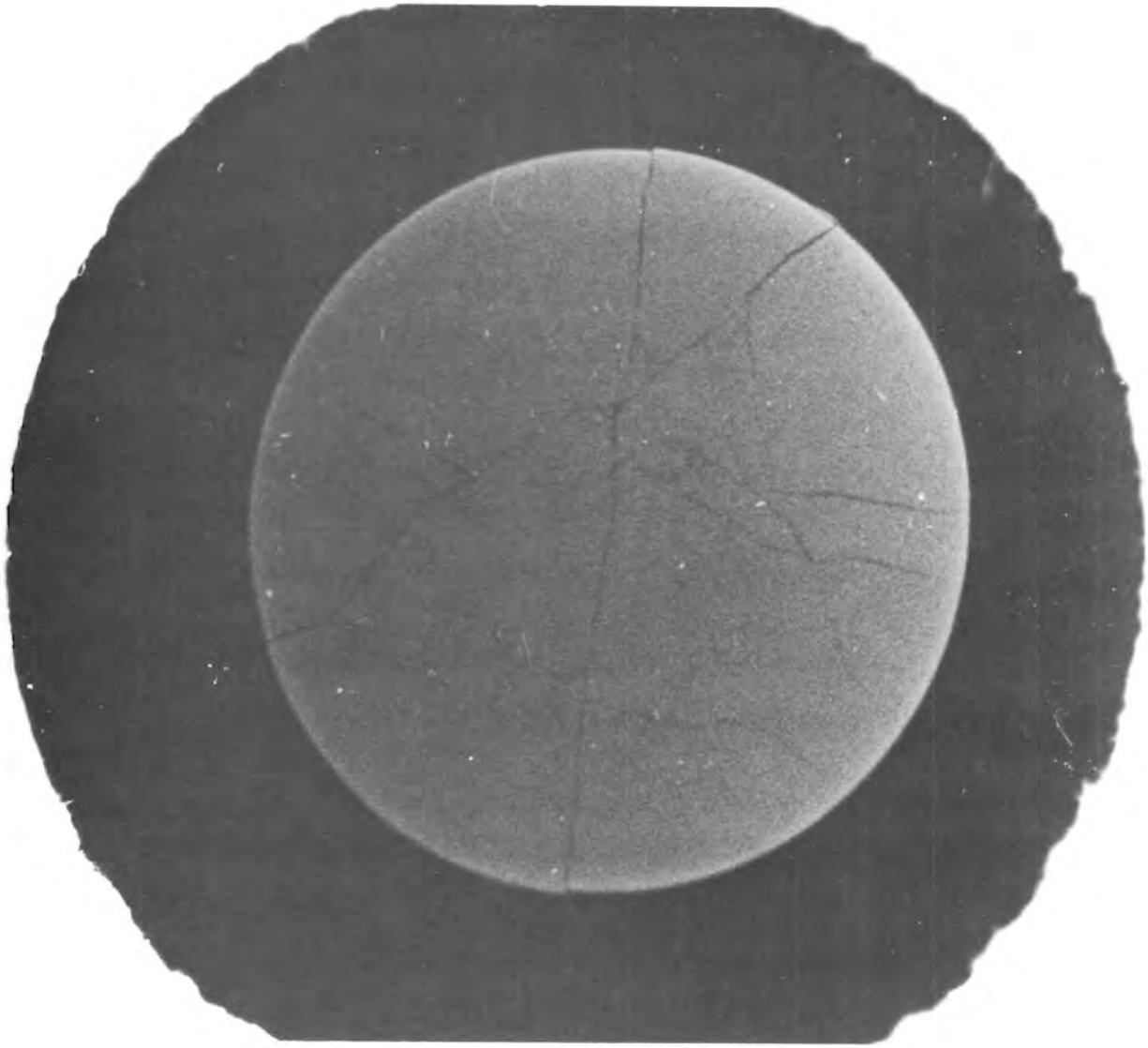

FIGURE 67. Alpha Autoradiograph from Rod AHR at 56.75 in. (144 cm) Above the Bottom of the Rod Showing the Increase of Alpha Emitter Concentration Over a Very Short Distance at the Fuel Periphery

The fabrication welding process can generate localized residual stresses and can degrade local mechanical and corrosion properties. Neutron irradiation affects the defect structure of the metal microstructure which, in turn, affects both mechanical and corrosion properties. Thermal environments during reactor operation can also affect metal microstructure and properties through creep processes. The fuel rod also contains fission products that provide a potentially corrosive and embrittling internal atmosphere for the cladding.

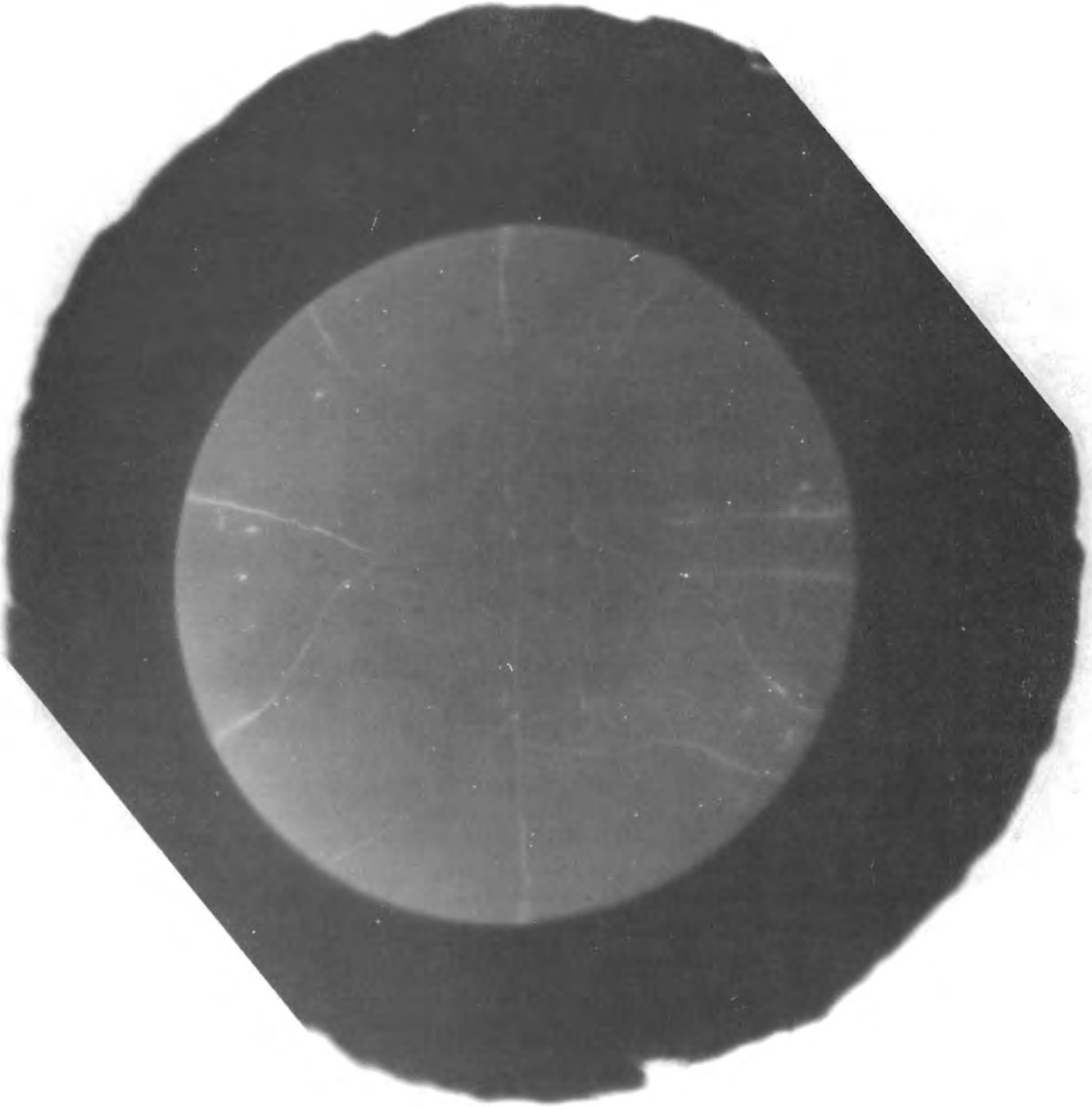

FIGURE 68. Beta-Gamma Autoradiograph from Rod AHR at 56.75 in. (144 cm) Above the Bottom of the Rod Showing a Steep Increase in Beta-Gamma Emitter Concentration at the Fuel Periphery, Along Cracks and at Some Voids

The external environment of the assembly is another factor. The coolant in an operating PWR is potentially more aggressive than the pool environment as a result of higher temperatures and more intense radiation. Crud deposits

82A916-1

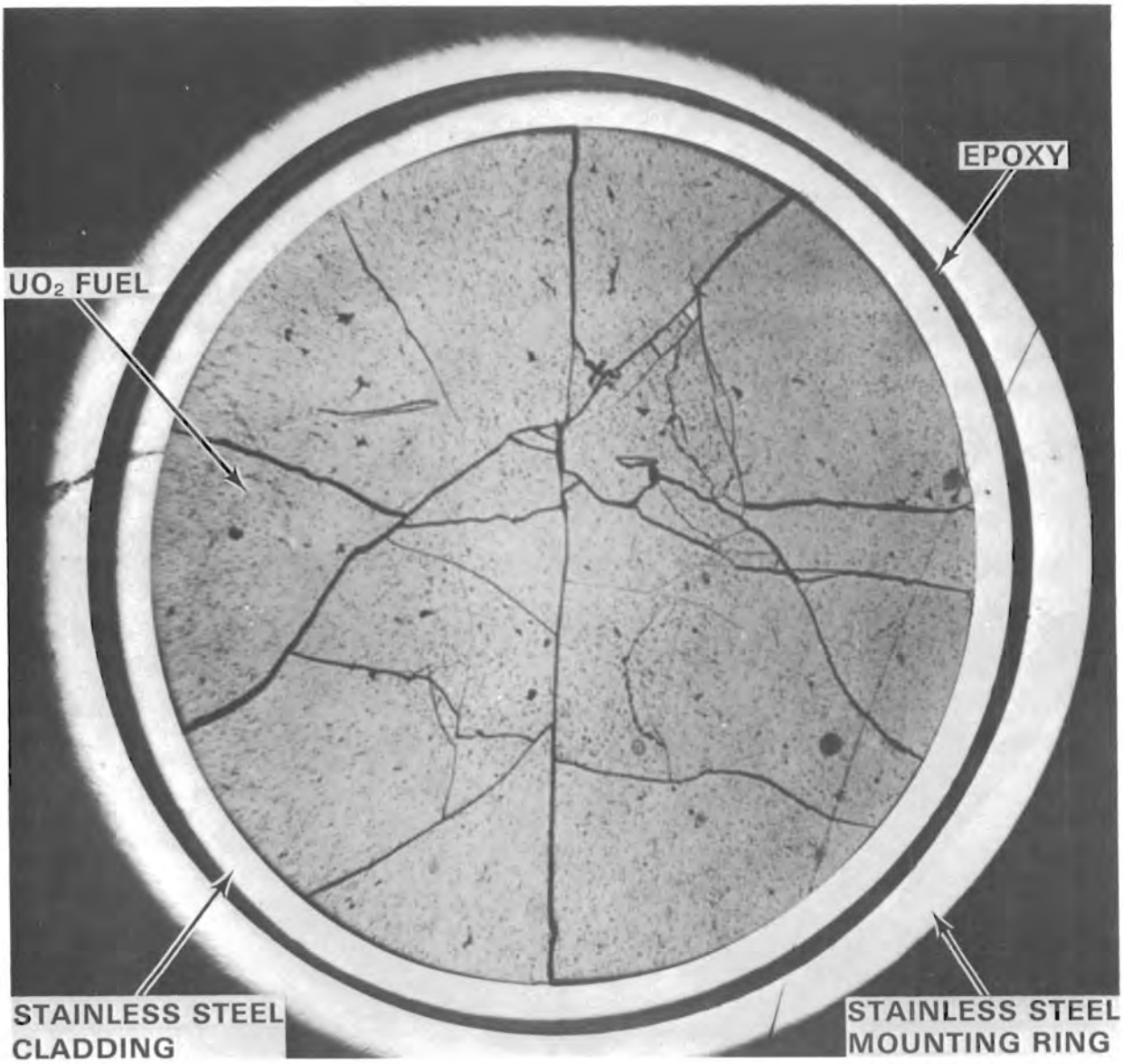

FIGURE 69. Macrograph of the As-Polished Surface from Rod AHR at 56.75 in. (144 cm) Above the Bottom of the Rod Showing the Structure of the Fuel Seen in the Autoradiographs in Figures 67 and 68

on the cladding surface can increase local temperature and local impurity concentrations in the coolant trapped under or in the crud deposits. The controlled environment in the fuel storage pool is probably the mildest of all the environments that the irradiated fuel assembly encounters.

The potential for material degradation from environmental effects must be considered. Accordingly, ring crush and tensile tests were conducted to determine postirradiation mechanical properties and deformation behavior of cladding exposed to the normal range of environments.

Cladding specimens for mechanical testing were cut from S004 rod AHR in 1/2-in. (1.3-cm) and 5-in. (13-cm) lengths by a water-cooled abrasive cut-off wheel. An attempt to defuel 1/2-in. (1.3-cm) long specimens on the fuel removal punch press was unsuccessful. The specimens were defueled on a drill rig with an end mill instead of a water-cooled diamond drill. Drilling was slow because much fission gas release was encountered. The retained fisson gas accumulated in unconnected porosity in the fuel and remained there until it was released during drilling (Zimmerman 1975). Very little fission gas moved from the trap sites in the fuel after the fuel was discharged from the reactor, i.e., when the fuel was no longer at the high temperature of reactor operation (Bouffioux and De Meulemeester 1979). Normally this procedure leaves a thin annulus of fuel tightly adhering to the cladding. The annulus is often removed by soaking the sample in nitric acid. We specifically requested that the specimens not be exposed to nitric or any other acid. The 1/2-in. (1.3-cm) long specimens were visually examined before testing to ensure that no nicks or scratches were present that could affect test results.

Ring Crush Test

Side-pressing compression tests (Greenberg and Prager 1951; Johnson 1956; and Sorverby et al. 1968) on 1/2-in. (1.3-cm) long defueled sections of cladding from S004 fuel rods yielded information on the mechanical deformation behavior of the irradiated 304L stainless steel fuel cladding. Test were designed to provide insight into the effects of strain rate or deformation rate and specimen axial location (i.e., local irradiation and thermal environmental histories) on cladding mechanical deformation. A specimen of unirradiated archive material obtained from BNFL was included for comparison.

Specimens were tested on an Instron testing machine, side-pressing the rings in the compression mode. The average of three length measurements was the value used for each of the specimen lengths. Specimen load versus

displacement and load versus time were recorded. The limits on testing deformation rate were determined by the upper crosshead speed (2.00 in./min or 5.18 cm/min) and lower crosshead spead 0.002 in./min or 0.005 cm/min) of the Instron. An intermediate deformation rate of 0.05 in./min (0.13 cm/min) was also used. Specimens were selected from low, middle, and high axial rod locations lying within the area of relatively uniform power and burnup (Figures 7 through 9 and Table 28). The rings were loaded until metal-to-metal contact of the ring ID occurred; the cladding did not break or split. Some specimen spring-back occurred after the load was removed. Specimen 3H did fracture several months after testing while it was being handled for post-test photography in the hot cell. A photographic record of the specimen geometry was being made. No other specimens failed.

Table 28 lists the results of the ring crush tests. Figure 70 shows the strain-rate dependence of the collapse load (Pc) normalized for specimen length. Figure 71 shows the strain-rate dependence of the strain (i.e., crosshead displacement) at ring collapse. A correlation of the axial location of the specimen with deformation behavior is apparent in the strain-rate plots. Specimen 3F may be an anomaly (it was the first test in the series).

The general conclusion is that the irradiated cladding is not brittle under compressive loading (less than 1% uniform elongation). The mechanical deformation behavior in the ring crush tests is similar to that of archive material under these testing conditions.

The link between the crush test and conventional tensile test is the collapse load. Rosenfield (1978) developed a correlation between collapse load (Pc) and flow stress (σ_f). Figure 72 shows a schematic load versus displacement plot for a ring. The point Pc is the collapse load and is determined by extrapolating the lines from the two linear regions. The flow stress is described as the average of the 0.2% offset (YS) and the ultimate tensile strength (UTS). Figure 73 shows the correlation developed by Rosenfield between the normalized collapse load and the ratio of the inside diameter (Di) to the outside diameter (Do) of the ring. Rosenfield's investigation included rings with (Di/Do) values in the range of 0.25 to 0.75. The (Di/Do) of the rings tested in this program was 0.92.

TABLE 28. Side-Pressing Ring Crush Test Results[a]

Specimen Designation (See Figure 13)	Crosshead Speed (in./min)	Specimen Center Location (in. above rod bottom)	Specimen Length (in.)	Load (lb)	Normalized Load (lb/in.)	Displacement (mils)
3F	2.000	34.75	0.5040	127	252.0	36
12B	2.000	59.50	0.5313	146	275.0	55
7D	0.050	50.00	0.5054	130	257.0	35.8
17B	0.050	49.00	0.5292	140	265.0	33.8
3H	0.002	35.75	0.5244	112	214.0	29
17C	0.002	90.75	0.5527	126	228.0	25.5
Archive	0.200	---	0.2500	51	204.0	

(a) Fuel cladding from assembly S004. Cladding material is 304L SS drawn-welded tubing, nominally 12% cold-worked. Nominal cladding OD is 10.76 mm (0.4235 in.); wall thickness is 0.42 mm (0.0165 in.).

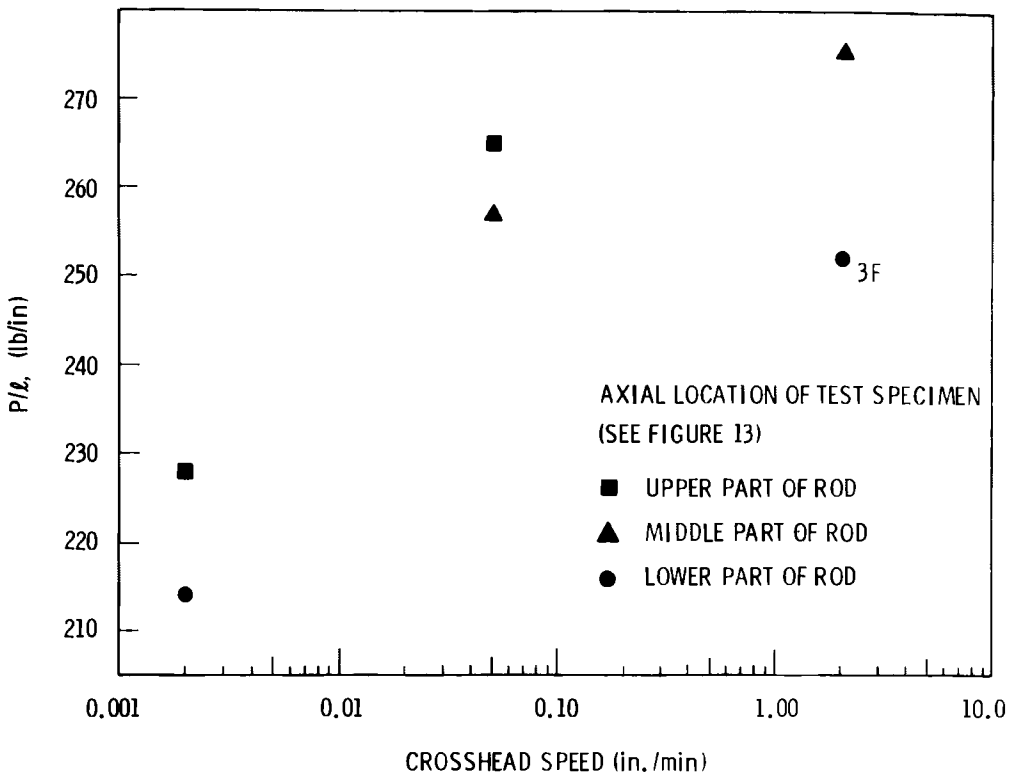

FIGURE 70. Results of Side-Pressing Crush Tests of Rings of Irradiated 304L Stainless Steel Cladding Showing the Dependence of Collapse Load on Deformation Rate. The collapse load, Pc, has been normalized for specimen length, ℓ (250 lb/in. = 44.6 kg/cm; 1.00 in./min = 2.54 cm/min)

The normalized collapse load is Pc/σ_f Doℓ, where Pc = collapse load, σ_f = flow stress, Do = outside diameter of ring, ℓ = length of ring. Table 29 lists the values of normalized collapse loads calculated for the ring crush tests. The average of these values constitutes a reasonable extrapolation of Rosenfield's results. The agreement with Rosenfield's results and the consistency of the tests themselves support the results of the ring crush tests as being representative of the mechanical deformation behavior of cladding.

Tensile Test

Tensile tests on 5-in. (13-cm) long defueled sections of irradiated Type 304L stainless steel cladding from S004 fuel rods yielded information on the mechanical strength and ductility during uniform mechanical deformation.

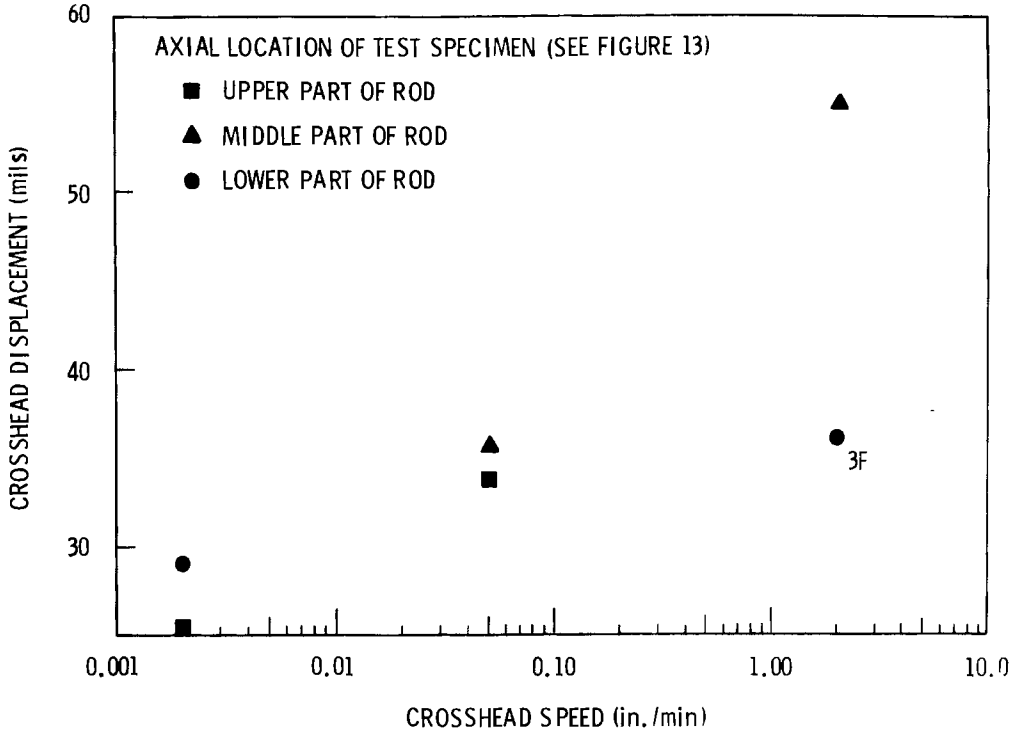

FIGURE 71. Collapse Deformation Versus Deformation Rate from Ring Crush Tests on Irradiated 304L Stainless Steel Showing the Dependence of Deformation at Collapse on Deformation Rate (50 mils = 1.27 mm; 1.00 in./min = 2.54 cm/min)

Deformation was continued until specimen fracture occurred. A test matrix similar to that developed for the ring crush tests provided insight into the effects of strain rate or deformation rate and specimen axial location (i.e., local irradiation and thermal environmental histories) on cladding strength and ductility during uniform deformation.

Again, specimens were tested on an Instron testing machine. To support the specimen ends gripped in the Instron, 1 1/2-in. (3.8-cm) long plugs were prepared; one was inserted into each end of the specimen. Axial strain of the 2-in. (5 cm) gage length was measured with a clip gage. Specimen load versus displacement, as well as load versus time behavior, was recorded. Nominal as-fabricated cladding dimensions were used to compute the stresses.

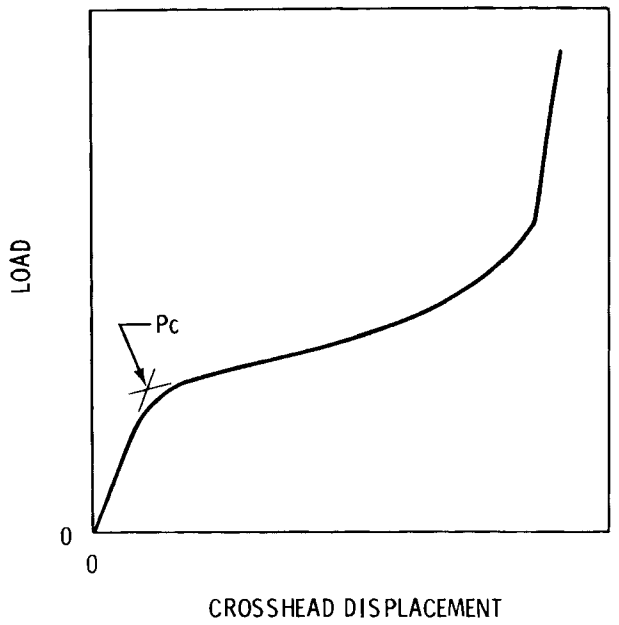

FIGURE 72. Schematic Load Versus Displacement Curve for Side-Pressing Ring Crush Test

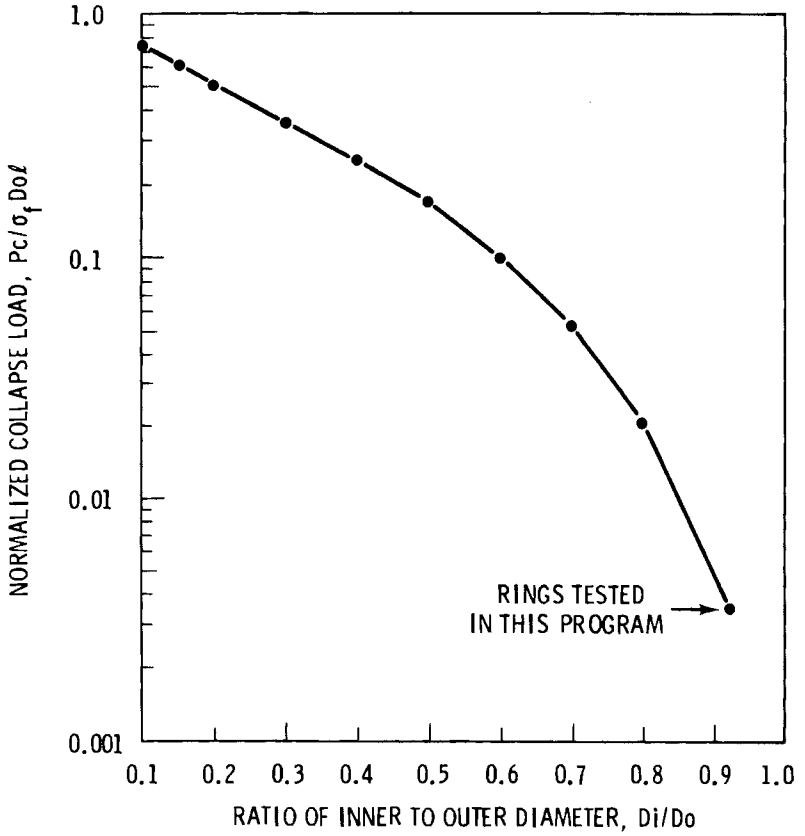

FIGURE 73. Dependence of Collapse Load on Ring Geometry in the Side-Pressing Ring Crush Test

TABLE 29. Normalized Collapse Loads for Ring Crush Tests of Cladding from S004 Rod AHR

Specimen	Collapse Load (lb)	Length of Ring (in.)	Flow Stress(a) (psi)	Normalized Collapse Load
3F	127	0.5040	171,848.	3.46×10^{-3}
12B	146	0.5313	169,787.	3.82×10^{-3}
7D	130	0.5054	167,180.	3.63×10^{-3}
17B	140	0.5292	164,337.	3.80×10^{-3}
3H	112	0.5244	166,825	3.02×10^{-3}
17C	126	0.5527	160,308.	3.36×10^{-3}
			AVERAGE	3.52×10^{-3}

(a) The flow stress, $\sigma_f = 1/2(UTS + YS)$, is calculated from the tensile test results (see Table 30). UTS is the ultimate tensile strength and YS is the yield stress.

Table 30 lists the results of the longitudinal tensile tests on six specimens. Figure 74 shows the low strain-rate dependence of the yield strength (0.2% offset). Figure 75 shows the strain-rate dependence of the difference between the ultimate tensile strength (UTS) and the yield strength (YS). Figure 76 illustrates the strain-rate dependence of the cladding uniform elongation. Ultimate tensile and yield strengths showed some correlation with the axial location of the specimen. There was no consistent variation of uniform elongation with axial location.

The tensile strength of the irradiated cladding has increased and the elongation has decreased significantly compared to the nominal values for unirradiated samples of other comparable Type 304 stainless steel cladding used in other Connecticut Yankee fuel assemblies. However, the irradiated cladding retained sufficient ductility to withstand crushing without breaking or splitting. Only six irradiated specimens were tested and the results for total elongation varied over quite a range. The single tensile specimen that broke in the center of the specimen gage length had a total elongation of 20%. The other five speciments exhibited less total elongation (1.7 to 6.0%) but similar uniform elongations (1.1 to 1.6%). Similar but unirradiated cladding exhibits an elongation of 46%.

TABLE 30. Tensile Test Results[a]

Specimen Designation (see Figure 13)	Crosshead Speed (in./min)	Specimen Center Location (in. above rod bottom)	Fracture Location	Maximum Load (lb)	UTS (ksi)	YS (ksi)	Uniform Elongation (%)
3C	2.000	26.50	Top, near knife edge	3720	176.3	167.4	1.6
7F	2.000	53.25	Top break	3685	174.6	164.9	1.5
7A	0.050	46.25	Bottom break	3585	169.9	164.5	1.2
17	0.050	87.00	Top break	3535	167.5	161.1	1.2
3D	0.002	31.50	Top, above knife edge	3570	169.2	164.5	1.1
17E	0.002	94.00	Mid-gage length	3435	162.8	157.8	1.36

(a) Fuel cladding from fuel rods from assembly S004.
Cladding material is 304L SS drawn, seam-welded tubing.
Nominal cladding OD is 0.4235 mils; wall thicknes is 0.0165 mils.
Assumed cross-sectional area for all samples is 0.0211 $in.^2$
Samples are 5 in. long with a 2-in. gage length.
Similar unirradiated 304 SS tubing has the following properties:
UTS = 105 ksi; YS = 78 ksi; elongation = 46%.

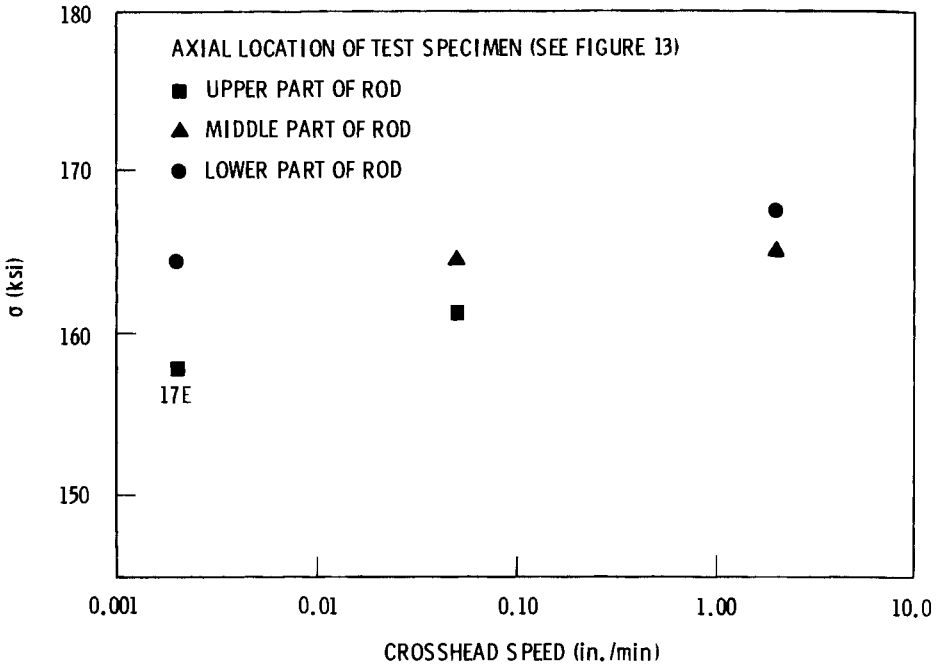

FIGURE 74. Cladding Tensile Test Results for Irradiated 304L Stainless Steel Showing the Low Strain-Rate Dependence of the Yield Strength, σ (0.2% Offset), (160 ksi = 1100 MPa; 1.00 in./min = 2.54 cm/min)

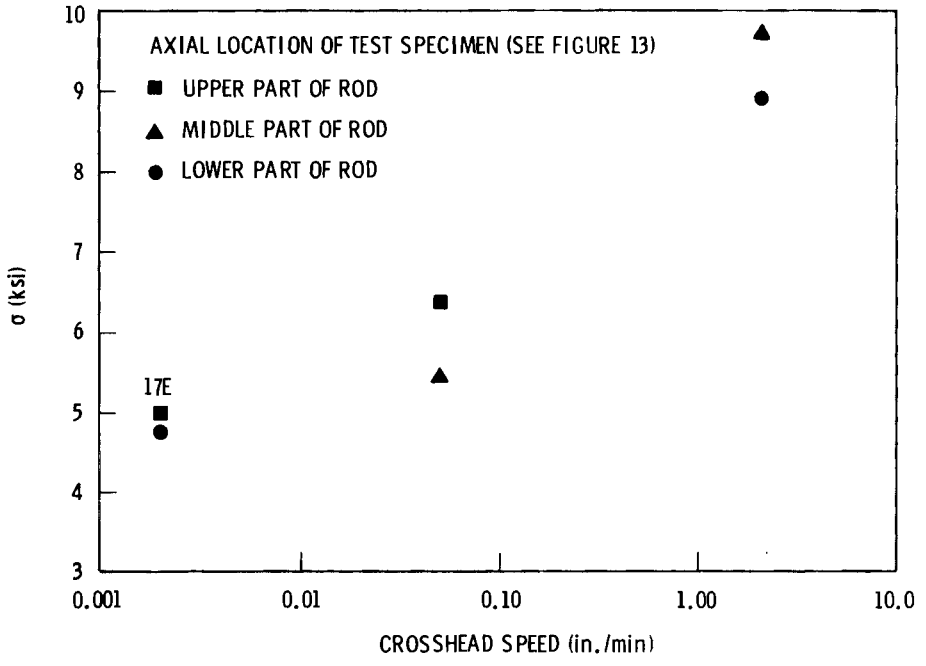

FIGURE 75. Cladding Tensile Test Results Showing the Strain-Rate Dependence of the Difference Between the Ultimate Tensile and Yield Strengths for Irradiated 304L Stainless Steel (6 ksi = 41 MPa; 1.00 in./min = 2.54 cm/in.)

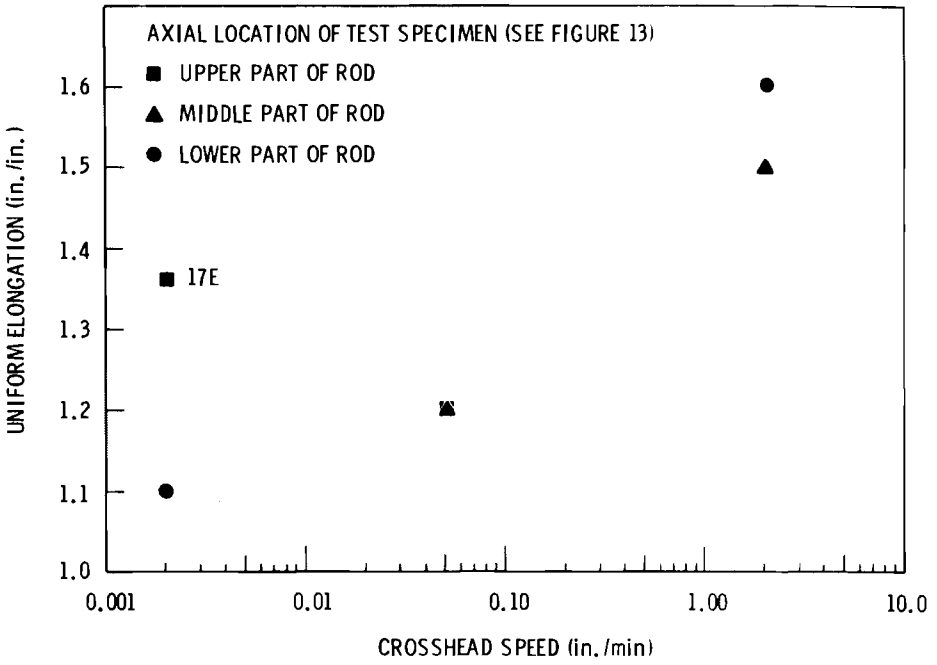

FIGURE 76. Cladding Tensile Test Results Showing the Dependence of Strain-Rate on the Specimen Uniform Elongation for Irradiated 304L Stainless Steel (1.00 in./min = 2.54 cm/min)

REFERENCES

Anderson, P. A., and H. S. Meyer. 1980. Dry Storage of Spent Nuclear Fuel. NUREG/CR-1223. U.S. Nuclear Regulatory Commission, Washington, DC.

Barney, W. K., and B. D. Wemple. 1958. Metallography of Irradiated UO_2-Containing Fuel Elements. KAPL-1836, Knolls Atomic Power Laboratory, Schenectady, New York.

Bouffioux, P. and E. De Meulemeester. 1979. "Prediction of Fission Gas Release at High Burnup." Proceedings of the ANS Topical Meeting on Light Water Reactor Fuel Performance, Portland, Oregon.

Carter, W. L. 1980. Spent Fuel and Waste Inventories and Projections. ORO-778, Oak Ridge National Laboratory, Oak Ridge, Tennessee.

Fuhrman, N. et al. 1976. Evaluation of Fuel Rod Performance in Maine Yankee Core 1. EPRI NP-218, Electric Power Research Institute, Palo Alto, California.

Garzarolli, F., D. Jorde, R. Manzel, G. W. Parry, and P. G. Smerd. 1980. Review of PWR Fuel Rod Waterside Corrosion Behavior. EPRI NP-1472. Prepared by Kraftwerk Union AG, F.R.G. and Combustion Engineering, Inc., Windsor, Connecticut, pp. 3-15 and 4-5.

Garzarolli, F. and R. Manzel. 1979. "High Burnup Performance in LWRs." Trans. Am. Nuclear Soc. 31:162-163.

Giacobbe, F. S. 1981. "Examination, Evaluation, and Repairs of Stress Corrosion Cracking in a PWR Borated Water Piping System." Corrosion 81, Toronto, Ontario, Canada.

Greenberg, H. J. and W. Prager. 1951. "Limit Design of Beams and Frames." Proc Am. Soc. Civil Eng. 77(59):1.

Heal, T. J., J. E. Littlechild, and H. Page. 1980. "Fuel Production-An Advanced Technology. Nuclear Engineering International, pp. 48-51.

Johnson, A. B., Jr. 1975. "A Review of Corrosion Phenomena on Zirconium Alloys, Niobium, Titanium, Inconel, Stainless Steel, and Nickel Plate Under Irradiation." Reviews on Coatings and Corrosion. J. Yahalom (ed.), Freund Publ. House, Tel Aviv, Israel, pp. 352-356.

Johnson, A. B., Jr. et al. 1980. Annual Report - FY-1979, Spent Fuel and Fuel and Fuel Pool Component Integrity. PNL-3171, Pacific Northwest Laboratory, Richland, Washington.

Johnson, A. B., Jr., E. R. Gilbert, and R. J. Guenther. 1982. Behavior of Spent Nuclear Fuel and Storage System Components in Dry Interim Storage. PNL-4189, Pacific Northwest Laboratory, Richland, Washington.

Johnson, W. 1956. "The Compression of Circular Rings." J. Royal Aero. Soc. 60:484.

Klingensmith, R. W. 1980. "Airborne Contamination Released During Underwater Unloading of Failed PWR Spent Fuel Assembly." Proceedings-PATRAM 80.

Littlechild, J. E. and G. G. Butler. 1976. "The Specification and Quality Control of UO_2 Fuel Pellet Microstructure to Ensure Density Stability and Low Moisture Content." Proceedings of Seminar on Nuclear Fuel Quality Assurance. International Atomic Energy Agency.

Multer, I. 1975. "European Operating Experience," a paper presented at the Joint Topical Meeting on Commercial Nuclear Fuel Technology Today, held in Toronto, Ontario, Canada, April 1975.

Northern States Power Company. 1982. Licensee Event Report No. 81-031/01X-1, Docket No. 50-282 (Prairie Island-1).

Pasupathi, V. and R. W. Klingensmith. 1981. Investigation of Stainless Steel Clad Fuel Rod Failures and Fuel Performance in the Connecticut Yankee Reactor. EPRI NP-2119, Electric Power Research Institute, Palo Alto, California.

Phillips, J. R. et al. 1980. Application of Nondestructive Gamma-ray and Neutron Techniques for Safeguarding of Irradiated Fuel Materials. LA-8212. Los Alamos Scientific Laboratory, Los Alamos, New Mexico.

Raven, L.F.A. 1976. "The Performance of BNFL Controlled Porosity Nuclear Fuel," Paper No. 45-N-76 presented at the 78th Annual Meeting of the American Ceramic Society, held in Cincinnati, Ohio, May 1976.

Rosenbaum, H. S., J. S. Armijo, and U. E. Wolf. 1966. Fission Fragment Damage to 304SS Fuel Cladding. GEAP-5002, General Electric Company, San Jose, California.

Rosenfield, A. R. 1978. "Diametral Compression of Rings." Strain 14(4):150.

Sorverby, R., W. Johnson and S. K. Samanta. 1968. "The Diametrical Compression of Circular Rings by 'Point' Loads." Int. J. Mech. Sci. 10:369.

Storev, J., and D. H. Locke. 1970. "High Burnup Irradiation Experience in Vulcain." Nuclear Engineering International. February 1970, pp. 93-99.

Zhou, S. Y., and D. R. Olander. 1981. "Thermal Gradient Redistribution of Ruthenium in UO_2." Trans. Am. Nucl. Soc. 38:314-315.

Zimmerman, H. 1975. "Fission Gas Behavior in Oxide Fuel Elements of Fast Breeder Reactors." Nuclear Technology 28:127-133.